KTH Architecture and
the Built Environment

Ground Improvement by Dry Deep Mixing Lime-Cement Column Panels as Excavation Support

Razvan Ignat

Doctoral Thesis

Department of Civil and Architectural Engineering

Division of Soil and Rock Mechanics

KTH, Royal Institute of Technology

Stockholm, 2018

TRITA-ABE-DLT-1834

ISBN 978-91-7729-969-1

PREFACE

The work presented in this thesis was conducted between 2012 and 2018 at the Division of Soil and Rock Mechanics, Department of Civil and Architectural Engineering, KTH Royal Institute of Technology in Stockholm, Sweden. The work was supervised by Professor Stefan Larsson, Head of the Division of Soil and Rock Mechanics, with assistance from Dr. Sadek Baker and Dr. Sven Liedberg at Skanska AB.

This study is part of BIG (Better Interaction in Geotechnics). The project was founded by the Development Fund of the Swedish Construction Industry (SBUF), the Swedish Transport Administration, and Skanska AB. Sincere thanks go to the funders for making this project possible.

I would like to give my supervisors Professor Stefan Larsson, Dr. Sadek Baker, and Dr. Sven Liedberg the warmest of acknowledgement and my gratitude for their encouragement, great support and guidance throughout this project.

The field test work would not have been possible without the equipment provided by the Skanska Foundation Group, the practical work conducted by Johan Jandelius, the help with installation, programming and surveillance of the measurement systems conducted by Ivar Nöre and Patrick Andersson at Geometrik and the geotechnical field experience of Ingemar Forsgren at Ingefors Geoteknik AB. My warmest sincere thanks to Martin Holmén at the Swedish Geotechnical Institute (SGI) for all assistance and help in the planning and execution of the laboratory tests presented in this thesis. Professor Minna Karstunen, Dr. Tara Wood and Niklas Dannewitz have provided valuable comments throughout this project and their contribution is highly appreciated. I would also like to express my gratitude to all my colleagues at Skanska and KTH for their support and encouragement during these years.

Finally, I would like to thank my family, my wonderful wife Heam, for her unconditional support, love, and patience, my sons Victor and Julian, for all the joy, love, and happiness they bring to my life, and the rest of my family and friends, for their help in making this work possible. Without their support, this work would not have been possible.

Stockholm, August 2018

Razvan Ignat

SUMMARY

Many urban areas near the coastal regions of Sweden are characterized by post-glacial clay deposits with very low undrained shear strength and high compressibility. Column type ground improvement by the Deep Mixing, DM, method using a binder mixture of lime and cement is commonly used in areas with poor soil conditions due to its cost-effectiveness, predominantly for settlement reduction and to improve the stability of embankments. With increasing urbanization and infrastructural development in these areas there is great interest in the industry in extending the practice of the Deep Mixing method to include other applications such as deep excavation and temporary and permanent improvement of natural slopes. Swedish experience related to use of the DM method for excavation support is limited and the current design recommendations for DM columns installed in the passive zone are very restrictive regarding the allowable mobilized column strength, resulting in a design which is often not cost-effective.

In order to increase the use of the method to include applications where DM columns are subjected to unloading and lateral loading conditions, the mobilized strength and stiffness properties of the columns as well as the soil-column interaction need to be reliably predicted. The main objective of this study is to present a consistent method to adequately predict the behavior of lime-cement columns installed as excavation support in the passive zone of the structure and to investigate the strength and stiffness properties of lime-cement improved clay under different unloading and laterally loading conditions together with the soil-column interaction under these conditions.

In order to investigate the field behavior of lime-cement column panels as excavation support, two experimental full-scale tests were performed. In each of these tests, a braced steel sheet pile wall supported by panels of overlapping lime-cement columns was first excavated to a pre-determined depth and thereafter loaded to failure by stepwise increasing a load applied behind the sheet pile wall. The tests provided a case record of deformations, stresses, and pore pressure responses, and failure mechanisms of the structures focusing on the improved soil. These tests showed that column-type ground improvement installed as panels of overlapping columns in the passive zone of a sheet pile wall significantly increases stability and reduces both excavation- and loading-induced structural forces and vertical and horizontal displacements in the soil.

This thesis also presents the results of a laboratory study involving undrained and drained isotropic consolidated triaxial compression, extension and tension tests on laboratory improved clay with a binder of lime-cement similar to that used in the experimental field tests. Based on undrained triaxial test results, a relationship between the undrained strength, effective consolidation stress, and overconsolidation ratio is presented for different stress paths to failure. From the drained triaxial tests it was found that a failure surface comprising of two failure functions, one for tension failure and one for shear failure, similar to that observed for cemented sand, is consistent with the experimental data. Finally, a 3D FE-study of the experimental field tests considering the laboratory observed stress-strain behavior and mobilized strength of lime-cement improved clay was conducted. The results of these analyses are promising and failure load, deformations and structural forces in the retaining structure were predicted reasonably well.

Summarizing the most important findings and conclusions from this study:

- Lime-cement columns panels installed in the passive zone acting as excavation support for a sheet pile wall will significantly increase the stability of the structure.
- Lime-cement column panels installed as excavation support are effective in reducing excavation induced displacements that can be of major concern for deep excavations conducted in areas with soft clay layers.
- The undrained strength of lime-cement improved clay at low consolidation stresses, corresponding to approximately 10 m of depth in field conditions, is dependent of the stress path to failure and it was found to be significantly lower for unloading stress paths compared to lateral loading stress paths, i.e. stress induced anisotropy.

- The Young's Modulus of lime-cement improved clay evaluated from undrained triaxial extension tests was significantly higher, 2.7 to 4.1 times, compared to the corresponding Young's Modulus evaluated from the undrained triaxial compression tests. Also, significantly more brittle stress-strain behaviour was observed for triaxial extension tests compared to triaxial compression tests, regardless of applied stress path to failure and type of test, i.e. undrained/drained.
- Results of the Finite Element analysis of the conducted experimental tests show that the current Swedish Design Guide for lime-cement columns installed in the passive zone overestimates the material undrained strength when based on results from Unconfined Compression tests, but also significantly underestimates the material drained strength. Since the Swedish Design Guide specifies that the lowest of the undrained/drained column strength should be chosen in the design, the consequence is often a too conservative design as the strength increase in the improved clay is not properly considered.

SAMMANFATTNING

Många bebyggda områden runt Sveriges kuster karaktäriseras av postglaciala leror med mycket låg skjuvhållfasthet och hög kompressabilitet. Jordförstärkning med kalkcementpelare (Dry Deep Mixing) används ofta i områden med dåliga grundförhållanden på grund av metodens kostnadseffektivitet, dock i huvudsak för reducering av sättningar och för att öka stabiliteten vid byggnation av bankar. Till följd av ökad byggnation och infrastrukturutveckling finns det ett starkt intresse att öka användningen av kostnadseffektiva metoder såsom djupstabilisering med kalkcementpelare till att i större omfattning förstärka djupa schakter och temporära och permanents slänter där pelarna riskerar bli lateralt belastade eller dragbelastade till följd av en avlastning. Svenska erfarenheter av förstärkning av djupa schakter med kalkcementpelare är begränsade och dagens dimensioneringsmetodik för pelare installerade i passiv zon är mycket restriktiv gällande tillåten hållfasthet i pelarna vilket ofta resulterar i en oekonomisk design.

För att öka metodens användbarhet till att i större grad omfatta ovan nämnda användningsområden behöver materialets hållfasthets och styvhetsegenskaper kunna tillförlitlig beskrivas för de aktuella belastningarna. Huvudsyftet i denna avhandling är att presentera en metod för att adekvat beskriva hållfastheten i kalkcementpelare installerade i passiv zon och att undersöka hållfasthet och styvhetsegenskaper hos lateralt och dragbelastade kalkcementförstärkt lera samt samverkan pelare-jord under dessa belastningsförutsättningar och.

För att undersöka materialens beteende och samverkan pelare-jord för stabilisering av djupa schakter genomfördes inom ramen för denna forskningsstudie två stycken fältförsök. I vart och ett av dessa försök, installerades en stålspont strävad mot en mothållspont som förstärktes med överlappande kalkcement pelarskivor installerade i passiv zon mellan de två sponterna. Avschaktning utfördes till en i förväg bestämd nivå innan konstruktionen drevs till brott genom att stegvis öka belastningen bakom sponten på aktiv sida. Genom dessa tester kunde en omfattande dokumentation insamlas avseende deformationer, spänningar, portrycksrespons och brottmekanism i konstruktionen med fokus på den stabiliserade jorden. Dessa tester visade att kalkcementpelarförstärkning utförd som skivor av överlappande pelare i passiv zonen av en spont signifikant ökade konstruktionens säkerhet mot brott, minskade schakt- och belastningsinducerad laster i stödkonstruktionen och minskade såväl vertikala som horisontella deformationer.

I denna avhandling presenteras också resultat av en omfattande laboratoriestudie som innefattar odränerade och dränerade isotropisk konsoliderade aktiva och passiva triaxialförsök. De passiva triaxialförsöken utfördes under olika spänningsvägar till brott som ska spegla både lateral belastning och avlastning av materialet. Baserad på utförda odränerade triaxialförsök, en relation mellan materialets hållfasthet, konsolideringsspänning och överkonsolideringsgrad presenteras för olika spänningsvägar till brott motsvarande aktiv belastning, lateral belastning och avlastning. Från de dränerade triaxialförsöken konstaterades att beskrivning av materialets brottyta med hjälp av två brottfunktioner, en för dragbrott och en för skjuvbrott, liknande dem som har rapporterats för cementerat sand, stämmer väl överrens med test resultaten. Slutligen, en 3D – Finita Element studie av båda fältförsöken presenteras där den i laboratoriestudien observerade materialbeteendet gällande spännings-töjningssamband och mobiliserbar hållfasthet beaktas. Resultaten av denna studie är lovande och predikterad belastning vid brott, deformationer och storlek på belastningar i spontkonstruktionen stämmer relativt väl överrens med de i fält observerade.

De viktigaste upptäckterna och slutsatserna från denna studie kan summeras enligt:

- Kalkcementpelarskivor installerade i passiv zon som support för en spontkonstruktion kommer att avsevärt öka säkerheten mot stabilitetsbrott i jorden.
- Kalkcementpelarskivor installerade i passiv zon som support för en spontkonstruktion är en effektiv metod att minska schaktinducerade deformationer som kan vara av stor betydelse vid djupa schakter i områden med lös lera.

- Den odränerade hållfastheten hos kalkcement stabiliserad lera vid låga konsolideringsspänningar, motsvarande cirka 10 m djup under markytan, är starkt beroende av valt spänningsväg till brott, dvs. materialet uppvisar spänningsinducerad anisotropi
- Elasticitetsmodulen utvärderad från odränerade passiva triaxialförsök var i storleksordningen 2.7 till 4.1 gånger högre jämfört med motsvarande elasticitetsmodul utvärderad från aktiva odränerade triaxial försök. Också, en signifikant mer spröd spännings-töjningsbeteende erhölls från alla passiva triaxial försök, både odränerade och dränerade, oberoende av valt spänningsväg till brott.
- Finita Element analyser av de utförda fältförsöken visar att den Svenska Dimensioneringsanvisningen för kalkcementpelare installerade i passiv zon dels överskattar materialets odränerade hållfasthet när denna baserar på resultat av Enaxliga Tryckförsök, men också signifikant underskattar den dränerade hållfastheten som kan mobiliseras. Eftersom den Svenska Dimensioneringsanvisningen anger att den lägsta av den odränerade och dränerade hållfastheten i pelaren ska väljas i varje situation blir konsekvensen en alltför konservativ design.

LIST OF PUBLICATIONS

Paper I

Ignat R., Baker S., Larsson S., Liedberg S., 2015, "Two- and three-dimensional analyses of excavation support with rows of dry deep mixing columns", Computers and Geotechnics, Vol. 66, p. 16-30.

Ignat performed the analyses and wrote the paper, supervised and assisted by Baker, Larsson and Liedberg.

Paper II

Ignat, R., Baker, S., Liedberg, S., & Larsson, S. 2016, "Behaviour of braced excavation supported by panels of deep mixing columns", Canadian Geotechnical Journal; Vol. 53(10); p. 1671-1687

Ignat and Baker conducted the experimental tests and analyzed the tests. Ignat wrote the paper. Larsson and Liedberg assisted in planning of the tests and in preparation of the manuscript.

Paper III

Razvan Ignat, Sadek Baker, Martin Holmén and Stefan Larsson, "Triaxial Extension and Tension behavior of lime-cement improved clay", submitted to Soil and Foundations

Ignat and Baker planned and analyzed the tests. Holmén conducted the test and assisted in analyzing of the tests. Ignat and Larsson wrote the manuscript.

Paper IV

Razvan Ignat, Sadek Baker, Minna Karstunen, Sven Liedberg and Stefan Larsson, "Numerical analyses of an experimental full scale excavation supported by panels of lime-cement columns", submitted to Computers and Geotechnics.

Ignat performed the analyses and wrote the paper. Baker and Karstunen assisted in analyzing the results and preparation of the manuscript. Liedberg and Larsson supervised the work and assisted in preparation of the manuscript.

CONTENTS

LIST OF SYMBOLS

Latin letters

a	SHANSEP constant for normalized undrained shear strength
a_q	SHANSEP constant for normalized undrained shear strength of lime-cement improved clay
a_s	Area improvement ratio
b	SHANSEP exponent
c'	Effective cohesion
c'_c	Effective cohesion for compression loading
c'_e	Effective cohesion for extension loading
e_0	Initial void ratio
f_p	Resonant frequency for compression wave
f_s	Resonant frequency for shear wave
q	Deviator stress, $q = \sigma'_1$ - σ'_3
q_f	Deviator stress at failure
q_{peak}	Maximum applied load
q_{fail}	Load at failure
q_y	Yield stress
q_{load}	Applied load
q_t	Unconfined tension strength
q_{ult}	Ultimate load
q_{UC}	Unconfined compression strength
m	Exponent controlling the stress dependency in the Hardening Soil model
n	Porosity of the soil
p_0	Initial absolute pressure corresponding to S_{r0}
p^{ref}	Reference pressure in the Hardening Soil model
p'	Mean effective stress, $p' = (\sigma'_1+\sigma'_2+\sigma'_3)/3$. For triaxial stress state $\sigma'_2=\sigma'_3$
p'_y	Mean effective stress at q_y
p'_{iy}	Isotropic yield stress

$p'_{t\,min}$	Intersection between the tensile failure line and the compression failure line
$p'_{t\,max}$	Intersection between the tensile failure line and the extension failure line
s_u	Undrained shear strength
s_u^C	Undrained shear strength for compression loading
s_u^E	Undrained shear strength for extension loading
s_u^{re}	Remolded undrained shear strength
s_{col}	Center distance between DDM columns
s_{panel}	Center distance between DDM column panels
$s_{u\,clay}$	Undrained shear strength of clay between the DDM column panels
$s_{u\,col}$	Undrained shear strength of DDM columns
$s_{u\,comp}$	Undrained shear strength of the composite soil
$s_{u\,o}$	Undrained shear strength in the overlap zone of DDM columns
$\mathrm{u}_{BP\,100}$	Back pressure required for full sample saturation
u_h	Horizontal displacements
$u_{h\,SPW}$	Horizontal deformation of SPW
w	Water content
w_{col}	Water content of lime-cement improved clay
w_L	Liquid limit
B	Skempton pore pressure coefficient
B_{100}	Skempton pore pressure coefficient at full saturation
BP_{100}	Back pressure at full saturation
C_d	Compressibility of soil skeleton
C_w	Compressibility of water
E_0	Initial elastic modulus
E_{50}	Undrained secant modulus at 50% strength
E'_{50}	Drained secant modulus at 50% strength
$E_{50}^{\prime\,ref}$	Reference elastic modulus at 50% strength in the Hardening-Soil model
E_{oed}^{ref}	Reference oedometer modulus in the Hardening-Soil model
E_{ur}^{ref}	Reference unloading/reloading modulus in the Hardening-Soil model
F_s	Normal force in the struts

G_0	Initial shear modulus (also G_{max})
G_s	Specific gravity
H	Henry's coefficient of air solubility in water
I_1	First invariant of the stress tensor σ'_{ij}, $I_1 = 3p'$ for σ'_2=σ'_3
J_2	Deviatoric stress tensor
K	Bulk modulus
K_0	Lateral earth pressure coefficient
S_r	Degree of saturation
S_{r0}	Initial degree of saturation
S_t	Sensitivity ($S_t = s_u/s_u^{re}$)
T_f	Tensile strength from direct tension test
T_{fd}	Tensile strength from drained triaxial extension tests
V_p	Compression wave velocity
V_s	Shear wave velocity

Greek symbols

Δ	Increment
ε_a	Axial strain
ε_{af}	Axial strain at failure
$\varepsilon_{x\ 2D}$	Horizontal strain in 2D FE-analyses
$\varepsilon_{x\ 3D}$	Horizontal strain in 3D FE-analyses
Δu_h	Incremental horizontal displacements
Δu	Excess pore water pressure
ΔBP	Back pressure increment
Δz	Vertical distance between two inclinometers
$\Delta\sigma_h$	Horizontal stress increment
$\Delta\sigma_{h\ col}$	Horizontal stress increment in the DDM column panel
$\Delta\sigma_{h\ clay}$	Horizontal stress increment in the clay between the DDM column panel
$\Delta\sigma'_{h\ clay}$	Effective horizontal stress increment in the clay between the DDM column panel
$\emptyset'$	Effective friction angle

$\emptyset'_c$	Effective friction angle for compression loading
$\emptyset'_e$	Effective friction angle for extension loading
$u_{h\ SPW}$	Horizontal deformation of SPW
θ	Lode's angle
γ	Shear strain (%)
γ_{col}	Unit weight of lime-cement improved clay
γ_s	Unit weight of soil
γ_w	Unit weight of water
ρ	Mass density
σ'_1	Major principle stress
σ'_2	Intermediate principle stress
σ'_3	Minor principle stress
σ_a	Axial stress in triaxial tests
σ_r	Radial stress (confining stress) in triaxial tests
σ'_c	Effective confining stress
σ'_{qp}	Quasi-preconsolidation stress of lime-cement improved clay
σ'_p	Vertical preconsolidation stress
σ'_v	Vertical effective stress
$\tau_{d\ col}$	Drained shear strength of DDM columns
τ_{mob}	Mobilized shear stress in FE-analyses
τ_{max}	Maximum shear stress in FE-analyses
ν	Poisson's ratio
υ'_{ur}	Poisson's ratio for unloading /reloading

Acronyms

BP	Back pressure
CID	Consolidated drained triaxial test
CIDC	Isotropic consolidated drained triaxial compression test
CIDE-L	Isotropic consolidated drained triaxial extension test (radial loading)
CIDE-U	Isotropic consolidated drained triaxial extension test (axial unloading)

CIU	Consolidated undrained triaxial test
CIUC	Isotropic consolidated undrained triaxial compression test
CIUE-L	Isotropic consolidated undrained triaxial extension test (radial loading)
CIUE-U	Isotropic consolidated undrained triaxial extension test (axial unloading)
CIUE-UL	Isotropic consolidated undrained triaxial extension test (simultaneous axial unloading and radial loading)
CK_0UC	K_0 – consolidated undrained triaxial compression test
CK_0UE	K_0 – consolidated undrained triaxial extension test
CPT	Cone penetration test
CRS	Constant rate of strain oedometer test
DM	Deep Mixing
DDM	Dry Deep Mixing
FFR	Free-free resonance test
FV	Field vane shear test
LCC	Lime cement columns
LDP	Load distribution platform
KPS	Column penetration test
POP	Pre-overburden pressure
OCR	Overconsolidation ratio
SHANSEP	Stress History and Normalized Soil Engineering Properties
SPW	Sheet pile wall
UC	Unconfined compression test

1. INTRODUCTION

1.1 Background

Improving the strength and stiffness properties of soft clays using the deep mixing method, DM, is nowadays a well-established practice in many parts of the world. In Scandinavian countries, the dry deep mixing method, DDM, where a binder, usually of lime and cement, is mixed with the soil, known as "lime-cement columns", is the most common ground improvement method (Larsson 2005). In the DDM method a mixture, usually of powdered lime and/or cement, is mixed in-situ with the soil using compressed air, forming columns of improved soil to depths of, typically in Sweden, 10-25 m. The wet deep mixing method, where slurry, typically of cement, is mixed in situ with the soil, is the leading method in Japan and other Asian countries as well as North and South America and some European countries. The work presented in this thesis is limited to the DDM method using a mixture of dry lime and cement as binder material.

When introduced in the mid-1970s the DM method was initially applied mainly to reduce settlement and improve stability in road/railroad embankments constructed in locations with poor soil conditions. With increasing urban development the DM method's area of use has also been extended to include other applications such as stability of cut slopes, reducing the influence of nearby construction during excavations and support of braced excavations, liquefaction prevention and mitigation, among others (Terashi 2005, Massarsch & Topolnicki 2005, Kitazume & Terashi 2013). In recent years, different ground improvement techniques, above all jet grouting and DM soil-cement columns installed using the wet method, have been applied successfully in deep excavations to reduce settlement and heave displacements related to excavation works, reduce structural loads in the retaining structure, and improve safety against basal heave failure (Tanaka 1993, O'Rourke and O'Donnell 1997, O'Rourke and McGinn 2004 and 2006, Hsieh et al. 2003, Hsi and Yu 2005). Good experience of the use of the DDM method to improve the stability of excavations has been reported from Norway for up to 18 m deep excavations (Karlsrud and Andresen 2008, Karlsrud et al. 2015). In general, the columns are installed between the retaining walls, usually steel sheet pile walls, in a continuous panel configuration, single or double panels formed by overlapping columns. However, Swedish experience related to use of the DM method for excavation support is very limited.

One important reason for very few reported projects where DDM columns are used as excavation support in Sweden is believed to be related to the formulation of the current Swedish design recommendations (TK Geo 13, Larsson 2006). In order to consider previous research that highlighted a lower mobilized strength for DDM columns subjected to lateral loading compared to the material's unconfined compression strength, that is normally used in the design of improved soil, the design guidelines recommend selecting the lowest value of the undrained column's shear strength, $s_{u\,col}$, (determined on the basis of a combination of unconfined compression tests, UC, and field control) and the drained column shear strength, $\tau_{d\,col}$, (determined from a Mohr-Coulomb, MC, failure criterion) in each situation. Furthermore, for DDM columns installed in the passive zone, the drained strength is evaluated based only on the normal stress and friction angle, $\emptyset'$, disregarding the cementation effect expressed as cohesion intercept, c', (assumed equal to zero in the passive zone). These recommendations result in a design where the effect of DDM columns installed as excavation support in passive zones will be very limited and not economical. In order to increase the likelihood of employing ground improvement by means of DDM in applications where the columns are subjected to lateral loading/unloading conditions it is necessary to increase the knowledge regarding the material's behavior in the passive zones of a construction and to advance a design procedure that can adequately predict the strength and stiffness properties of DDM columns in passive zone.

1.2 Previous research

A majority of the research studies emphasizing the mobilized strength and failure mechanisms of laterally loaded DM columns presented in the last 20 years, which include analytical, numerical, and small-scale model tests, focused on laterally loaded columns due to embankment loading. The analytical expressions presented by Kivelö (1998) for calculating the stability of embankments considering the location of single columns relative to the failure surface (active-shear - passive zone) and the loading condition acting on the columns (compression-shear-tension) was the first attempt to address the shear resistance of lime-cement columns that can be mobilized for different failure conditions. Broms (1999a and 1999b) further investigated failure of singular columns and column panels based on the same principles described by Kivelö and also highlighted the possibility of progressive failure by analyzing two real embankment failures. Larsson and Broms (2000) and Larsson et al. (2012) investigated the failure mechanism of lime-cement columns installed in different configurations due to lateral loading by means of small-scale tests conducted in a specially designed shear-box test device. Bearing capacity as well as internal and external stability of a group of columns under embankment loading were investigated by Kitazume et al. (1999 and 2000), Kitazume & Maruyama (2006, 2007) and Nguyen et al. (2016a and 2016b) by means of centrifuge model tests. These studies revealed that a bending failure of the columns due to low tensile strength and a tilting failure pattern in the embankment are the most probable internal and external failure modes, respectively. The main conclusions were that the effect of singular columns to improve the stability of embankments is limited in the shear and passive zones of a failure surface and increasing the column diameter but above all overlapping the columns to form continuous panels significantly increases the bending moment capacity and the factor of safety against shear failure.

The increase in computer capacity and development of numerical computational tools has led to a number of 2D and 3D FE-analyses focusing on failure mechanisms and a difference between the factor of safety predicted by numerical methods and limit equilibrium methods (Han et al. 2005, 2007 and 2010, Huang et al. 2006, Navin and Filz 2006, Larsson et al. 2012, Jamsawang et al. 2015a, 2015b, 2015c and 2016, Nguyen et al. 2016c, Chai et al. 2017 among others). In addition to shear failure, FE-analyses are able to capture failure mechanisms not included in the limit equilibrium slope stability analyses. As a consequence, lower factors of safety are generally predicted by the numerical analyses. Furthermore, for overlapping columns installed in a panel wall configuration Larsson et al. 2012 showed that the overlapping zone between the columns has a significant influence on the failure mechanism. Similar results were presented by Adams (2011) and Adams et al. (2008 and 2009) who investigated the stability of levees supported by deep-mixed shear panels through 2D FE-analyses and showed that the factor of safety for a slip failure is substantially higher for a panel configuration compared to isolated columns at the same area replacement ratio. Based on these studies, Filz et al. (2011) have presented a simplified analytical solution for calculation of the safety factor for external and internal stability of levees supported by DM panels of overlapping columns.

FE-studies regarding the effect of soil improvement by means of DM columns in reducing excavation-induced wall displacements and structural forces in the retaining structures have been presented by Khan et al. 2008, Ou et al. 1996, 2008 and 2013, Ruggeri et al. 2014, Liao et al. 2008, Su & Liao 2017. In most of these studies a concept of composite material has been adopted to represent the material properties of the improved soil. Isotropic column strength, normally evaluated from isotropically consolidated triaxial compression tests, CIUC, or unconfined compression tests, UC, is commonly used in practice. However, several researchers (Ou et al. 1996, Su 2009, Liao and Su 2011, Yang et al.2011) have highlighted that isotropic column strength may not represent the actual performance of DM columns in the passive zone. Also, the effect of spatial variation of the strength and stiffness properties and geometric imperfection on the behavior of laterally compressed cement admixed clay column slabs has been investigated by using random FE-analyses (Liu et al. 2015 and Liu et al. 2018, Comodromos et al. 2018). Therefore, strength reduction factors applied on the column strength before the material composite strength is calculated have been introduced in order to consider a lower mobilized strength of laterally loaded columns. A similar approach for both groups of columns

and longitudinal/transversal panels of overlapping columns, based on large simple shear tests on soft clay improved with soil-cement columns, was presented by Sukpunya and Jotisankasa (2016).

The tensile strength of DM columns has been investigated primarily using methods originating from concrete engineering, such as split tension tests, unconfined tension tests or bending tests and a linear relationship between the unconfined tensile strength and the unconfined compression strength, has been reported by Terashi et al. 1980, Kivelö 1998, Koseki et al. 2005, Namikawa & Koseki 2007, Consoli et al. 2009 and 2012 among others. It was found that the relationship between the unconfined tension strength, q_t, and unconfined compression strength, q_{UC}, was independent of the type and amount of binder and also the initial water content of the soil. Generally, a ratio q_t/q_{UC} equal to 0.15 up to values of $q_t \leq 200$ kPa is recommended for the design of cement improved soil subjected to tensile stresses (Kitazume & Terashi 2013).

Very few studies involving triaxial extension tests on lime-cement improved clay have been presented. Åhnberg (2007) performed a series of stress controlled undrained extension tests in a conventional triaxial cell by increasing the radial stress, σ_r, while keeping the axial stress, σ_a, at a constant level. Åhnberg concluded that the influence of a quasi-preconsolidation stress could be observed in the extension tests and evaluated effective stress parameters that were largely similar to those evaluated from triaxial compression tests.

1.3 Research Objectives

This project aims at increasing the knowledge regarding the behavior of lime-cement DDM columns installed in the passive zone and to present a method to adequately predict the strength and stiffness properties of DDM columns acting as excavation support for a retaining structure.

First, the field behavior of overlapping panels of lime-cement columns installed in the passive zone of a sheet pile wall was investigated with a focus on excavation and lateral loading induced propagation of stresses and deformations in the DDM column panels, in the clay between the panels, and also in the steel structures. Two full-scale tests, where only the area improvement ratio, a_s, of the improved soil was varied between the two tests, were conducted in order to document the effect of DDM column panels as excavation support. To enhance understanding of how the strength of DDM columns is mobilized in a passive zone, a series of consolidated undrained and drained triaxial extension tests on laboratory-mixed lime-cement stabilized soft clay was conducted under various stress paths to failure. The aim of these laboratory tests was to investigate the material's behavior under loading conditions essentially similar to those expected for DDM columns used as excavation support and to present an adequate method for assessment of the mobilized column strength for these stress conditions. The proposed methodology for DDM columns is then validated by performing FE-analyses of the field tests and the results are compared with the experimental data and also with FE-results predicted by using the current Swedish design guide for determining the columns' strength and stiffness properties.

1.4 Outline of Thesis

This thesis consists of an introductory part and four appended papers, two published in peer-reviewed journals and two submitted journal papers. The introductory part, presenting background information and summary of previously conducted research and motivation of the conducted research study, is intended to act as complement to the appended papers.

Chapter 2 presents the results of an FE-study, described in Paper I, with the objective to investigate if a simplified 2D model can accurately predict the ultimate limit state behavior of an excavation with a tied back sheet pile wall supported with perpendicular panels of overlapping DDM columns compared to a 3D model with a focus on failure load, failure mechanism, and stress-strain relationship.

Chapter 3 presents the set-up and results of two instrumented full-scale tests of a braced sheet pile wall supported by panels of overlapping DDM columns that was first excavated then loaded to failure. The objective of these tests was to provide a first case record of deformations, stresses, and pore pressures responses, and also failure mechanisms of lime-cement improved clay in the passive zone. The tests are comprehensively described in Paper II and this chapter summarizes the test set-ups and provides additional photographs and results that are not included in the papers.

Chapter 4 summarizes the results from laboratory tests conducted on lime-cement improved clay, presented in paper III. The aim of these tests is to enhance understanding of how the strength of lime-cement improved clay is mobilized in the passive zone.

Chapter 5 is an FE-study of the conducted full-scale tests where the mobilized strength and the stress-strain behavior of lime-cement improved clay observed from the triaxial extension tests are considered in the analysis. This study is also presented in Paper IV.

Chapter 6 contains a summary of the appended papers.

Chapter 7 summarizes the main conclusions from this study and gives suggestions for future work related to this study.

1.5 Limitations

Some of the limitations associated with this study can be summarized as follows:

1.5.1 Full-scale tests

The main aim of these tests was to investigate the behavior of the DDM column panels acting as excavation support. The geometrical layout of the tests was therefore chosen with the intension to achieve a controlled failure of the retaining system (sheet pile wall and DDM column panels) in view of the geotechnical conditions at the test site. One important limitation is therefore related to the imposed test conditions, particularly the depth of the excavation prior to loading to failure and the number of bracing levels. The test configuration with one in advance predetermined excavation depth was limited by the thickness of the soft clay layer at the test location. Due to limited excavation depth only one bracing level was installed, with the purpose of inducing a highest possible lateral stress increase in the DDM column panels below the excavation.

Also, in addition to the two tests performed and presented in this study, a similar experimental braced excavation without panels of DDM columns acting as support of the sheet pile wall, i.e. a reference test, could not be conducted within the margin of this project. Even though the behavior of the excavation without panels of DDM columns could be studied through FE-analyses, presented in

Chapter 5, a reference excavation without the support of DDM column panels at the same location would have provided valuable additional information.

Another limitation is the geotechnical conditions at the test site. The presence of strikes of sulfide bearing clay to a depth of approximately 5 m below the ground surface has an important role in the gain in strength and stiffness properties of the improved clay and resulted also in DDM columns of relatively low strength in this clay layer. It is very likely that a similar field test conducted at a site with homogenous clay characteristics would have resulted in DDM columns of higher strength and stiffness.

1.5.2 Laboratory tests

The tests conducted in this study were performed only on laboratory-mixed samples from the clay collected at the test site and no tests were performed on DDM field samples. Although the type, amount and ratio of the binders used in the laboratory tests was chosen similar to that used for the DDM columns in the experimental full-scale tests, the laboratory-mixed samples are generally expected to be more homogeneous compared to in situ DDM columns. The effect of "poor" mixing on the tensile strength of in situ DDM columns needs to be investigated in future work.

Furthermore, due to limitation in the number of triaxial testing equipment available, additional tests with the purpose to study the triaxial extension and tension behavior for different types of clays and different type/amount of binder could not be performed within the margin of this project.

2. 2D AND 3D NUMERICAL ANALYSES OF LATERALLY LOADED PANELS OF DRY DEEP MIXING COLUMNS

2.1 Background and Study Objective

As part of the planning and preparation of the full-scale tests, a numerical study involving an excavation followed by loading to failure of a sheet pile wall supported by panels of overlapping lime-cement columns was conducted. Several research studies concerning reported case histories and numerical studies of excavations of retaining structures supported by deep mixing columns (Tanaka 1993, O'Rourke & O'Donell 1997, O'Rourke and McGinn 2004 and 2006, Ou et al. 1996, 2008 and 2013, Hsieh et al. 2003) or by means of short slabs of jet grouting columns below the excavation (Hsi and Yu 2005, Ho and Hu 2006, Yang et al. 2011) have been presented in recent years. In the majority of these studies, 2D plane strain numerical analyses have been used for simplicity and to reduce the computational time of complex problems. The DM columns and the soil in between are thereby modeled as an ideal composite material with weighted strength and stiffness properties, regardless of the actual column configurations, including group columns, panels of overlapping columns or block type improvement (often in the case of jet grouting slabs below the excavation base). However, excavation and loading of a sheet pile wall, SPW, where the soil on the passive side of the wall is improved by means of panels of deep mixing columns installed perpendicular to the direction of the SPW is a three-dimensional mechanical system in which the retaining structure, the column panels and the soft soil between the panels interact.

When columns are overlapped in order to form continuous panels, grids or block type improvement, the overlap zone between columns could have a significant effect on both internal and external failure mechanisms. In addition to failure mechanisms of single columns, vertical internal shear failures in the overlap zone and extrusion of the soft clay between the panels (Terashi et al. 1983, Adams 2009, Larsson et al. 2012, Kitazume and Terashi 2013) also need to be considered in the design of DM column panels. Aside from the distance between the column panels and distance between the columns within the panel, q_{UC} in the overlapping zone between the columns is also believed to be of substantial importance for the behavior of laterally loaded DM columns. Tests performed by Yoshida (1996) and Yoshizawa et al. (1997) on cores extracted from overlapping DM columns indicate that q_{UC} in the overlap zone is usually lower compared to that obtained in the center of the columns and decreases with increasing time of installation of adjacent columns.

It has not yet been clarified whether the 3D behavior of DDM panels installed as excavation support can be adequately described by an idealized composite material regarding the mobilized strength, failure mechanisms, and predicted deformations. The scope of these FE-analyses was to investigate the ability of a composite soil model, commonly employed in a 2D plane strain model, to accurately predict the 3D behavior of panels of overlapping DDM columns subjected to lateral loading regarding failure load, failure mechanism, stress-strain relationship, and deformations up to failure load. In order to investigate the effect of lower strength and stiffness properties in the overlap zone, a method to model the vertical overlap between the columns in a 2D plane strain model is introduced. The effect of different spacing between the column panels, s_{panel}, center distance between columns in each panel, s_{col}, and the strength and stiffness properties of the overlapping zone between the columns was investigated in this study.

2.2 Geometrical Model and Analyses Set-up

A brief presentation of the geometrical model, analyses set-up and some clarifications are presented here. Material properties of the soil, DDM columns and retaining structure, and also model boundary conditions are presented in detail in Paper I.

At the time this study was conducted only an overall site investigation and no laboratory test had been performed at the location of the yet to come full-scale test. Chosen material properties of the soft clay and DDM columns and also geometrical layout were therefore not fully consistent with the laboratory test results and geometrical layout of the field tests conducted later. The strength and stiffness parameters chosen for the soft clay and columns are typical for DDM projects in Sweden while the properties of the structural elements (sheet pile, anchors, wale beam) were chosen as typical for construction projects involving excavation works.

The analysis with the improved clay modeled as two separate materials, panels of overlapping columns and soft clay between the panels are hereafter referred to as 3D model, and the analysis with the improved clay modeled as a composite soil volume are hereafter referred to as 2D model. However, both type of analysis were performed with the finite element program PLAXIS 3D 2012 in order to eliminate possible sources of uncertainty related to the two principal geometrical problems. The analysis was performed as an undrained effective stress analysis with undrained strength parameters since the excavation and the loading were executed rapidly and the consolidation process is thus very limited. The soil profile was assumed to consist of a 1 m thick layer of dry crust on top of a 10.5 m thick layer of normally consolidated soft clay over a stiff bearing stratum of frictional soil. The groundwater table was set at the top of the soft clay, 1 m below the ground surface. The vertical model boundaries parallel to the yz plane were fixed in the x direction and free in the y and z directions while vertical model boundaries parallel to the xz plane were fixed in the y direction and free in the x and z directions. The model bottom condition was chosen fixed in all directions while the ground surface was free in all directions. In order to avoid boundary effects, the width of the model was chosen to be 35 m and the unexcavated side was chosen to be 20 m from the side boundary of the model. The length of the excavation was chosen, due to symmetrical effects, to be 3 m, presented in Fig. 2-1a.

In the 3D model, the DDM column panels and the soil between the panels were modeled as two separate materials, shown in Fig. 2-1b. The “volume pile” technique was used for the overlapping DDM column panels installed perpendicular to the SPW. A large number of overlapping cylindrical volumes requires a very large number of elements, resulting in mesh generation problems. Each column was therefore modeled with an octagonal prism shape and cross-sectional area equal to that of columns with a diameter of 0.6 m. The column panels in the model extended 7.0-7.2 m (depending on the actual overlap width) from the SPW and the columns were installed to a depth of 10 m, floating type improvement, starting from the top of the soft clay. A floating type ground improvement was considered to be more representative of Scandinavian conditions compared to the case where the columns penetrate the stiff frictional soil, as the typical mixing tools for installation of DDM columns (Larsson 2005) are not designed to penetrate stiff bearing strata below the clay unless special actions like predrilling of the stiff soil are taken. Due to a floating type ground improvement analyzed in this study, the stiff frictional soil below the soft clay was not believed to influence the failure mechanism of the column panels and was therefore not included in the model.

In the 2D model, the DDM column panels and soft clay between the panels were represented by a composite soil. The overlapping zone between the columns in the panels was considered by defining vertical joints as illustrated in Fig 2-1c. The material properties of the composite soil volume were calculated based on the area ratio, a_s, of the columns and the overlap zones, respectively.

The length of the SPW below the ground surface, 7.0 m, and the bracing system, horizontal steel wire anchors located 1 m below the ground surface and a center-to-center spacing of 3 m, were chosen with the purpose to induce a rotational stability failure of the structure. The analyses were performed by defining calculation phases in order to model the stage excavation inside a braced SPW followed by a loading procedure until failure. The excavation was performed in two steps to a final excavation depth

of 4 m below the ground surface, before a uniformly distributed surface load, q_{load}, was applied behind the SPW. The load was thereafter stepwise increased in constant increments of 10 kN/m^2 until a failure collapse mechanism was reached. By increasing q_{load} behind the SPW increasing lateral stresses are also induced in the column panels due to mobilization of passive earth pressure in the improved soil below the excavation level. By adopting this procedure the gradual development of the emerging failure mechanism and the stress-strain behavior in the column panels subjected to lateral loading until failure could be analyzed.

The effect of s_{panel} and s_{col}, i.e. the width of the overlapping zone, and the effect of reduced strength and stiffness properties of the overlapping zone was investigated by varying these parameters according to Table 2-1.

Table 2-1: Varied parameters of conducted 2D and 3D FE- analyses

Center-to-center spacing between panels, s_{panel} (m)	Column center-to-center spacing in the panel, s_{col} (m)	Reduction of strength and stiffness properties of overlapping zone (%)
1.0	0.6 (tangential columns)	-
1.5	0.5	0/50/75
3.0	0.4	0/50/75

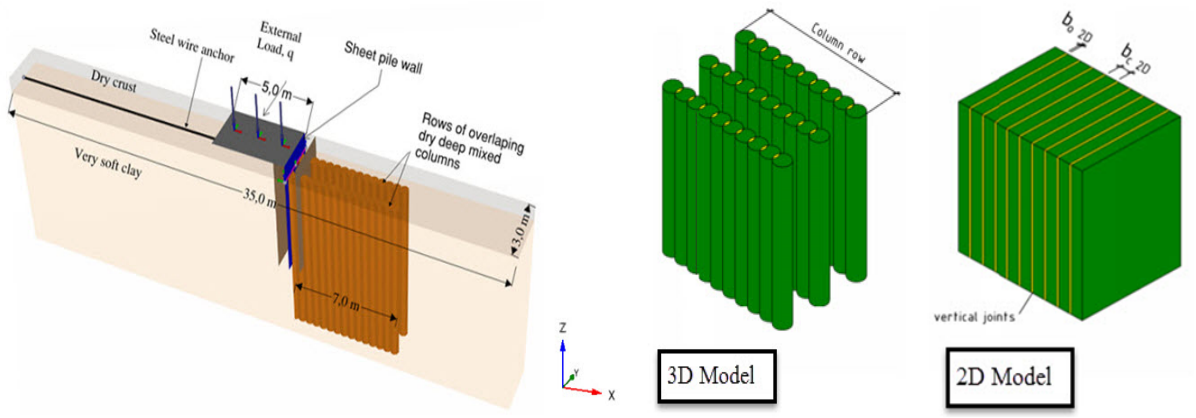

(a) *(b)* *(c)*

Fig. 2-1: Geometric model of FE-analyses
(a) 3D model geometry
(b) Row of overlapping columns; 3D model
(c) Composite material with vertical joints representing column overlap; 2D model

2.3 Analysis Results

Here, only selected results and conclusions obtained from this study are presented, and for full results, analyses and discussion the reader is referred to the appended paper (Paper I).

2.3.1 Predicted ultimate load and failure mechanism

In general, the 2D model can predict an ultimate load, q_{ult}, (evaluation of the ultimate load is described in detail in Paper I) that agrees reasonably well with the corresponding "3D" analyses regardless of s_{panel} and s_{col} for full overlap strength, presented in Table 2-2. The ratio between the mobilized shear stress and the maximum shear stress, τ_{mob}/τ_{max}, at 25, 50, 75, and 100% of q_{ult}, presented in Fig. 2-2 for s_{panel}=1.5 m, shows the development of the failure mechanism in the DDM column panels and the composite soil. The results clearly indicate that the failure mechanism in the panel is initiated by a vertical shear failure in the overlapping zone in the DDM column panel closest to the SPW as also reported by Adams (2011) and Larsson et al. (2012). By introducing vertical joints in the composite soil volume, the 2D model can predict the load-induced shear stress in the column panels during the initial loading stages. However, in the 3D model, the applied load is transferred mainly to the column rows due to the large stiffness difference between the soft soil and the columns at the interface with the SPW. In the 2D case, where the soft soil and the column panels are replaced with a composite soil volume, the stress increment is instead evenly distributed due to idealization of the material properties and stress concentration in the column panels is therefore not considered. As a consequence, even though $s_{u,col}$ is higher than the shear strength of the composite soil, $s_{u\,comp}$, τ_{mob}/τ_{max} in the columns in the 3D model is significantly higher than in the 2D composite soil volume at q_{ult}. This implies that at q_{ult}, the yielding criterion has been reached in more parts of the columns than in the composite soil volume.

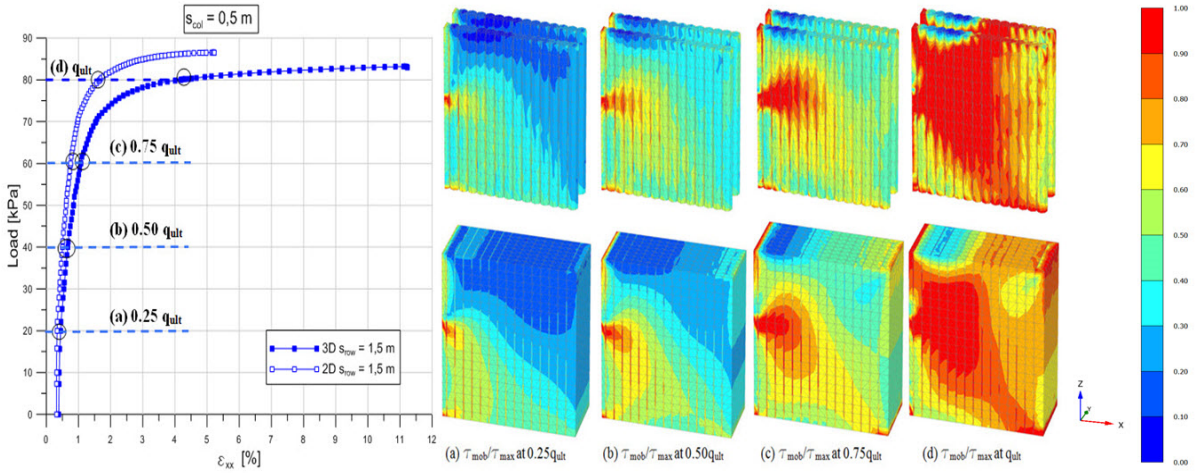

Fig. 2-2: Load-strain curve of 3D and 2D analyses with s_{panel} = 1.5 m and s_{col}= 0.5 m. Snapshots of ratio between mobilized shear stress and maximum shear stress at 25, 50, 75 and 100% of q_{ult}.

Table 2-2: Ratio of predicted ultimate load between 2D and 3D analyses

s_{panel} (m)	Reduction of shear strength in overlap zone (%)	s_{col} (m)	
		0.5 $q_{ult\ 3D}/q_{ult\ 2D}$	0.4 $q_{ult\ 3D}/q_{ult\ 2D}$
1.0	0	(1.00*)	(1.00*)
1.5		0.96	0.95
3.0		0.94	0.94
1.0	50	1.00	1.00
1.5		1.00	0.99
3.0		0.98	0.93
1.0		1.07	1.15
1.5	75	1.04	1.05
3.0		1.00	0.79

**For s_{panel} =1.0 m and full overlapp strength the failure mechanism predicted was a bearing capacity failure below the applied load on the active side of the SPW.*

Similar results are obtained if the reduction of strength and stiffness properties in the overlap zone between the columns is 50% of the column strength and stiffness properties, presented in Table 2-2. However, for a very poor overlap quality, 75% reduction of overlap strength combined with increased s_{col} to 0.2 m, the 2D model generally predicts significantly lower q_{ult} for a high a_s (s_{panel} =1.0 m) respectively significantly higher q_{ult} for a low a_s (s_{panel} =3.0 m) compared to the 3D model.

2.3.2 Predicted deformations

Regarding full overlap strength, the 2D analyses underestimated both the deformation in the improved soil and the displacement of the SPW compared to the deformation predicted by the 3D analyses. The ratio between the 3D and 2D predicted horizontal strain in the improved soil beneath the excavation at the same load level is shown in Fig. 2-3a and the horizontal displacement in the SPW is shown in Fig. 2-3b. The horizontal strain ratio, $\varepsilon_{x\ 3D}/\varepsilon_{x\ 2D}$, between the 3D and 2D analyses as a function of q_{load} is presented up to the level $q_{load} = q_{ult}$. Presented $\varepsilon_{x\ 3D}/\varepsilon_{x\ 2D}$ is located 0.5 m inside the excavation pit (the center of the second column in the 3D analyses) and 3 m below the bottom of the excavation (bottom of the sheet pile wall). After the excavation and before the load is applied, there is no significant difference regarding s_{panel}. After the load is applied, $\varepsilon_{x\ 3D}/\varepsilon_{x2D}$ increases at first almost linearly in all studied cases. In all cases there is a distinct non-linear increase in $\varepsilon_{x\ 3D}/\varepsilon_{x2D}$ when q_{load} exceeds 65-90% of the evaluated q_{ult}.

When the strength and stiffness properties of the column overlap are reduced, the results of predicted strains and deformation of the SPW show different trends in the 2D and 3D analyses, illustrated in Fig. 2-4. For a high a_s, s_{panel}= 1.0 m, $\varepsilon_{x\ 3D}/\varepsilon_{x2D}$ is constant until approximately 80-90 % of q_{ult} is reached, Fig 2-4a. Above this load level, $\varepsilon_{x\ 3D}/\varepsilon_{x2D}$ increases as q_{load} is further increased for an overlap strength equal to the column strength ($s_{u\ o} = s_{u\ col}$), but $\varepsilon_{x\ 3D}/\varepsilon_{x2D}$ decreases as the overlap strength is reduced. The results also show that for an equal reduction in overlap strength, $\varepsilon_{x\ 3D}/\varepsilon_{x2D}$ decreases faster when the overlap area is increased (s_{col} decreases). For a low a_s, $s_{panel} = 3.0$ m, the overall trend is that $\varepsilon_{x\ 3D}/\varepsilon_{x2D}$ increases when q_{load} is increased, i.e. the 3D analysis predicts larger strains at q_{ult} regardless of overlap strength, Fig. 2-4b.

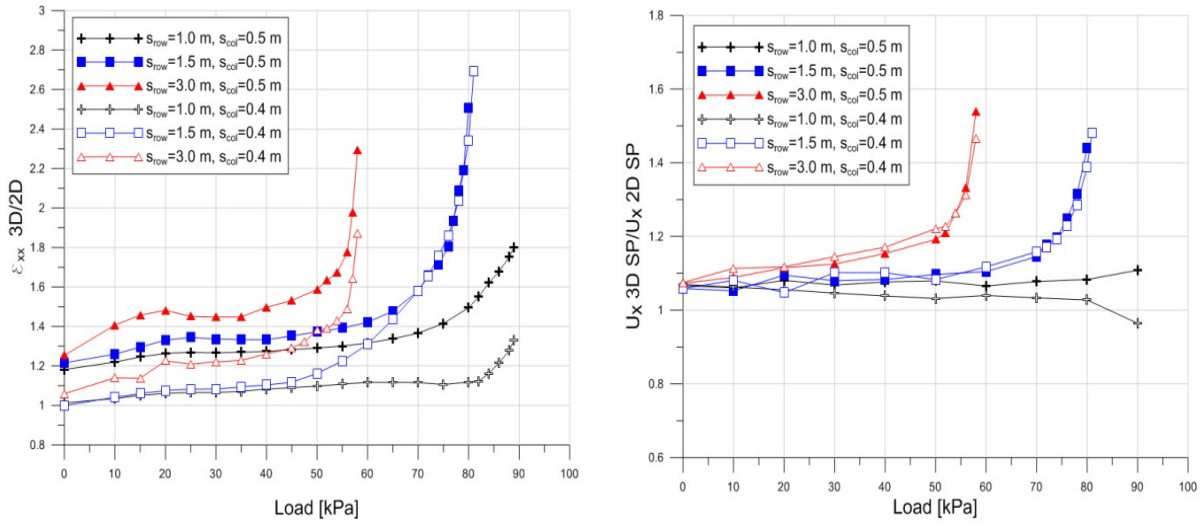

(a) *(b)*

Fig. 2-3: Results of calculated deformations for full overlap strength
(a) Horizontal strain ratio, $\varepsilon_{x\,3D}/\varepsilon_{x\,2D}$,
(b) Ratio between the maximum horizontal deformations of the sheet pile wall

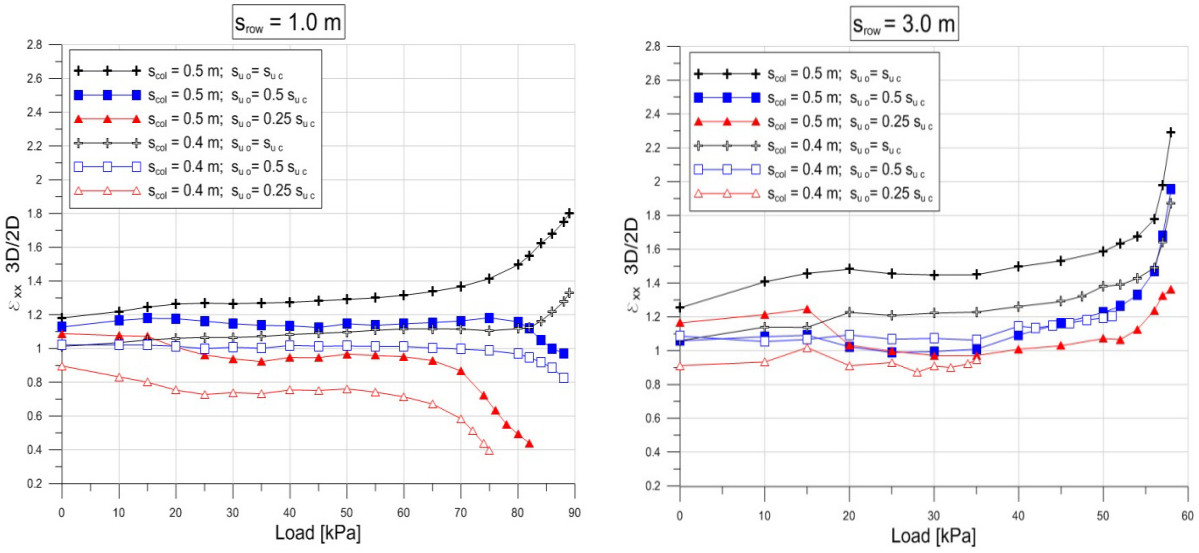

(a) *(b)*

Fig. 2-4: Results of calculated deformations for reduced overlap strength
(a) Horizontal strain ratio, $\varepsilon_{x\,3D}/\varepsilon_{x\,2D}$, s_{panel}= 1.0 m
(b) Horizontal strain ratio, $\varepsilon_{x\,3D}/\varepsilon_{x\,2D}$, s_{panel}= 3.0 m

2.4 Summary

The most important findings of this study can be summarized as follows:

- Regarding full overlap strength, there is good agreement between ultimate load predicted by the 2D and 3D analyses, regardless of spacing between the panels or overlap width. However for or a very poor overlap quality, 75% reduction of overlap strength, the 2D model generally predicts a lower ultimate load for a high area improvement ratio and a significantly higher ultimate load for a low area improvement ratio compared to a 3D model.
- By taking into consideration the effect of the overlap zone between columns installed in a row pattern, a 2D plane strain model shows reasonably good agreement regarding obtained deformations compared to a 3D model, as long as the stress level in large parts of the stabilized soil does not reach the stated yielding criteria.
- The area improvement ratio has a significant influence on how well the prediction of calculated deformations agrees between the two models. In addition to the area replacement ratio, the quality of the overlap zone between columns impacts strongly on the predicted deformation but also the predicted ultimate load and the failure mechanism that occurs.

3. FIELD TESTS OF BRACED EXCAVATION SUPPORTED BY PANELS OF DRY DEEP MIXING COLUMNS

3.1 Background and Study Objective

This study includes two experimental full-scale tests, performed during the spring-summer period of 2014. In these tests a braced SPW was excavated and thereafter loaded to failure. The clay was improved in both cases on the excavation side with panels of overlapping DDM columns. Both tests were extensively instrumented, which made it possible to follow the propagation of stresses and deformations in the clay, in the DDM column panels, and also in the steel structures. This is the first time the pre- and post-failure behavior of a column type ground improvement supported excavation has been documented in an instrumented full-scale test. The objective of these tests was to provide a case record of deformations, stresses, and pore water pressure responses, and also failure mechanisms of the structures with a focus on the improved soil. The test layout, test execution and tests results are described in detail in Paper II and are only briefly presented here.

3.2 General Site Description and Geotechnical Conditions

The full-scale tests were performed in the eastern part of Sweden, about 70 km northwest of Stockholm in the proximity of the city of Enköping. The site chosen for the tests is an unexploited open field with an area of about100 x 200 m situated approximately 100-120 m north of the Enköping creek. The area is relatively flat, with an elevation above sea level at the site that varies between +5.9 and +6.2 m. Both test areas, with dimensions of about 20 x 30 m, were located in the south central part of the site where the greatest thickness of the soft clay layer occurred, about 35 m from each other.

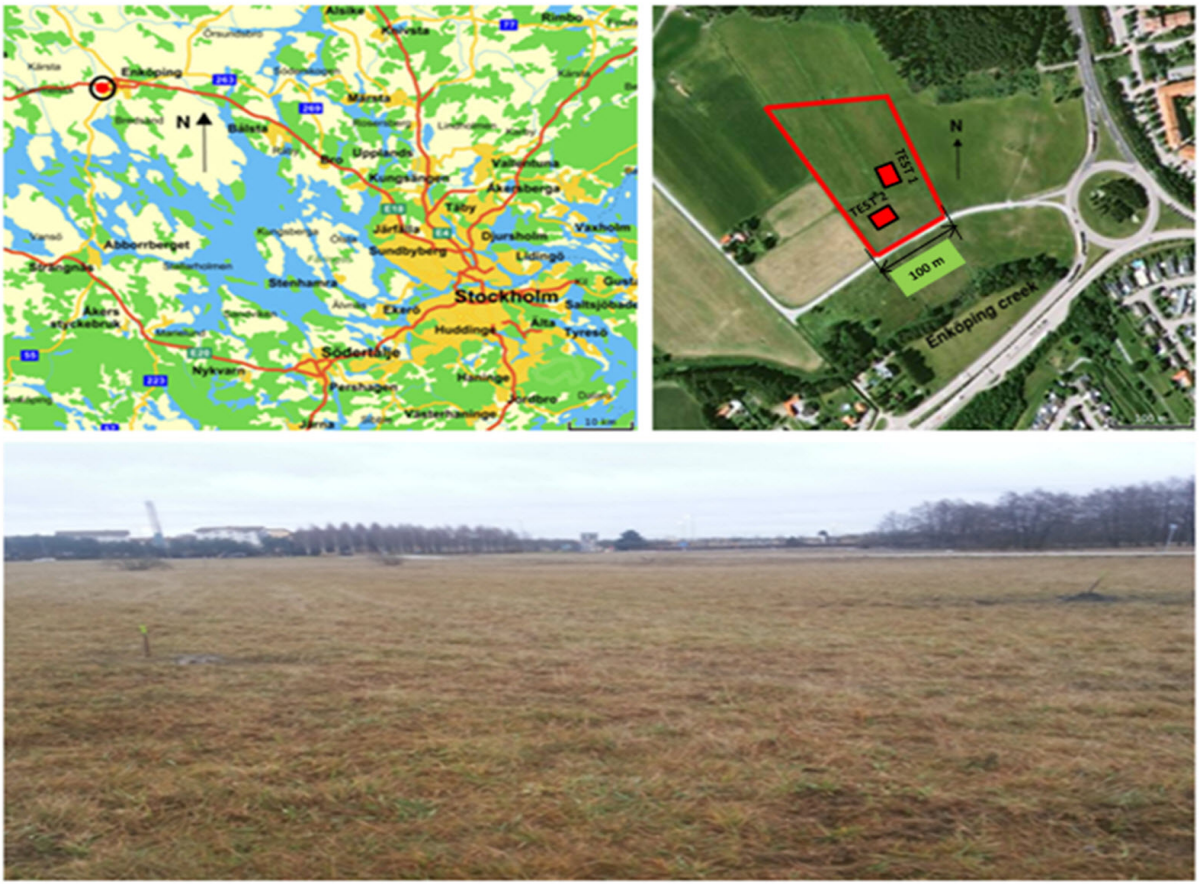

Fig. 3-1: Location of the test site

An extensive soil investigation program, described in Paper II, was conducted prior to the experiment to characterize the soil conditions within each test site. The soil conditions at the two test sites were very similar and the stratigraphy can be summarized as follows: a 1.2-1.5 m thick layer of dry crust followed by a soft post-glacial clay layer with a thickness of 7-9 m. Beneath the clay there is a 3-7 m thick layer of sand which overlays a layer of very stiff till closest to the bedrock, which was located at a depth of 14-20 m below the ground surface.

The general characteristics of the clay at the two test locations are presented in Fig. 3-2. Down to a depth of approximately 5-5.5 m below the ground surface lenses of sulfide bearing clay exist and the clay has a water content, w, of 80-90% and a liquid limit, w_L, of 67-81%. The clay layer below this depth was classified as banded silty clay with a significantly lower w and w_L, 55-70% and 40-53%, respectively and unit weight, γ_s, increasing with depth. The vertical preconsolidation pressure, σ_p', evaluated from constant rate of strain oedometer tests, CRS tests, specifies that the clay is lightly overconsolidated with an OCR of about 1.5 and 1.2 at 5 and 7 m depth, respectively. The undrained shear strength of the clay, s_u, determined from site field vane shear tests, FV, and CPT tests was 9-11 kPa from the top of the soft clay layer to a level of about 4 m below the ground surface and an average strength increase of about 1.1 kPa/m below this level. From conducted fall cone tests the remolded shear strength, s_u^{re}, was measured to be in the order of 0.75 - 0.26 kPa. The sensitivity of the clay, S_t, increased with depth from about 20 at 2 m depth to 50 at 7 m depth, and was classified as highly sensitive below 5 m depth, S_t >30.

In general, s_u of soft Scandinavian clays is dependent on the stress path followed during undrained shearing, i.e. stress-induced anisotropy, (Bjerrum 1973, Larsson 1977, Länsivaara 1999, Karstunen et al. 2005, Karlsrud and Hernandez-Martinez 2013, Koskinen 2014, D'Ignazio 2016). The anisotropy of the clay at the test site was investigated by anisotropic (K_0) consolidated undrained compression and extension triaxial tests, CK_0UC and CK_0UE, conducted on undisturbed clay samples collected from depths of 5 and 7 m, Ignat (2015). Selected results of the tests, illustrated as the shear stress normalized by vertical consolidation stress, σ_v', versus axial strain, and normalized effective stress paths in meridian stress space are presented in Fig. 3-3.

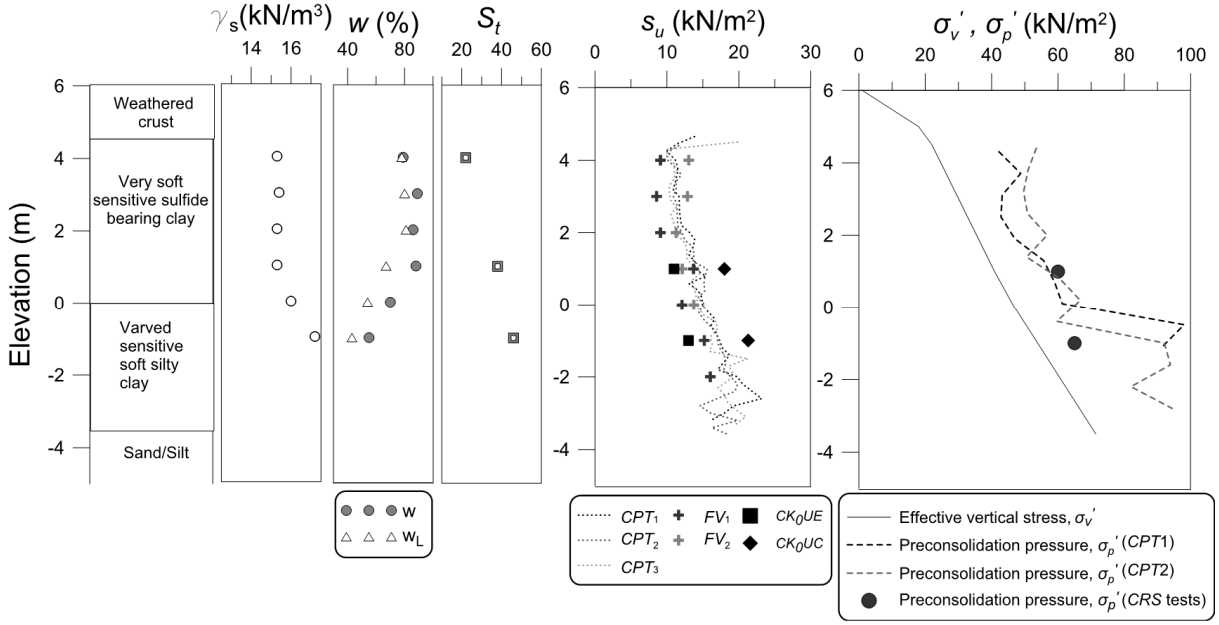

Fig. 3-2: Basic material properties of soft clay at the Enköping test site

The clay at the test site exhibits anisotropic s_u but also significant reduction of s_u with further straining after reaching a peak value (Fig. 3-3a), i.e. strain softening, was observed in the CK_0UC tests, a behavior characteristic of very sensitive soft clays (Thakur 2007, Gylland et al. 2014). The results of s_u normalized by σ_v', as a function of OCR are presented in Fig. 3-4, together with established empirical relationships of s_u anisotropy for Scandinavian clays (Larsson et al. 2007, Fig. 3-4a and Karlsrud and Hernandez-Martinez 2013, Fig. 3-4b) derived from the SHANSEP methodology presented by Ladd & Foot (1974). The anisotropy ratio defined as the ratio between s_u from triaxial extension and compression tests, s_u^E/s_u^C, varied between 0.66 and 0.75, values that are in line with previously presented results for Scandinavian clay (Larsson 1977) and also other soft clays (Mayne 1985, Ladd 1991, Tanaka et al. 2001, Won 2013).

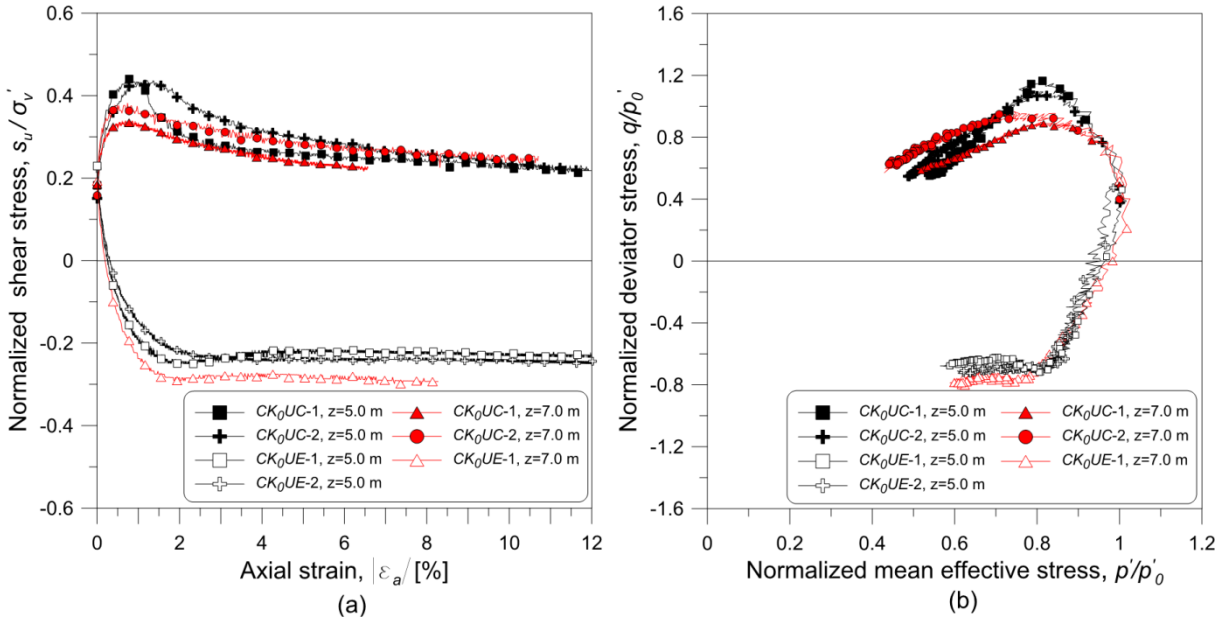

Fig. 3-3: Results of anisotropic (K_0) consolidated undrained triaxial tests on soft clay: (a) Normalized stress-strain behavior; (b) Normalized effective stress paths

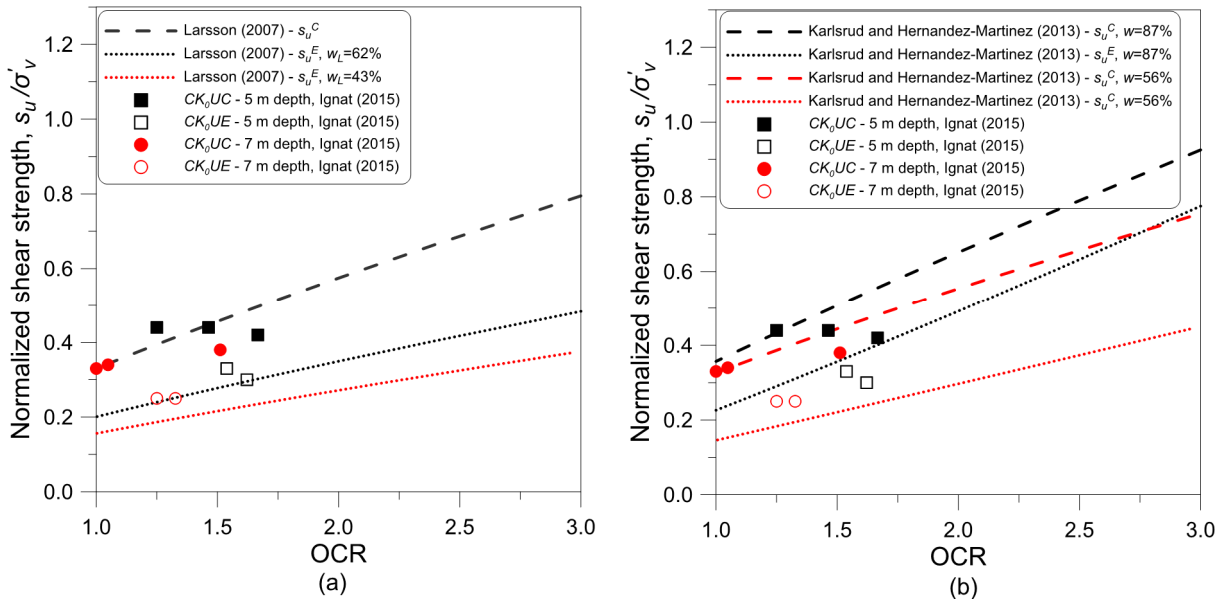

Fig. 3-4: Measured peak normalized shear strength versus OCR and empirical relationship for Scandinavian clays.

3.3 Test Description

The choice of geometrical layout of the full-scale tests, illustrated in Fig. 3-5, was largely governed by the soil conditions at the test site such as area size with similar stratification and thickness of the soft clay. Except for the center to center spacing between the DDM column panels, s_{panel}, chosen to be 3.0 m in Test A and 1.5 m in Test B, all other geometrical and material parameters of the retaining structure were designed as identical. A similar construction sequence, as described in Table 3-1 and illustrated in Fig. 3-6, was adopted in both tests. In Test A, s_{panel}=3.0 m, a failure emerged about 10 h after the loading process started. In Test B, s_{panel}=1.5 m, a failure emerged about 50 h after the loading process started. Following an initial loading process with duration of approximately 30 hours, an additional excavation of 0.5 m was conducted after partial unloading of the containers. The structure was thereafter monitored for a period of 14 h before the load was again increased in one step and brought to failure.

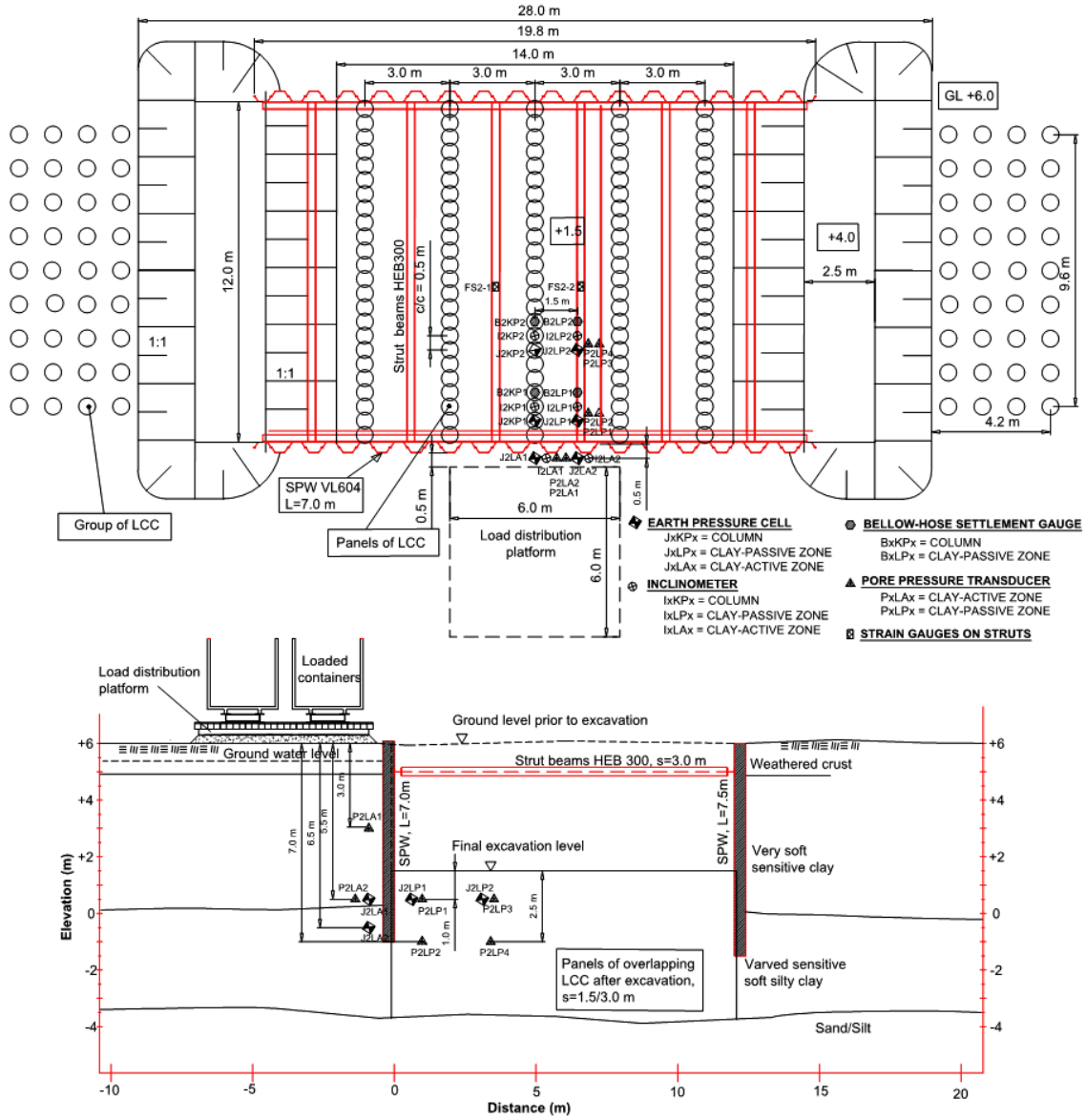

Fig 3-5: Test layout and location of conducted instrumentation

(a) *(b)*

(c) *(d)*

(e) *(f)*

Fig. 3-6: Full-scale tests. (a) Installation of DDM column panels. (b) Installation of SPW. (c) First excavation stage. (d) Final excavation stage. (e) Construction of LDP and placing of containers. (f) Ongoing loading to failure.

Table 3-1: Construction sequence of the experimental tests

Stage	Detail	Elapsed time Test A (days)	Elapsed time Test B (days)
1	Installation of DDM column panels	1	1
2	Installation of the SPW	1	1
3	Installation of group DDM columns	2	2
4	Excavation to level +4.0	22-24	24-28
5	Installation of the strut system	25-29	31-35
6	Excavation to level +2.0	30-31	-
7	Excavation to level +1.5	35	43*
8	Construction of stiff load distribution platform, LDP, 6×6 m, positioned 0.5 m from the sheet pile wall	35	44
9	Stepwise increased load - applied by filling two containers (L x B x H=6.3 x 2.6 x 2.5 m) with soil material, start of loading at t=0.	36 (failure at t=9:55 h after start of loading)	49-50
10	Unloading and additional excavation to level +1.0	-	50
11	Stepwise increased load	-	51 (failure at t=49:50 h after start of loading)

**Stages 6 and 7 were conducted simultaneously in Test B*

3.4 DDM Column Installation Procedure and Quality Control

The columns were manufactured using the Scandinavian dry deep mixing method, (CEN 2005). A binder content of 120 kg/m^3, 50% quicklime, QL 0-0.1 KÖ, and 50% Portland cement, CEM II/A-LL 42.5 R was used in both tests. Each panel of overlapping columns, 5 panels in Test A and 9 panels in Test B, consisted of 24 columns with a diameter of 0.6 m and a center-to-center spacing of 0.5 m giving an improvement ratio, a_s, of 17.5% for Test A and 35% for Test B. The columns were installed with a rotational speed of the mixing tool of 175 rev/min and a retrieval rate of 20 mm/rev and were installed before the installation of the SPWs. In order to ensure connection between the SPWs and the column panels, the SPWs in both test areas were installed 4-12 hours after the installation of the columns close to the center of the last column in each panel, shown in Fig. 3-7. The DDM columns were installed to the frictional soil underneath the soft clay layer, resulting in a column length of between 7.5 and 9.5 m in Test A and 8.0 and 10.4 m in Test B. The group of DDM columns used to improve the stability of the open end slopes were installed in a rectangular pattern with a center-to-center spacing of 1.2 m to a depth of 6.5 m below the ground surface.

Quality control of the DDM columns was performed 10-12 days after installation by means of the column penetration test, KPS, the most frequently used test method in Sweden (Axelsson and Larsson 2003, Bergman et al. 2013). In each panel, one KPS test was performed according to the Swedish design guideline, TK Geo 13 (2014) and Larsson (2006). Pre-drilling in the center of the DDM column was conducted in order to facilitate the verticality of the KPS probe. The KPS probe was attached to a CPT (cone penetration test), allowing bar friction to be differentiated from the penetration resistance. Evaluated undrained column shear strength, $s_{u\,col}$, is presented in Fig. 3-8. Although the variability in strength measured between individual columns was large, the average $s_{u\,col}$ evaluated in Test A and Test B were very similar. A relatively low average $s_{u\,col}$, ranging between 100 and 200 kPa, was evaluated in the sulfide bearing clay with the lowest values obtained between 3 and 4 m of depth in both test areas. Below this depth the average $s_{u\,col}$ increases and values above 300 kPa were evaluated in the silty clay below 7 m depth.

(a) *(b)*

Fig. 3-7: (a) KPS test in LCC panel; (b) Excavated LCC panel 2.5 m below ground surface

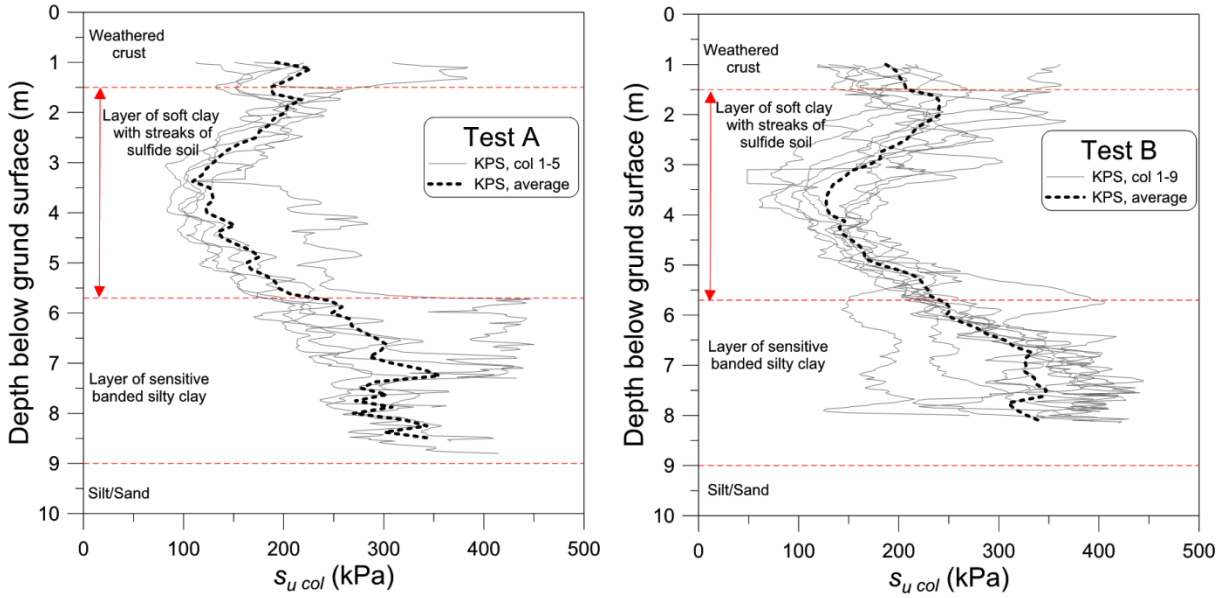

(a) *(b)*

Figure 3-8: Results of KPS tests: (a) Test A; (b) Test B

3.5 Results of Full-scale Tests

Evaluation of the shear strain, γ, in the column panel and the clay between the panels at different stages of the tests are presented in Fig. 3-9. Measured horizontal displacements perpendicular to the SPW, u_h, in the inclinometers were used to calculate the magnitude of the shear strain at the different stages according to Eq. 1.

$$\gamma = \Delta u_h / \Delta z \quad (1)$$

where γ is the calculated shear strain, Δu_h is the incremental horizontal displacement in the inclinometer between two adjacent measurement points, and Δz is the vertical distance between the two points.

Different behavior of the improved soil is indicated for Test A and Test B during excavation stages. In Test A, at a distance of 1.5 m from the SPW the shear strain in the clay between the DDM column panels is larger than the shear strain in the DDM column panel at the same depth and the difference increased for each stage until failure. The opposite behavior was observed in Test B at a distance of 1.5 m from the SPW, as γ in the column panel is larger than γ in the clay at the same depth and the difference increased for each stage until failure. At failure the increase of γ in the clay in Test A was significantly larger compared to the column panels, indicating a failure initiated in the clay between the DDM column panels, located approximately 1.5 m below the excavation, Fig. 3-9a, i.e. directly below the toe of the SPW. No increment of γ, either in the clay or column panel, was observed at a distance of 4.0 m from the SPW, Fig. 3-9c, indicating a local failure with limited propagation. In Test B it is clear that the instrumented column in the panel at a distance of 1.5 m from the SPW was completely broken at failure (represented by decrease of γ at a depth of approximately 1.0 m below the excavation and a large increase below the SPW), Fig. 3-9b, initiating a simultaneous failure in the clay and DDM column panel. The location of the failure surface indicated by the inclinometers in Test B was located at a larger depth below the SPW compared to Test A, approximately 2.5 m below the excavation. Also, a large shear strain increment was observed in the column panel at a distance of 4.0 m from the SPW, Fig. 3-9d, indicating that the propagation of the failure mechanism in the DDM column panel was significantly more extended in Test B compared to that obtained in Test A.

Fig. 3-10 presents the behavior of the improved soil in the passive zone in each test during the final loading hours until failure. The top graphs, Fig. 3-10a-b, show the horizontal stress change, $\Delta\sigma_h$, with evolution of the applied load, q_{load}, in the column panel and the clay between the panels in the respective test at the same depth, 5.5 m, and distance from the SPW, 1.0 and 3.5 m, respectively. The lower graphs, Fig. 3-10c-d, show the excess pore water pressure in the clay, Δu_{clay}, between the panels at the same locations as $\Delta\sigma_h$ and also at the depth of 7.0 m corresponding to the toe of the SPW. In Test A, the change in $\Delta\sigma_{h\,col}$ after the last load step was applied, interpreted as possible yielding of the columns ($\Delta\sigma_{h\,col}$ started to decrease under constant q_{load}) was followed by an increase in $\Delta\sigma_{h\,clay}$ between the panels and a decrease in Δu_{clay} at the same level (resulting in a significant increase in $\Delta\sigma'_{h\,clay}$) prior to failure. At failure a simultaneous equal decrease in $\Delta\sigma_{h\,clay}$ and Δu_{clay} occurred at a distance of 1.0 m from the SPW, indicating a collapse failure in the clay resulting in very large deformations.

However, the same behavior was not observed in the column panel where although a large decrease in $\Delta\sigma_{h\,col}$ at a distance of 1.0 m from the SPW occurred at failure, a significant amount of stress was redistributed in the column panel, represented by an instant increase in $\Delta\sigma_{h\,col}$ at 3.5 m from the SPW. In Test B yielding of the columns at a distance of 1.0 m from the SPW started at approximately the same stress level as in Test A before the end of the last loading stage but the decrease in $\Delta\sigma_{h\,col}$ evolved at a significantly faster ratio compared to Test A. At failure a large sudden drop in $\Delta\sigma_{h\,col}$ ($\Delta\sigma_{h\,col}$ dropped below 0 to negative values) occurred, confirming breaking of the column.

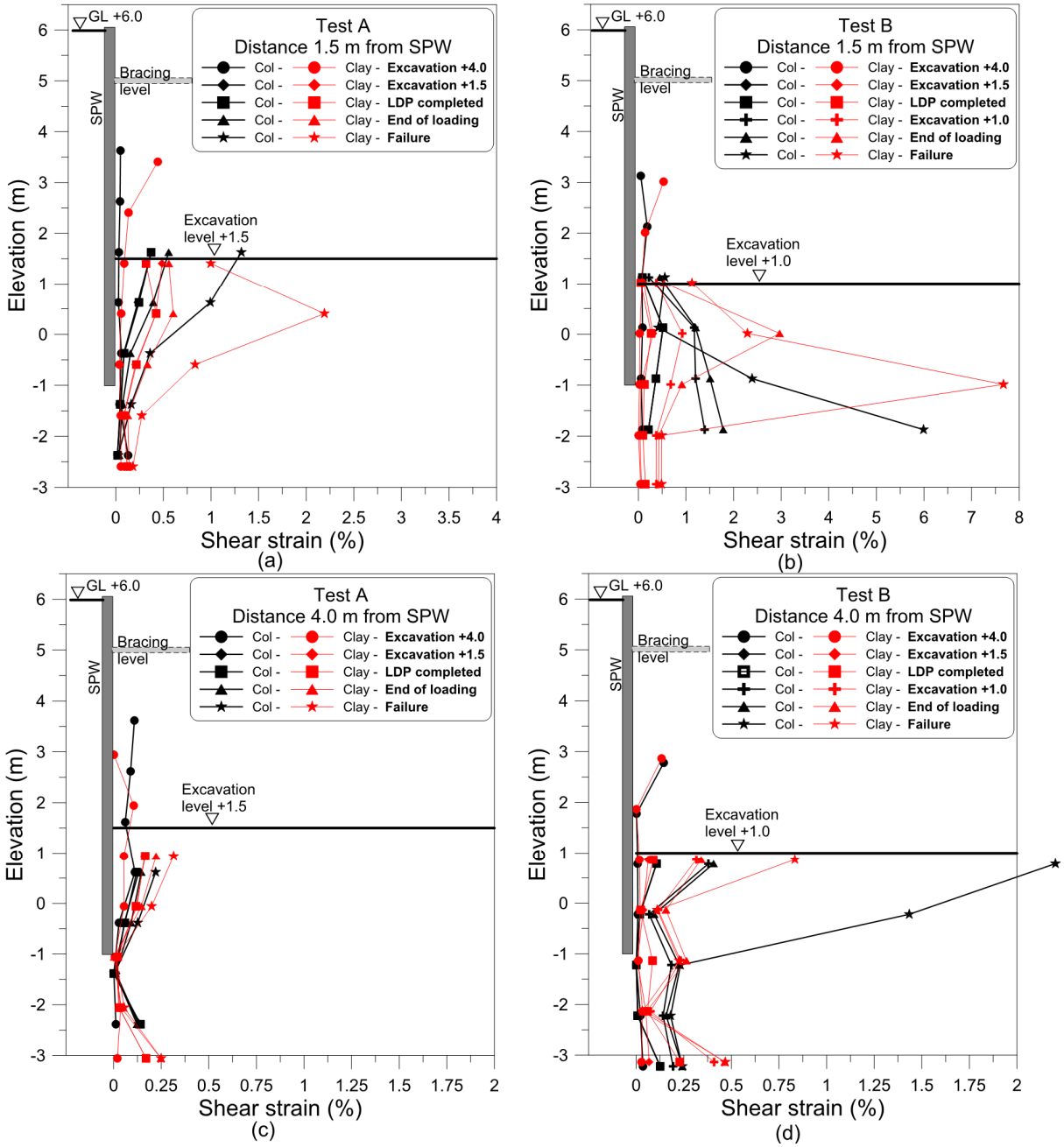

Fig. 3-9: Calculated shear strains from horizontal displacement at different stages

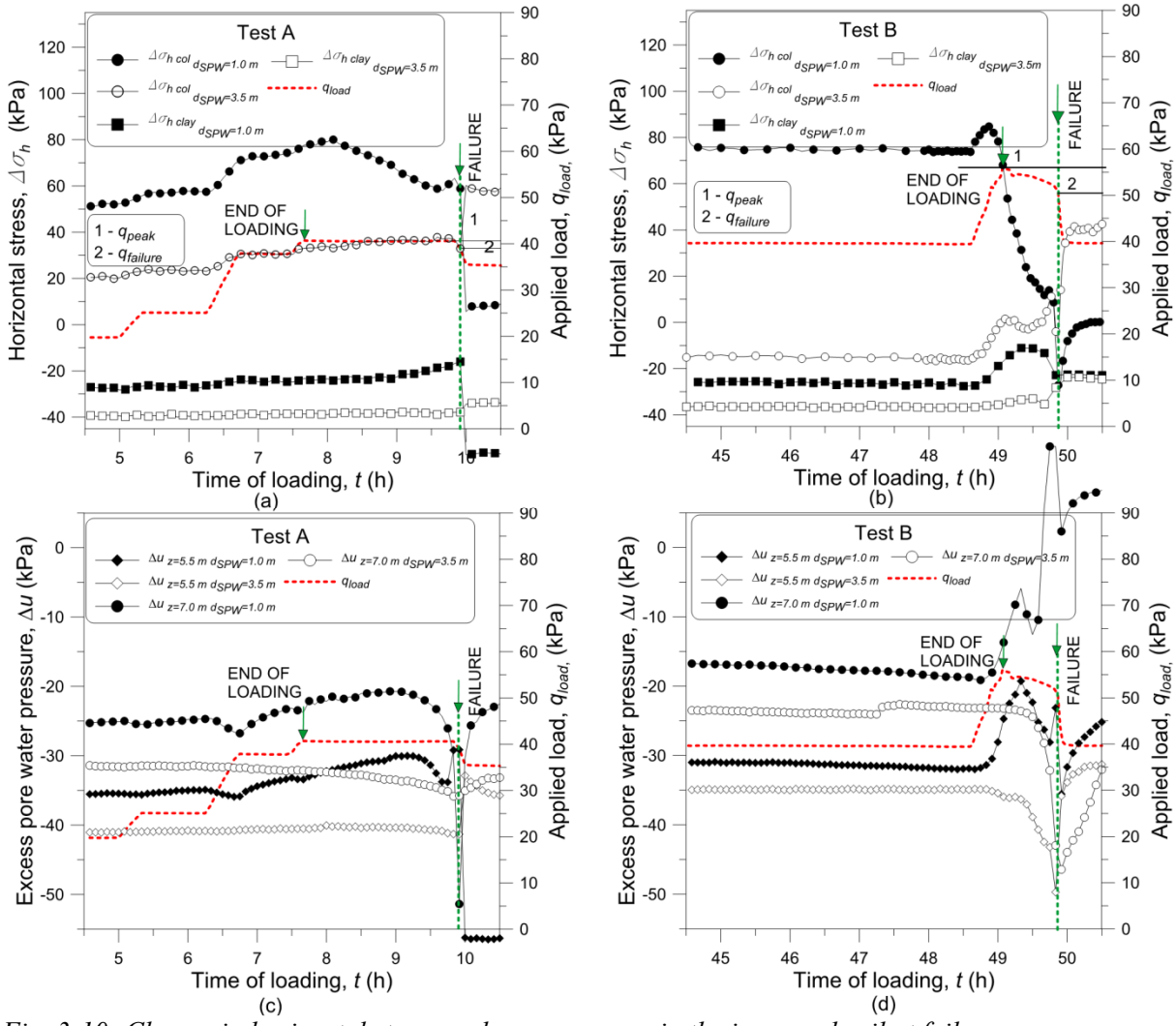

Fig. 3-10: Change in horizontal stress and pore pressure in the improved soil at failure

The horizontal stress-shear strain behavior during the loading stage in the column panels and the clay between the columns at the same distance from the SPW is presented in Fig. 3-11. In Test A, Fig. 3-11a, yielding of the columns below the excavation at a distance of 1.0 m from the SPW implies stress redistribution to the clay between the column panels at the same distance from the SPW. The increase in $\Delta\sigma_{h\ clay}$ results in increased mobilization of $s_{u\ clay}$ followed by yielding initiated at a γ value of approximately 0.4 % and finally failure initiated in the clay (extrusion between the panels) at a γ value of approximately 1.8 %. Very small values of γ were observed in the column panel and the clay between the panels at a distance of 3.5 m from the SPW and the increase in $\Delta\sigma_h$ indicates that either $s_{u\ col}$ or $s_{u\ clay}$ was completely mobilized at failure. The partial unloading followed by reloading conducted in Test B between the first and second day of loading as well as the partial unloading followed by the additional excavation conducted during the second day of loading are clearly indicated in both the column panel and the clay between the panels, Fig. 3-11b and 3-11d. Also in Test B yielding of the columns at a distance of 1.0 m from the SPW implies stress redistribution to the clay between the column panels at the same distance from the SPW. However, due to the much closer distance between the panels, failure occurred in both the columns and the clay between the panels after $s_{u\ clay}$ was completely mobilized.

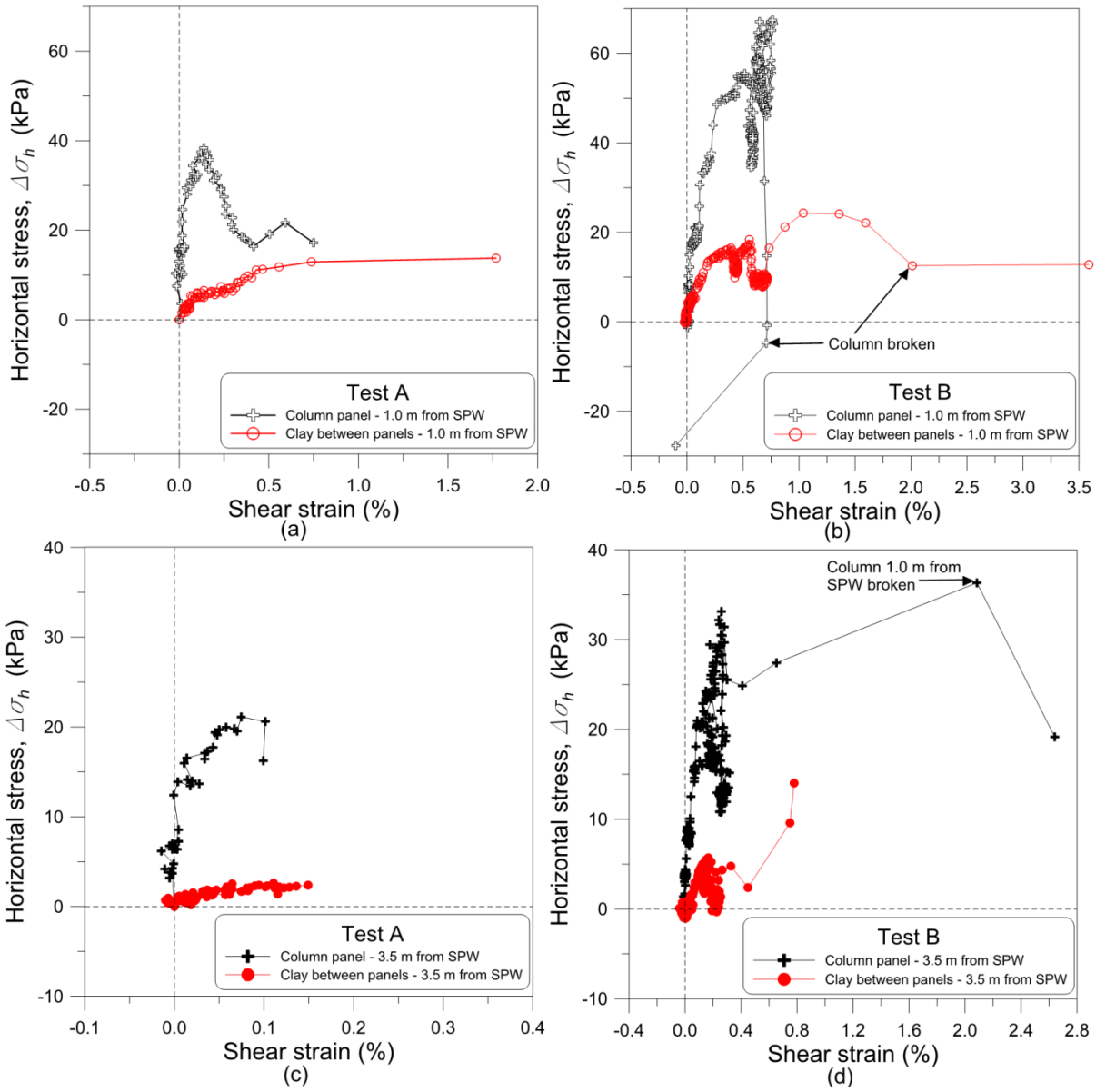

Fig. 3-11: Horizontal stress-shear strain behavior of the LCC panels and the clay between the panels

Fig. 3-12 shows the development of the normal forces, F_s, measured in the instrumented struts in front of the LDP, together with $\Delta\sigma_{h\,col}$ during the final loading stage until failure. The increament ratio of F_s after the last load step was applied was significantly higher in Test B, Fig. 3-12b, due to the larger decrease in $\Delta\sigma_{h\,col}$. In Test B, breaking of the column at failure resulted in a very large instant increase in F_s, indicating that the applied load was transferred to the strut supporting system. However, only a small increase in F_s was observed in Test A at failure, Fig. 3-12a, indicating that the support system provided by the column panels did not break and the failure was initiated in the clay between the panels.

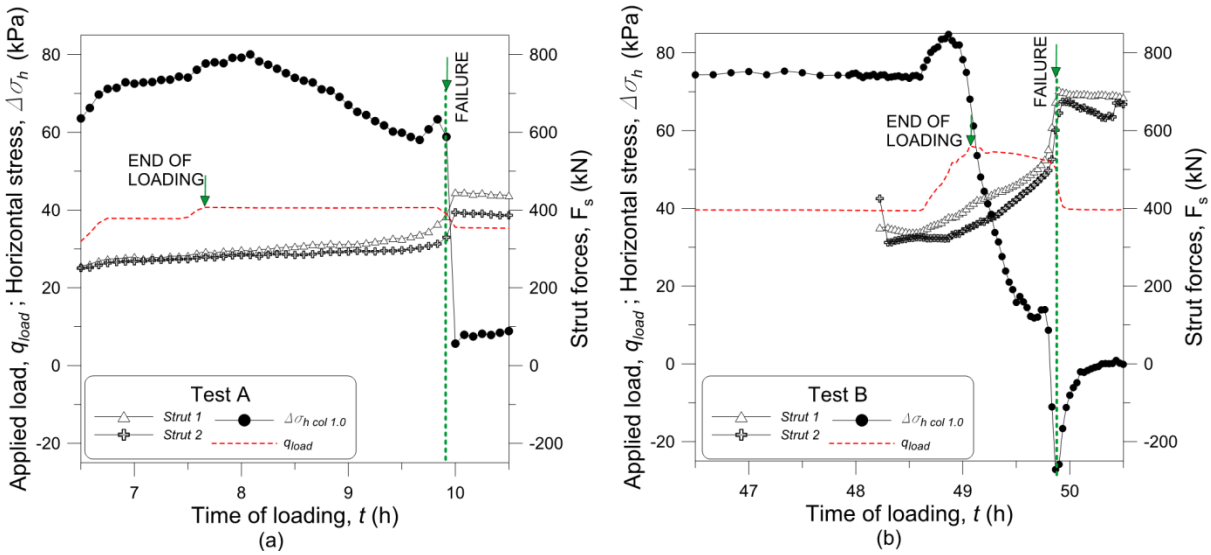

Fig. 3-12: Measured strut forces and column horizontal stress increment at failure

3.6 Summary

The main outcomes of the full-scale field test are summarized as:

- Column-type ground improvement installed as panels of overlapping columns in the passive zone of a sheet pile wall significantly increases stability and reduces excavation- and loading-induced structural forces as well as vertical and horizontal displacements in the soil.
- The lime-cement column panels installed in the passive zone acted as support for the sheet pile wall below the bottom of the excavation by creating a strut-like effect.
- Excavation- and loading-induced stress increments were transferred mainly to the DDM column panels even at spacing between the panels as great as 3.0 m, due to the large difference in strength and stiffness properties between the soft soil and the DDM columns.
- The pre-failure behavior differed significantly between the two tests. For a center spacing between the DDM columns panels equal to 3.0 m, a very sudden failure developed initially in the clay between the panels with small deformations prior to failure. A simultaneous failure of both the DDM column panels and the clay between the panels was observed at a center spacing of 1.5 m between the DDM column panels.

4. LABORATORY TESTS ON LIME-CEMENT ADMIXED CLAY

4.1 Background and Study Objective

The strength and stiffness properties of laboratory mixed lime-cement improved clay from the full-scale test site were investigated through a laboratory test program comprising unconfined compression tests, UC, free-free resonance testing, FFR, constant rate of strain oedometer tests, CRS, and consolidated undrained/drained triaxial tests, CIU/CID.

Laboratory strength and stiffness properties of clays improved by different types of binders are generally assessed based on results from unconfined compression tests, UC, and the column field strength is thereafter verified by column penetration tests (in Scandinavian countries), CPT tests or UC tests on field samples. However, DM columns located in the passive zone of an embankment/slope or excavation support are subjected to extension/tension loading conditions and the material stress-strain behavior may differ significantly compared to the behavior from conventional compression loading tests (UC, CIUC).

The tensile behavior of cement improved soils has been investigated primarily by methods originating from concrete engineering, such as split tension tests, unconfined tension tests or bending tests. A linear relationship between the unconfined tensile strength and the unconfined compression strength has been reported by Terashi et al. 1980, Koseki et al. 2005, Namikawa & Koseki 2007, Consoli et al. 2010 and 2012 and is recommended for the design of cement improved soil subjected to tensile stresses (Kitazume & Terashi 2013). Nevertheless, in these types of tests originating from concrete engineering, some important parameters that may have a significant effect on the materials' strength properties, such as confining stresses, loading conditions (i.e. undrained/drained conditions), and effective stresses (excess pore pressure development during undrained loading) are not considered. The tensile strength as well as the effect of principal stress rotation and intermediate principal stress on artificially cemented granular soils has been investigated in conventional triaxial and true triaxial tests (Lade & Overton 1989, Reddy and Saxena 1993, Lade & Trads 2014, Malandraki and Toll 2000 and 2001, Toll et al. 2006, Namikawa and Mihira 2007, Namikawa et al. 2017). However, very few triaxial extension or tension tests on lime-cement improved soft clay have been presented.

To enhance understanding of how the strength of lime-cement improved clay is mobilized in the passive zone, a comprehensive series of 26 isotropic consolidated triaxial tests (16 undrained tests and 10 drained tests) on lime-cement improved soft clay were conducted. The effect of varying the major and minor principal stress was investigated by conducting the tests for three different stress paths to failure under undrained conditions: triaxial extension, CIUE-L (increase in radial stress under constant axial stress), triaxial tension, CIUE-U (decrease in axial stress under constant radial stress), and a stress path where a decrease in axial stress and increase in radial stress were applied simultaneously, CIUE-UL (increase in radial stress and decrease in axial stress resembles the stress change in the DDM columns during excavation). The stress path to failure in the DDM columns during the excavation stage depends on several factors such as: panel center spacing, stiffness difference between the column panels and the clay between the columns and at the distance from the SPW towards the center of the excavation. In this study an equal decrease in axial stress and increase in radial stress were applied, resulting in a total stress path located in-between the total stress paths of CIUE-L and CIUE-U tests and at an inclination of 6:1 towards the Critical State Line. Drained tests with two different stress paths to failure were also performed: triaxial extension, CIDE-L and triaxial tension, CIDE-U. All tests were conducted in a conventional triaxial device. Followed stress paths to failure were chosen to resemble estimated stress paths of DDM columns located in the passive zone of a retaining structure acting as excavation support. In order to compare the test results with conventional testing methods, undrained and drained triaxial compression tests (increase in axial stress and constant radial stress), CIUC/CIDC, were also performed.

A frequently used procedure to ensure a high degree of saturation, S_r, of lime and cement improved soils is, due to its simplicity, to apply a high back pressure, BP, for a sufficient period of time to minimize the volume of entrapped air voids in the sample. However, it has been debated whether the field behavior of DDM columns where the soil is in-situ mixed with the dry binder under relatively high air pressure is consistent with the saturation procedure where high BP is applied, and how the material behavior is influenced by this procedure. Åhnberg (2004) investigated the effect of consolidating lime-cement improved clay samples at different confining stresses with very low and high BP (20 and 400 kPa, respectively) and found that samples with low BP behave during undrained shearing as partly drained and related this behavior to excess pore pressure being partly equalized by compression or extension of the entrapped air. The difference between $s_{u\,col}$ evaluated from samples saturated by low BP and samples saturated at high BP was found to increase with increasing confining stress. From the corresponding drained tests, no significant difference in $s_{u\,col}$ was found between the tests conducted at low and high BP, respectively. However, test conditions where the improved clay samples are consolidated at a very low BP combined with high confining stresses are not consistent with real field conditions where both the pore pressure and the confining stresses are expected to increase with depth below the ground surface.

4.2 Sample Preparation

The dry binder content used was 120 kg/m^3, 50% quicklime, QL 0-0.1 KÖ, and 50% Portland cement, CEM II/A-LL 42.5 R, similar to the dry binder content used in the full-scale field tests. The samples were prepared by mixing the dry binders of lime and cement with the soil for 5 minutes. Immediately thereafter, the mixture was gradually filled in layers of 10-20 mm into fiberglass tubes 50 mm in diameter and 150 mm in height. Each layer was compacted using a Ø30 mm cylindrical rod in order to produce uniform samples with a minimum of air pockets. The tubes were filled and then sealed with rubber lids before being stored in a climate room at 7°C without curing stress. This procedure is in accordance with the common procedure for testing of laboratory samples of improved soil in Sweden (Larsson 2006). Due to limitations in the number of triaxial tests that can be conducted each week, new batches containing 3-4 samples were prepared once or twice a week for a period of approximately 20 weeks, allowing the samples to be tested at the same curing time of 28 days.

After the curing period, the samples were extracted and trimmed to a height to diameter ratio of 2:1, 100 mm in height and 50 mm in diameter. Before testing, the specimens were cut and smoothed to obtain parallel end surfaces and any irregularities at both end and mantle surfaces were repaired with remolded trimmings from the sample and plaster.

4.3 UC Tests, FFR Column Tests and CRS Oedometer Tests

4.3.1 Testing procedure

Unconfined compression tests, UC, each test conducted on samples from different batches, were performed at a strain rate of 1.2 %/min, in accordance with Swedish Standards, SIS (1991). The oedometer *CRS* tests, conducted in accordance with SIS (1992), were performed in order to assess the yield stress (quasi-preconsolidation stress) of the improved material, σ'_{qp}, at a strain rate of 0.01 %/min.

The resonant free-free column test, FFR, is an attractive alternative due to its simplicity and non-destructive testing procedure that has been utilized with good results to investigate the dynamic modulus of laboratory and field improved soils (Lindh et al. 2005, Rydén et al. 2006, Åhnberg &Holmén 2008 and 2011, Toohey &Mooney 2012, Guimond-Barrett et al. 2013, Ismail & Rydén 2014, Verástegui-Flores et al. 2015). The samples having a length to diameter ratio of 2:1 were placed "free" on a soft foam platform. The specimens were subjected to longitudinal and flexural excitation to measure resonant frequencies associated with compression and shear wave propagation recorded by an accelerometer of type PCB Piezotronics 352B10 with a frequency range of 2-10000 Hz.

The relationship for evaluating the wave length from the resonant frequency is an approximation applicable for specimens with free ends and a length-to-diameter ratio of two or more (Rydén et al. 2006). Knowing the specimen's mass density, ρ, the dynamic Young's modulus, E_0, and dynamic shear modulus, G_0, could be determined using the following equations:

$$E_0 = \rho\left(2Lf_p\right)^2 = \rho V_p^2 \tag{2}$$

$$G_0 = \rho(2Lf_s)^2 = \rho V_s^2 \tag{3}$$

where L is the specimen length, f_p and f_s are the resonant frequency for compression wave and shear wave, respectively, and V_p and V_s are the compression wave velocity and the shear wave velocity, respectively. From Equations (2) and (3) and assuming homogeneous, isotropic linear elasticity, the Poisson's ratio, ν, can be determined by the following relationship:

$$\nu = E_0/2G_0 - 1 \tag{4}$$

4.3.2 Test results

The relationship between unconfined compression strength, q_{UC}, and $V_p$and V_s, respectively, obtained from these tests are presented in Fig. 4-1. The test results agree reasonably well with the equations proposed by Åhnberg &Holmén (2011), also presented in Fig. 4-1, and comprehended from tests performed on improved soil samples with water content higher than 40 % and a large diversity of soil types from 20 different geotechnical sites.

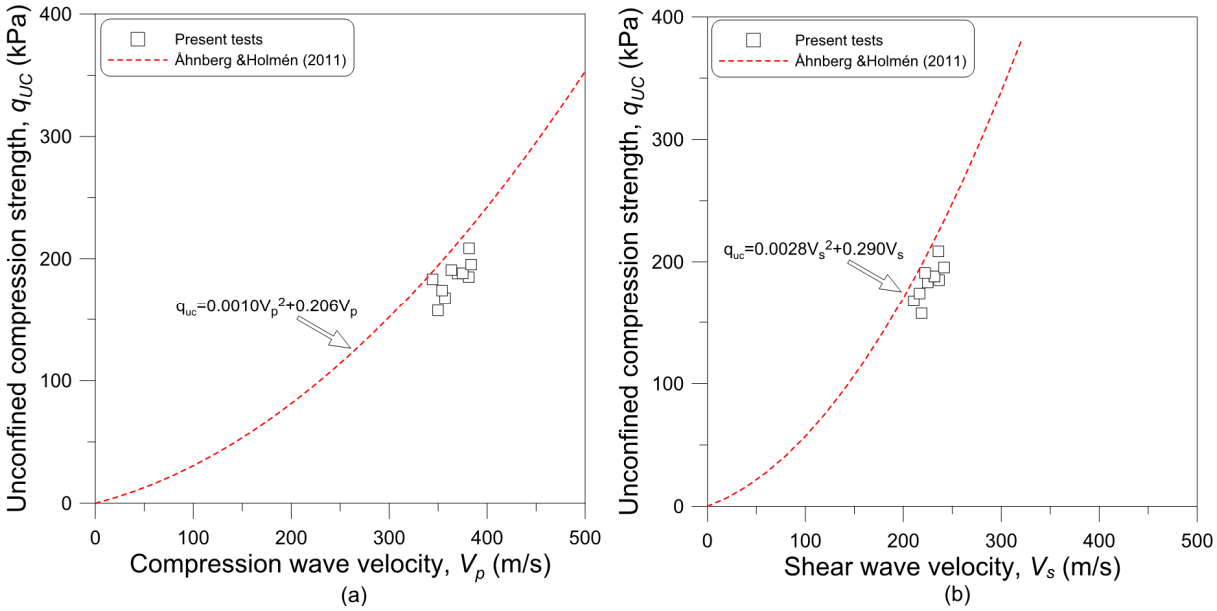

Fig. 4-1: (a) Relationship between compression wave velocity and unconfined compression strength; (b) Relationship between shear wave velocity and unconfined compression strength

The relationship between q_{UC} and dynamic modulus E_0 and G_0 as well as evaluated ν of these tests are presented in Fig. 4-2. The relationship between G_0 and q_{UC} indicates a trend close to the relationship between G_0 and undrained shear strength proposed for normally consolidated natural clays by Larsson & Mulabdic (1991):

$$G_0 = \frac{504 s_u}{w_n} \tag{5}$$

where s_u is the undrained shear strength and w_n is the natural water content. This relationship is included in the presented results for the improved samples, Fig 4-2a, assuming the shear strength of the improved soil to be equal to $q_{UC}/2$ and based on w_{col} measured in the samples after improvement. However, this relationship needs to be further investigated for improved soils of higher strength as the range of q_{UC} for these tests was very limited and varied only between approximately 150 and 220 kPa. The value of ν, Fig. 4-2b, was evaluated to approximately 0.3 and is similar to results presented by Åhnberg &Holmén (2008) for cement and lime-cement stabilizes samples and within the range of 0.28-0.45 reported by Kitazume & Terashi (2013) for clay improved by different types of binders.

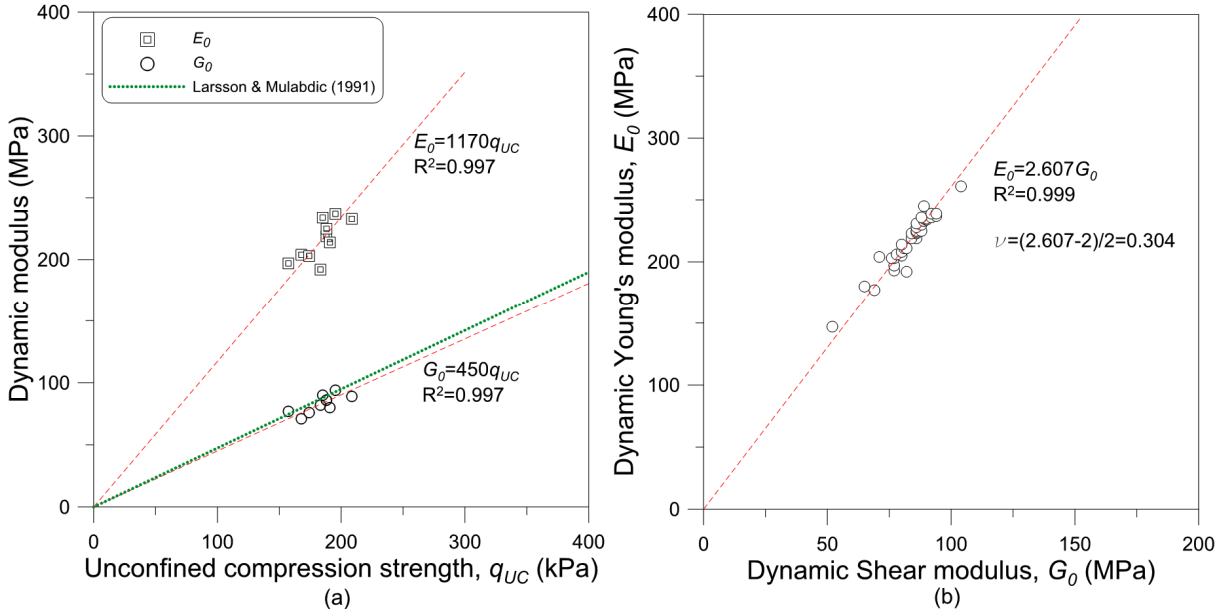

Fig. 4-2: (a) Relationship between dynamic modulus and unconfined compression strength; (b) evaluation of Poisson's ratio

The relationship between void ratio, e, and the logarithm of the vertical effective stress, $e - log\ \sigma'_v$ for improved clay obtained from the CRS oedometer tests is presented in Fig. 4-3 and the natural clay has also been included for comparison. The initial void ratio after curing, prior to one-dimensional loading, can be expressed as follows:

$$e_0 = \frac{(1+w_{col})G_s\gamma_w}{\gamma_{col}} - 1 \quad (6)$$

where w_{col} is the water content of the improved clay after curing, G_s is the specific gravity of the improved clay, γ_{col} is the unit weight of the improved clay, and γ_w is the unit weight of water. Measured γ_{col} varied between 16.0 and 16.3 kN/m^3 and w_{col} after curing varied between 56.6 and 57.8%. By assuming G_s of the improved clay to be equal to 2.71 as proposed by Baker (2000), the initial void ratio was estimated to be 1.64-1.66.

The results indicate a good reproducibility of the samples as the stress-strain properties of samples prepared from different batches were very similar. The one-dimensional yield stress, also called apparent or quasi-preconsolidation stress for improved clay (evaluated by the Casagrande method), σ'_{qp}, was significantly increased compared to σ'_p of the natural clay, Fig. 4-3a, due to the formation of cementation bonds, as also reported in other studies (Tremblay et al. 2001, Miura et al. 2001, Kamruzzaman et al. 2009). Evaluated σ'_{qp} varied between 220 and 250 kPa with a mean value of 240 kPa. A linear relationship between σ'_{qp} and q_{UC} is indicated, Fig. 4-3b, and the σ'_{qp}/q_{UC} ratio of these tests was approximately 1.26, which is in line with results reported in previous investigations of improved clays (Terashi et al. 1980, Indraratna et al. 1995, Åhnberg 2006, Lorenzo & Bergado 2006).

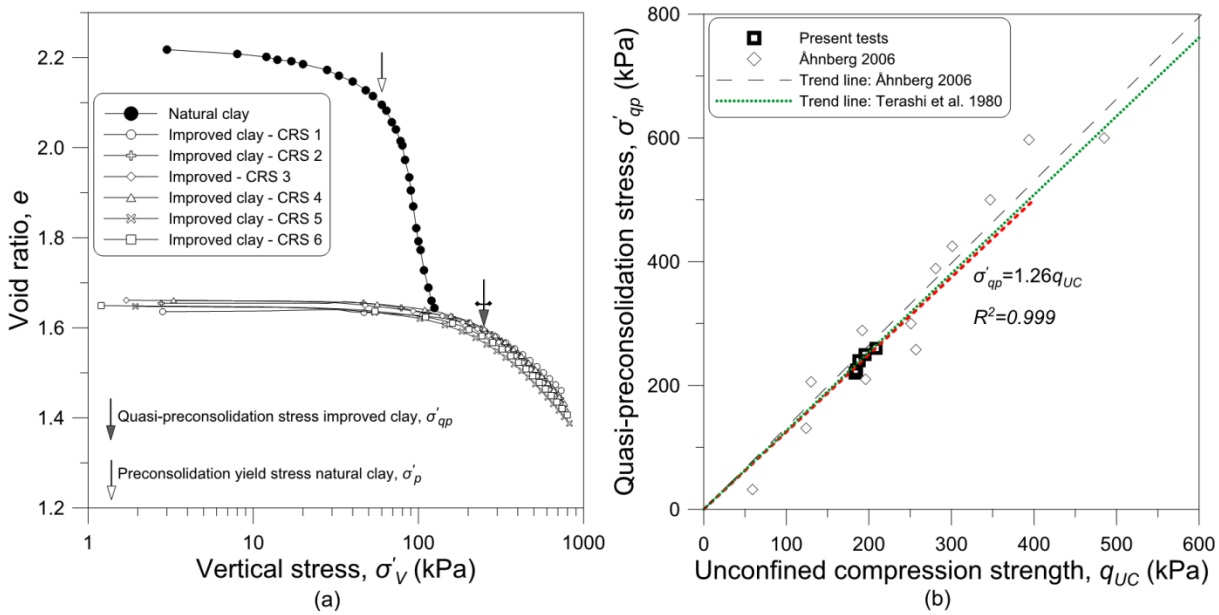

Fig. 4-3: (a) Evaluation of quasi-preconsolidation stress from CRS oedometer tests; (b) relationship between quasi-preconsolidation stress and unconfined compression strength

4.4 Triaxial Tests

4.4.1 Testing equipment

The triaxial tests were conducted at the SGI (Swedish Geotechnical Institute) laboratory with an SBEL HX-100-SA-1500 triaxial cell with a hydraulic servo actuator. The cell is controlled by an INSTRON 8800 digital servo controller. Load is applied by a hydraulic servo actuator in the lid of the cell. The displacement transducer is connected directly to the actuator piston. Load is measured by a load cell in the base pedestal and cell pressure is applied by a pneumatic servo valve. Back pressure and volume change measurement is provided by an ELDPC (1 MPa) from GDS.

Strip side drains on the side were used for faster consolidation during the consolidation stage. The paraffin method, described by Lacasse & Berre (1988), was used in all tests, thereby eliminating the need for membrane correction. A constant rate of stress change, 0.833 kPa/min, was used for the undrained tests. A much slower rate of stress change, 0.083 kPa/min, was chosen for the drained tests in order to ensure adequate dissipation of excess pore water pressure.

4.4.2 Sample saturation and consolidation

A Skempton B-value of at least 0.9 has been regarded as a measure of full saturation for cement improved soils, resulting in negligible suction during testing (Schnaid et al. 2001, Consoli et al. 2001). No attempt was made to fully saturate the samples in these tests. Instead, the BP applied during the saturation stage and consolidation stresses were chosen close to the prevailing in situ pore water pressure and effective confining stresses at depths within representative engineering consideration depths, i.e. less than 40 m of depth. The initial degree of saturation of the improved samples, S_{r0}, after curing and before sample saturation and consolidation, was estimated to be:

$$S_{r0} = \frac{\gamma_{col} \cdot G_s w_{col}}{\gamma_w \cdot G_s \cdot (1 + w_{col}) - \gamma_{col}} \quad (7)$$

Calculated S_{r0} based on Equation (7) varied between 93 % and 95 %, which is of the same order as in previous studies of laboratory mixed samples of improved clay (Baker 2000, Uddin & Buensucesco 2002, Åhnberg 2004).

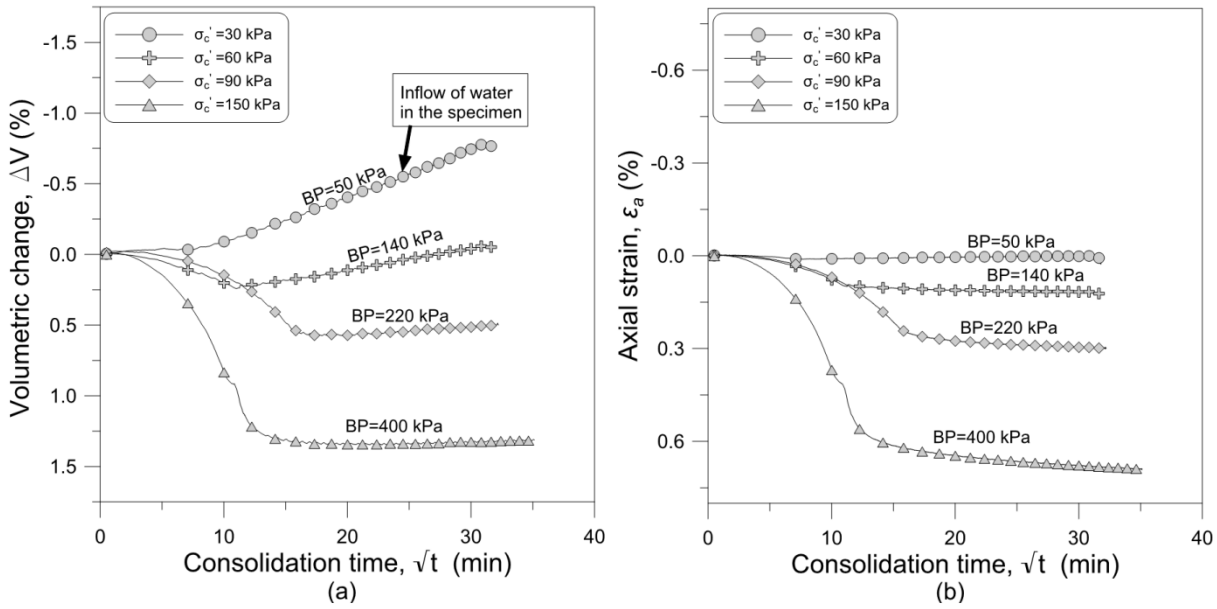

Fig. 4-4: (a) Volumetric change (measured as inflow/outflow of water in the sample) during consolidation; (b) Axial strain during consolidation

For saturation of the samples, an active application of BP (water is allowed to flow into the specimen to replace air being dissolved in the pore water and the soil skeleton is kept at its initial volume) was chosen and both volumetric change (volume change measured as the amount of water entering /exiting the sample, measured as negative/positive volume change), Fig. 4-4a, as well as axial strain during the consolidation stage, Fig. 4-4b, were used as a measure of when equilibrium conditions have been reached, as described by Lade (2016). This technique allows both saturation and consolidation to be achieved during the same time. First, the BP and cell pressure were simultaneously increased to targeted values during a time period of 1.5-2.5 h. Thereafter, the samples were isotropically consolidated at effective confining stresses, σ_c', ranging between 30 and 150 kPa, for 16-24 h, at which time no further axial strain or volumetric change (inflow of water due to saturation) was recorded and an equilibrium condition was obtained.

Theoretical BP to increase the degree of saturation in a sample from its initial value, S_{r0}, to another required value, S_r, by both compression and solution of the pore air has been defined by Lowe & Johnson (1960) as:

$$\Delta BP = p_0 \frac{(S_r - S_{r0})(1-H)}{1-S_r(1-H)} \tag{8}$$

where ΔBP is the required BP increment, p_0 is the initial absolute pressure corresponding to S_{r0} (atmospheric pressure for samples cured in a climate controlled room, assumed to be equal to 101.33 kPa), and H is Henry's coefficient of air solubility in water which is temperature and pressure dependent (equal to approximately 0.02 at room temperature, 20°C). By rearranging Equation (8), S_r after saturation and consolidation to the different applied BP was calculated as follows and is presented in Table 4-1:

$$S_r = \frac{p_0 S_{r0} - \frac{\Delta BP}{H-1}}{\Delta BP + p_0} \tag{9}$$

The BP required for complete saturation of a sample is:

$$BP_{100} = p_0 \frac{1-S_{r0}(1-H)}{H} \tag{10}$$

Based on S_{r0} equal to 93-95 % the BP required to fully saturate these samples is estimated to be 350-450 kPa. These values are in good agreement with recommendations presented by Åhnberg (2004), who recommended performing triaxial tests on lime-cement improved clay at a BP value of 400 kPa in order to yield results relevant for fully saturated conditions.

For stiff and very stiff soils, such as cement and lime-cement improved clay, a Skempton B-value lower than 1 can be expected even at full saturation. Black and Lee (1973) presented theoretical pore pressure response for different representative types of soils based on the material's compressibility at complete and nearly complete saturation. The B-value required for complete saturation, B_{100}, without system compliance can be determined as:

$$B_{100} = 1/(1 + n\frac{C_w}{C_d}) \quad (11)$$

in which n is the porosity of the soil, C_w is the compressibility of water (approximately $4.8 \cdot 10^{-7}$ m^2/kN) and C_d is the compressibility of the soil skeleton. According to Black and Lee (1973) an S_r between 99.0 % and 99.5 % implies for a stiff soil ($C_d \sim 1.45 \cdot 10^{-5}$ m^2/kN) a B-value of 0.51 - 0.69, and for a very stiff soil ($C_d \sim 1.45 \cdot 10^{-6}$ m^2/kN) a B-value of only 0.1 - 0.2 is expected for S_r between 99.0 % and 99.5 %.

The compressibility of the improved clay samples, C_d, was calculated as:

$$C_d = 1/K = 3(1-2\nu)/E_0 \quad (12)$$

With E_0 and ν values determined from the FFR tests, the mean C_d of these samples was evaluated to $5.1 \cdot 10^{-6}$- $6.6 \cdot 10^{-6}$ m^2/kN and the improved clay was categorized as a stiff to very stiff soil, according to the four different soil classes treated by Black and Lee (1973). Based on Equation (11) a B-value between 0.92 and 0.95 is required for these samples to achieve complete saturation. Calculated degree of saturation prior to and after saturation together with measured B-values after completed consolidation is presented in Table 4-1. The results show that practically complete or nearly complete saturation was obtained for samples consolidated at a BP of 220 kPa and higher. However, both calculated S_r and measured B-values for samples consolidated at the lower BP levels (50 and 140 kPa) indicate that these samples are not fully saturated. Calculated S_r of 96-97 % of the samples consolidated at BP equal to 50 kPa, corresponding to a depth of approximately 6 m below the ground surface, is in good agreement with the S_r of 96.5-98.1 % obtained by Baker (2000) for samples from DDM columns extracted from a depth of up to 7 m.

Table 4-1: Calculated degree of saturation before and after consolidation and measured Skempton B-values.

Consolidation stress, σ_c' (kPa)	Back pressure, BP (kPa)	Calculated S_{r0} before saturation (%)	Calculated S_r after consolidation (%)	Measured B-values after consolidation min - max
30	50	92.8 - 94.8	95.9 - 97.2	0.23 - 0.36
60	140	93.8 - 95.5	98.6 - 99.3	0.46 - 0.71
90	220	93.6 - 95.2	99.4 - 99.9	0.72 - 0.80
150	400	93.1 - 94.7	$\geq$ 99.9	0.92 - 0.94

4.4.3 Test results

4.4.3.1 Stress – strain behavior

The deviator stress - axial strain behavior, $q - \varepsilon_a$, of the undrained and drained test, respectively, is illustrated in Fig. 4-5 and the test results are summarized in Table 4-2 and Table 4-3. The post-peak behavior expressed as strain softening cannot be identified in these tests due to the test conditions implied, constant rate of stress change, although it has often been observed in strain controlled tests. The deviator stress at failure, q_f, was, for the undrained tests where a clear peak value could not be observed (alternatively occurred at very large values of ε_a), evaluated as q at an ε_a level where both the change in q and the change in excess pore pressure, Δu, become negligible.

The results show that q_f evaluated from undrained triaxial extension tests, Figs. 4-5b and 4-5c, is strongly influenced by the stress path to failure at low values of σ_c' but the difference in q_f reduces with increasing σ_c'. The trend of the stress-strain curves of CIUE-L tests and also CIUE-UL and CIUE-U consolidated at $\sigma_c' \geq 90$ kPa is analogous to that of CIUC tests, Fig. 4-5a. An initial linear elastic behavior followed by an elastoplastic behavior (strain hardening) with increasing ε_a is representative of these tests. The CIUE-UL and CIUE-U tests consolidated at low values of σ_c', i.e. heavily overconsolidated, exhibit to a certain extent different stress-strain behavior with significantly more rounded curves. The stress-strain behavior is influenced by the failure mode of these samples, which is a tension failure. The initial linear elastic part of the stress-strain curve corresponds to the stress path from the start of the test moving towards the tension failure line (effective stress paths are presented in Fig. 4.7a). During the test, negative Δu develops that continues to decrease with increasing strain, pushing the stress path of the sample downward to the right in the $p' - q$ plane (increasing q and p') and parallel to the tension failure line. The Δu behavior of these tests is analogues to the behavior observed from undrained triaxial extension (unloading) tests on overconsolidated clays with OCR > 2 (Parry 1960, Balasubramaniam and Uddin 1977, Zhu & Yin 2000). The significant stiffness degradation following the initial linear elastic part of the stress-strain curve observed in these tests is believed to be due to micro tension cracks that emerge and increase in the samples with continuous shearing until a tension failure is obtained, which is also indicated by post-failure photographs of the samples, presented in Fig. 4-6.

The CIDE-U tests, Fig 4-5f, indicated a very brittle behavior as the axial strain at failure, ε_{af}, was ≤ 0.1 % for samples consolidated at low values of σ_c'. Axial strain measurement was performed only by means of external transducer, making evaluation of ε_{af} at values < 0.1 % very uncertain. However, an increasing trend of ε_{af} with increasing σ_c' is indicated for all tests and the stress-strain behavior is analogous with results presented by Koseki et al. (2008) and Namikawa et al. (2017) from drained triaxial tension tests on artificially cemented sand conducted with ε_a measurements made by means of local displacement transducers.

Yielding of bonded or artificially cemented soils has been identified in experimental tests as a discontinuity in the stress-strain behavior or abrupt decrease in stiffness (Maccarini 1987, Jardine et al. 1991, Jardine 1992, Malandraki and Toll 1996, Leroueil and Vaughan 1990, Bergado et al. 2006, Rotta et al. 2003, Xiao et al. 2014, among others). Research on small strain behavior conducted by Jardine et al. 1991 and Jardine 1992 has suggested that three different yield conditions may be identified for cemented soils representing the limit of elastic behavior, the limit of recoverable behavior, and complete destructuration of the soil structure. Malandraki and Toll (1996, 2000, 2001) suggested that a bond yield, located between the initial yielding defining the end of the elastic region and the final yielding, could be determined as the point at which a major change in tangential stiffness occurs.

Yielding is not readily identified in a majority of the tests since the stress-strain curves do not show any abrupt change in the gradient. As a consequence, the yield stress, q_y , could not be evaluated from the methods proposed by Rotta et al. (2003) and Malandraki and Toll (1996).

As an alternative, q_y was evaluated at ε_a corresponding to the tangent of the maximum curvature of the q - ε_a curves. As these tests were conducted with only external strain measurements, evaluated q_y represents the yield stress at which level irrecoverable strains develop and should not be confused with the initial yield stress marking the purely elastic region. From the undrained tests the ratio q_y/q_f appears to be independent of the stress path to failure and varied between 0.77 and 0.84.

Table 4-2: Results of consolidated triaxial undrained tests

Test type	q_f (kPa)	q_y [2)] (kPa)	Δu_{max} [3)4)] (kPa)	ε_a at q_f [6)] (%)	ε_a at q_y (%)	E_{50} (MPa)	q_y/q_f	E_{50}/q_f
CIUC-30	216	175	(15.2)	4.00	1.24	26.7	0.81	124
CIUC-60	236	182	(39.1)	4.45	1.20	34.4	0.77	146
CIUC-90	244	200	70.9	4.73	1.30	41.0	0.82	168
CIUC-150	261	215	120.6	6.70	1.56	54.0	0.82	207
CIUE-L-30	165	128	(22.7)	-0.84	-0.21	122.6	0.78	743
CIUE-L-60	190	151	(56.4)	-0.83	-0.20	164.6	0.79	843
CIUE-L-90	200	155	85.9	-1.06	-0.23	120.9	0.78	593
CIUE-L-150	200	164	143.8	-1.16	-0.29	117.6	0.82	582
CIUE-UL-30	104	-	(2.0) [5)]	-1.00	-	61.3	-	589
CIUE-UL-60	165	-	(4.1)	-0.64	-	88.9	-	529
CIUE-UL-90 [1)]	(176)	146	20.4	(-0.62)	-0.24	(102.6)	(0.83)	(584)
CIUE-UL-150	207	173	50.0	-1.42	-0.32	114.1	0.84	551
CIUE-U-30	74	-	(-45.4)	-0.96	-	25.3	-	342
CIUE-U-60	126	-	-71.8	-1.00	-	56.2	-	446
CIUE-U-90	177	140	-105.8	-1.04	-0.25	86.4	0.79	462
CIUE-U-150	212	172	-71.3	-1.41	-0.35	93.8	0.81	442

1) *The vacuum pressure between the top cap and the sample could not be sustained and the test was terminated before failure occurred.*
2) q_y *was not evaluated for samples that failed in tension*
3) Δu_{max} *for samples with* $S_r \leq 99.0$ *% after consolidation are uncertain and specified in brackets*
4) *Negative values of* Δu *were measured from the start of all CIUE-U tests and* Δu_{max} *was evaluated at* q_f
5) *In CIUE-UL tests consolidated at low* σ_c' *small positive* Δu *are generated initially, followed by negative* Δu *until failure*
6) *A negative value of* ε_a *means the sample was elongated*

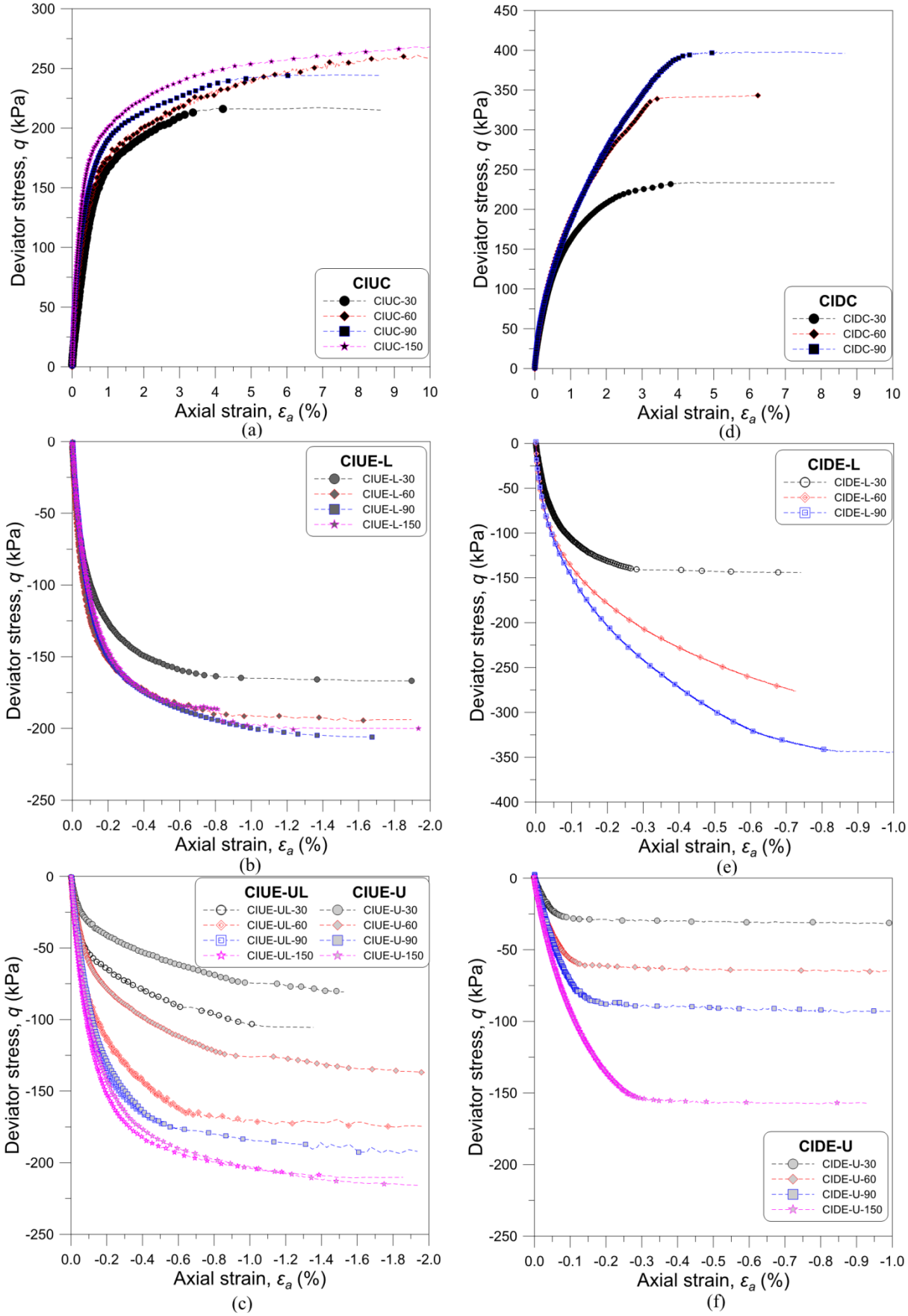

Fig. 4-5: Stress-strain relationship for (a) CIUC tests; (b) CIUE-L tests; (c) CIUE-UL tests and CIUE-U tests; (d) CIDC test; (e) CIDE-L tests; (f) CIDE-U tests

Table 4-3: Results of consolidated triaxial drained tests

Test type	q_f (kPa)	q_y [1] (kPa)	ε_a at q_f [2] (%)	ε_a at q_y [3] (%)	E'_{50} [4] (MPa)	q_y/q_f	E'_{50}/q_f
CIDC-30	230	171	3.61	1.14	29.0	0.74	126
CIDC-60	340	189	3.45	1.12	18.9	0.56	56
CIDC-90	395	222	4.12	1.38	17.7	0.56	45
CIDE-L-30	144	116	-0.30	-0.13	175.7	0.81	1222
CIDE-L-60	275	144	-0.72	-0.11	139.3	0.52	503
CIDE-L-90	344	151	-0.82	-0.10	124.6	0.44	362
CIDE-U-30	31	-	-[3]	-	(56.3)	-	(1816)
CIDE-U-60	64	-	-0.15	-	(85.1)	-	(1330)
CIDE-U-90	93	-	-0.18	-	(88.3)	-	(949)
CIDE-U-150	156	-	-0.30	-	(102.2)	-	(649)

[1] *q_y at values of $\varepsilon_a < 0.1\%$ and for samples that failed in tension is not evaluated*

[2] *A negative value means the sample is elongated*

[3] *Values of $\varepsilon_a < 0.1\%$ are not evaluated*

[4] *E'_{50} evaluated at values of $\varepsilon_a < 0.1\%$ are specified in brackets*

The secant Young's modulus defined as $E_{50} = q_{50}/\varepsilon_{a50}$ where q_{50} is the deviator stress equal to 50 % of q_f and ε_{a50} is the axial strain corresponding to q_{50}, cannot solely describe the nonlinear stress-strain behavior observed in a majority of the tests but is a good indication, commonly used in practice, of the soil stiffness. Generally, a linear relationship between E_{50} and q_f in the range of $E_{50} = 100 - 200\ q_f$ has been reported for laboratory improved clay samples with lime-cement (Åhnberg et al. 1995, Baker 2000) based on results from UC and CIUC tests. For CIUC, the relationship between E_{50} and q_f is in good agreement with previously reported values. A rather large scatter in the values of E_{50} was obtained from the CIUE tests but in general E_{50} was significantly larger compared to the CIUC tests and the ratio E_{50e}/E_{50c} varied between approximately 2.7 and 4.1, shown in Fig 4-6a. Nevertheless, it should be noted that E_{50} in a majority of the CIUE tests was evaluated at $\varepsilon_a < 0.1$ % and is uncertain but most probably an even larger E_{50} would be expected if measurement of ε_a had been performed with equipment able to adequately measure the small strain behavior.

The Young's modulus at 50 % of q_f evaluated from the drained tests, E'_{50}, was also significantly larger in CIDE tests compared to CIDE tests. However, a linear relationship between E'_{50} and q_f could not be identified, Fig. 4-6b, except for the CIDE-U test that failed in tension without reaching the yield surface. For CIDC and CIDE-L tests conducted at σ'_c =60 and 90 kPa, the stress-strain curve at a level corresponding to E'_{50} is highly curved, with continuous stiffness degradation, Figs. 4-5d and 4-5e. This implies that E'_{50} was evaluated in the elastic-plastic part of the stress-strain curve, explaining the decrease in E'_{50} with increasing σ'_c observed from these tests. It should be noted that the values of E'_{50} from the CIDE-U tests were similar to those in the undrained tests evaluated at $\varepsilon_a < 0.1\%$.

Examination of the samples post-failure revealed that the failure mode of the samples differed depending on the stress path applied during the test, illustrated in Fig. 4-7. In CIUC/CIDC tests, a bulging type of failure was initiated and eventually the samples split in shear upon further straining. The very brittle behavior shown in the triaxial tension tests is also indicated from the picture of the specimens after failure. Necking of the samples occurred in a majority of the CIUE-L/CIDE-L tests while a distinct horizontal split failure surface was observed for a majority of the CIDE-U tests and CIUE-U and also CIUE-UL tests consolidated at low values of σ'_c. Failure in the extension/tension tests occurred along a randomly located horizontal plane, indicating that for the extension type of test failure takes place along a weakness plane that depends on the quality and homogeneity of the actual sample tested.

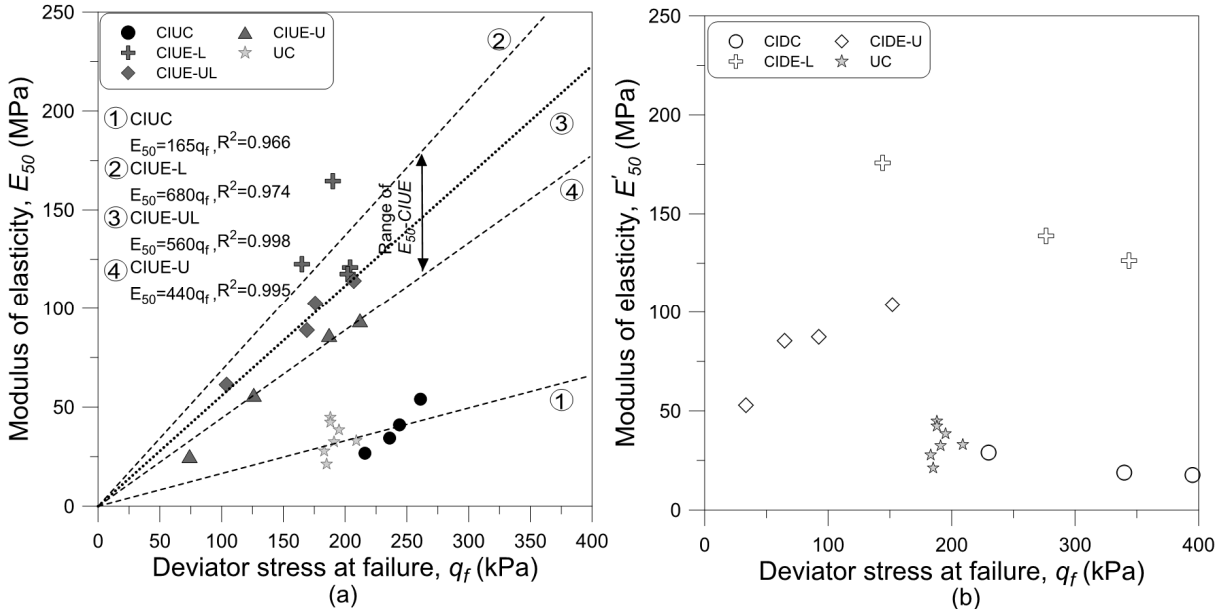

Fig. 4-6: Relationship between Modulus of Elasticity and deviator stress at failure: (a) Undrained tests; (b) Drained tests

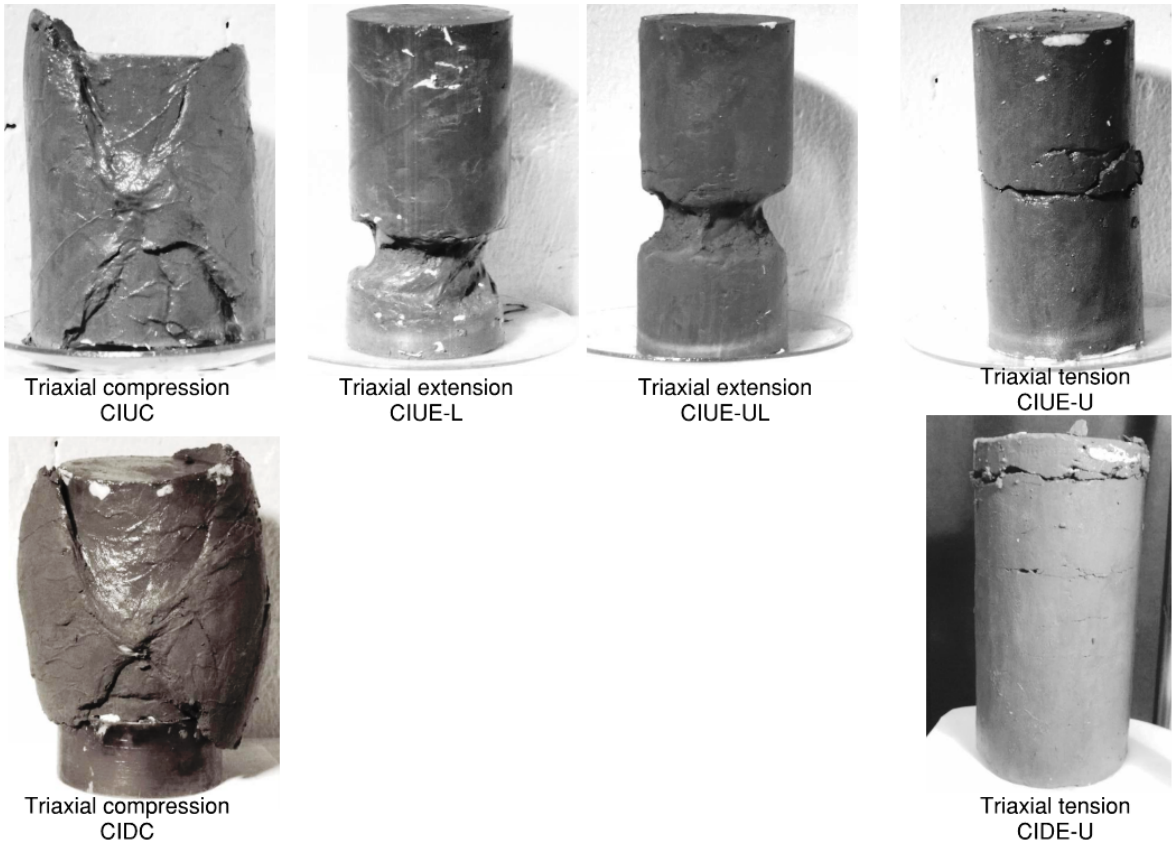

Fig. 4-7: Photographs of samples post-failure for different applied stress paths

4.4.3.2 Effective stress paths and yield locus

The effective stress paths measured in undrained and drained triaxial tests in the $p' - q$ effective stress plane ($q = (\sigma_1' - \sigma_3')$ and $p' = (\sigma_1' + 2\sigma_3')/3$ for $\sigma_2' = \sigma_3'$; where σ_1', σ_2' ,σ_3' are the effective principal stresses under the triaxial stress system) are presented in Fig. 4-8a, where also the compression/extension Critical State Lines, CSL, of the natural clay are included for comparison.

The slope of the compression and extension failure lines and tension failure line was determined from linear regression of q_f from the CIDC, CIDE-L and CIDE-U tests, respectively. All samples were consolidated in the quasi-overconsolidation region (σ_c'<σ_{qp}') prior to undrained shearing and the behavior of both compression and extension tests is very similar to the undrained behavior of overconsolidated cohesive soils. The effective stress paths of the undrained tests consolidated at low back pressure and σ_c' (corresponding to shallow depths) may have been influenced by the samples not being fully saturated. Due to the low positive Δu generated, the effective stress paths of CIUC and CIUE-L tests are located close to the stress paths of the corresponding drained tests. However, the low Δu generated is not believed to depend only on the degree of saturation but to a large extent on the *OCR*. Generally, low Δu are expected during shearing of heavily overconsolidated samples and very similar effective stress paths for fully saturated heavily overconsolidated samples were presented from CIUC and CIUC and CIUE-L tests on improved clay by Horpibulsuk et al. (2004) and Åhnberg (2007). This effect is very clear on the different extension stress paths. At low σ_c', the effective stress path of the CIUE-L and CIUE-U tests is initially very close to that of the CIDE-L and CIDE-U tests, resulting in a large difference in q_f. In CIUE-U tests with increasing σ_c', higher negative Δu are initially generated, making the effective stress path of these tests deviate to the right of the corresponding drained tests in the $p' - q$ plane. On the on the other hand, in CIUE-L tests with increasing σ_c' larger positive Δu are initially generated, causing the effective stress path of these tests to deviate to the left of the corresponding drained tests in the $p' - q$ plane. With increasing σ_c', and thereby also the Δu generated, the difference in effective stress paths and also q_f of CIUE-L, CIUE-UL and CIUE-U tests decreases and the stress paths of the undrained tests are located between the stress paths of the corresponding CIDE-L and CIDE-U tests. At the highest applied σ_c', at which stage the samples were also fully saturated, very similar effective stress paths were obtained in all three types of undrained extension/tension tests, although the difference in Δu between CIUE-L and CIUE-U was approximately 200 kPa at failure. For the CIUE-UL and CIUE-U test consolidated at low σ_c' (30 and 60 kPa), *OCR* $\geq$ 4, q_f was located on the tension failure line evaluated from CIDE-U tests, confirming that these tests failed in tension. On the other hand, q_f of CIUE-L and CIUE-UL and CIUE-U tests consolidated at higher values of σ_c' (90 and 150 kPa), OCR $\leq$ 2.7, was located between the evaluated tension and extension failure lines evaluated from CIDE-L tests.

The yield locus of the lime-cement improved clay is presented in Fig 4-8b and was evaluated by nonlinear regression of q_y, presented in Table 4-2 and 4-3, and the corresponding mean effective stress at yield, p_y', and defines the change from recoverable to irrecoverable strains. The shape of the yield locus is considerably rotated in the meridian plane indicating that the material exhibits significant anisotropy in the overconsolidated region. The intersection of the yield locus with the tension failure line in the negative stress region agrees with the observed behavior of the CIUE-U, CIUE-UL and CIDE-U tests conducted at low values of σ_c' for which a tension failure occurred prior to yielding. The yield locus was fitted with the relation proposed by Xiao et al. (2014):

$$\frac{q}{p_{iy}'} = N\sqrt{\left(\frac{p'}{p_{iy}'}\right) - \left(\frac{p'}{p_{iy}'}\right)^2} \tag{13}$$

by normalizing q and p' by the isotropic yield stress, p_{iy}', and is presented in Fig. 4-8c. A good agreement with the experimental data was obtained for N=1.70 in compression and N = -1.25 in extension. The value of N evaluated in compression is significantly smaller compared to N=3.65 proposed by Xiao et al. (2014), however, the N values obtained from these tests represent the yield locus at the change from recoverable strains to irrecoverable strains and not the primary yield stress.

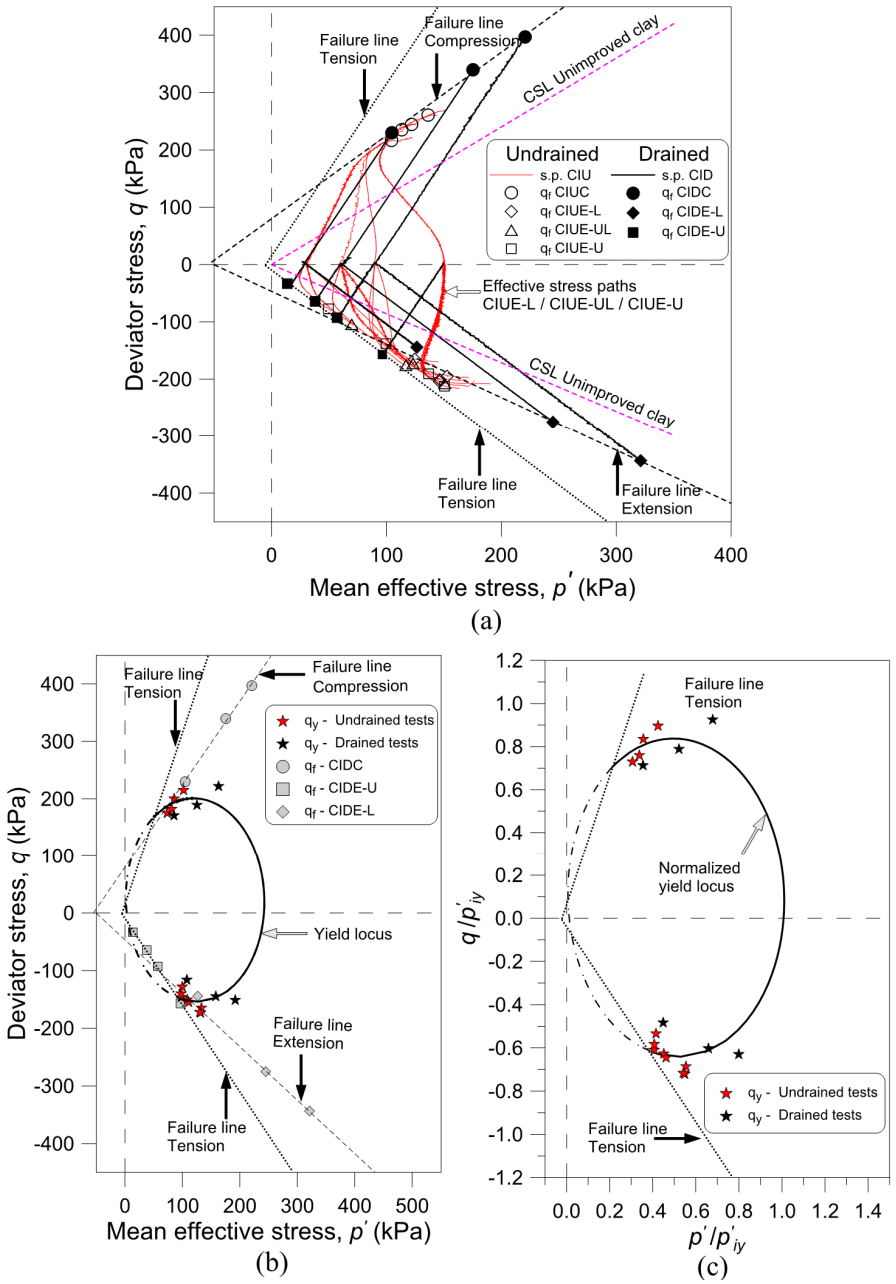

Fig. 4-8: (a) Effective stress paths of lime-cement improved clay; (b) Evaluated yield locus of lime-cement improved clay; (c) Yield locus normalized by isotropic yield stress of lime-cement improved clay.

4.4.3.3 Undrained strength

Test results strongly indicate that q_f is stress path dependent and the material exhibits significant stress-induced anisotropy at low values of σ_c'. A procedure that is extensively used to characterize the undrained strength of overconsolidated clays is the SHANSEP (Stress History And Normalized Soil Engineering Properties) procedure developed by Ladd and Foott (1974), where the undrained shear strength of the clay normalized by the effective vertical stress is related to OCR according to the relationship:

$$(s_u/\sigma_{vo}')_{OC} = a(OCR)^b \tag{14}$$

The parameter b is an empirical exponent and $a = (s_u/\sigma_{v0}')_{NC}$ is the normalized undrained shear strength of the NC clay.

Åhnberg (2006) showed that q_f of improved clay consolidated at stress levels below σ'_{qp} could be normalized analogous to Equation (14), presenting the following relationship between the normalized compressive strength and OCR:

$$\left(q_f/\sigma'_c\right)_{OC} = a_q(OCR)^b \tag{15}$$

For improved clay the OCR can be defined as:

$$OCR = \sigma'_{qp}/\sigma'_c \tag{16}$$

An analogous exponential function, where in addition to σ'_c an equivalent tensile stress was introduced to consider the cementation effect in the quasi-overconsolidated region, has been proposed by Kasama et al. (2006) to estimate the q_f of cement improved soils. Based on a large number of CIUC tests, Åhnberg (2006) proposed parameters a_q and b equal to approximately 1.0-1.2 and 0.9, respectively, for clays improved by means of different types of binders (fully saturated samples).

To determine whether the q_f of the lime-cement improved clay follows the SHANSEP normalization presented in Equation (15), the q_f normalized by σ'_c for the different stress paths investigated was plotted against OCR on a log-log scale, Fig. 4-9. The slope of a straight line in these plots is equal to the b parameter in Equation (15) while the intercept to the vertical axis at OCR=1 is the parameter a_q. For CIUC and CIUE-L tests, Figs. 4-9a and 4-9b, the relationship is almost a perfect straight line, which indicates a very good correlation between q_f and OCR, demonstrating the validity of Equation (15). The experimental data of the CIUE-UL and CIUE-U tests, Figs. 4-9c and 4-9d, show a slightly larger scatter. Nevertheless, the linear regression yielded R^2 values ≥ 0.9, indicating a correlation between OCR and q_f even for these tests. In both CIUC and CIUE-L tests, results clearly show that σ'_c has a minor influence on q_f for $\sigma'_c < \sigma'_{qp}$. Contrary to CIUC and CIUE-L tests, a significant decrease in q_f associated with a decrease in σ'_c was observed for CIUE-U tests at stress levels below σ'_{qp}. The experimental data points of both CIUE-L and CIUE-U tests consolidated at σ'_c = 150 kPa are located below the regression line, indicating that the linear regression on a log-log scale overestimates q_f in the range of $1 \leq$ OCR ≤ 2.

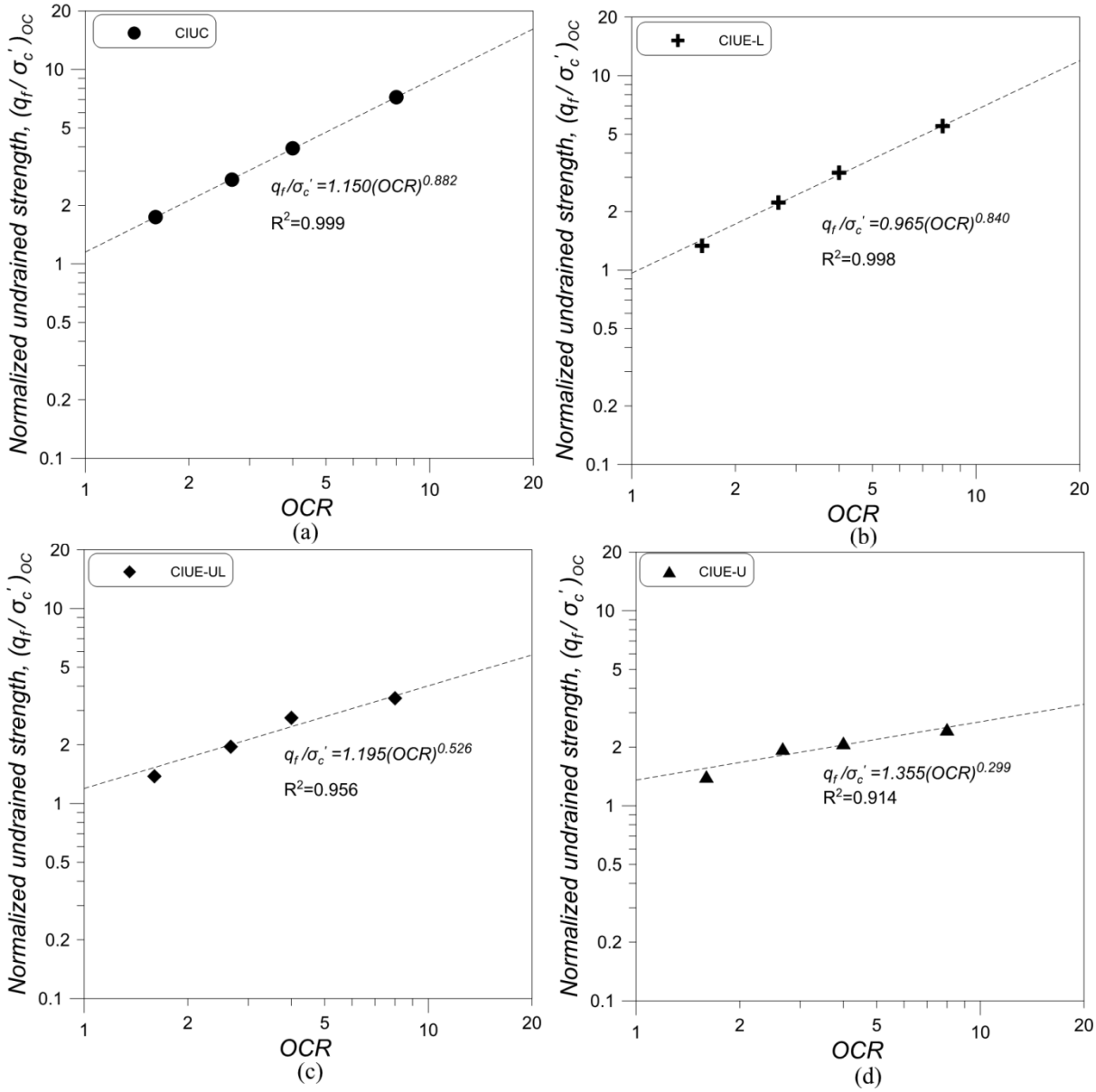

Fig. 4-9: Effect of the overconsolidation ratio on the normalized undrained failure strength: (a) CIUC tests; (b) CIUE-L tests; (c) CIUE-UL tests; (d) CIUE-U tests

A relationship between the normalized q_f and ln(OCR), presented in Fig 4-10, indicates a better agreement with the test data in the range of $1 \leq \text{OCR} \leq 2$ and also yield slightly higher R^2 values for the CIUE-UL and CIE-U tests compared to the linear regression. However, the number of tests is too small to draw any general conclusions and further investigations are needed in order to validate the presented relationships for these stress paths. The experimental data of CIUC and CIUE-L tests were compared to similar tests presented by other researchers, for which q_f, σ_c', and σ_{qp}' have been reported. The results of CIUC tests of cement admixed Ariake clay with a cement content of 9-18% conducted at $\sigma_c' < \sigma_{qp}'$ presented by Horpibulsuk et al. (2004) and the CIUE-L tests presented by Åhnberg (2007) on lime-cement admixed Linköping clay with a lime cement content of 70 kgm^3, are illustrated in Fig. 4-11. Although a slight change in the a_q and b parameters was predicted when all tests were considered, a very good agreement is obtained for both CIUC and CIUE-L that shows that Equation (14) is applicable to improved clays regardless of the amount and type of binder.

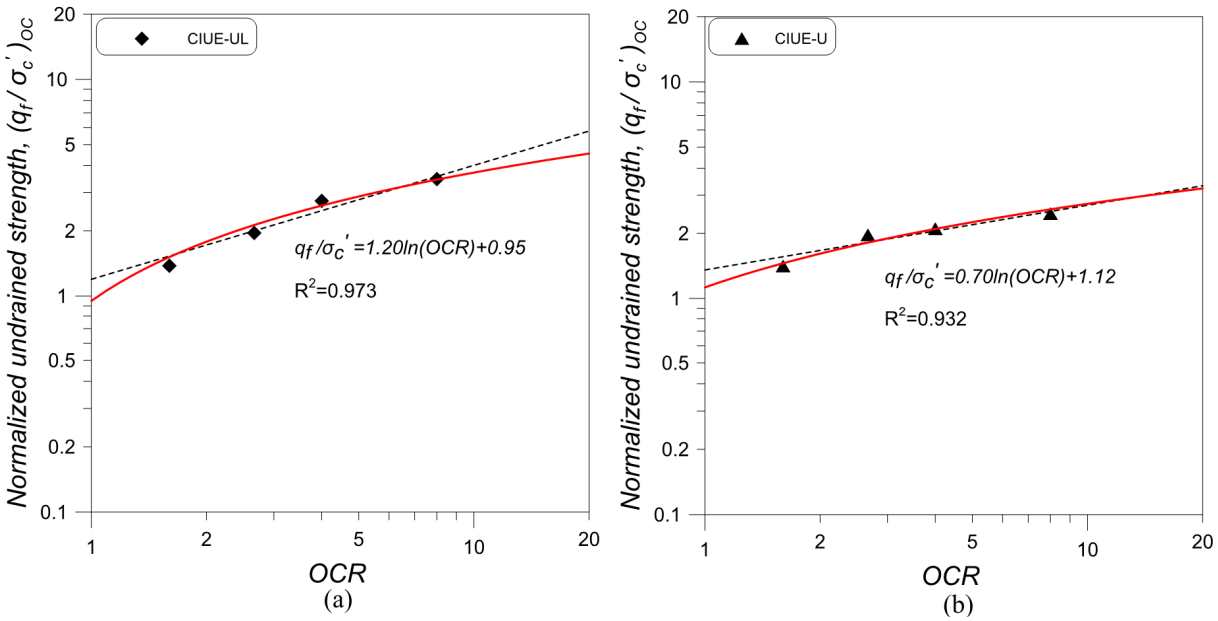

Fig. 4-10: Relationship between normalized failure strength and ln(OCR): (a) CIUE-UL tests; (b) CIUE-U tests

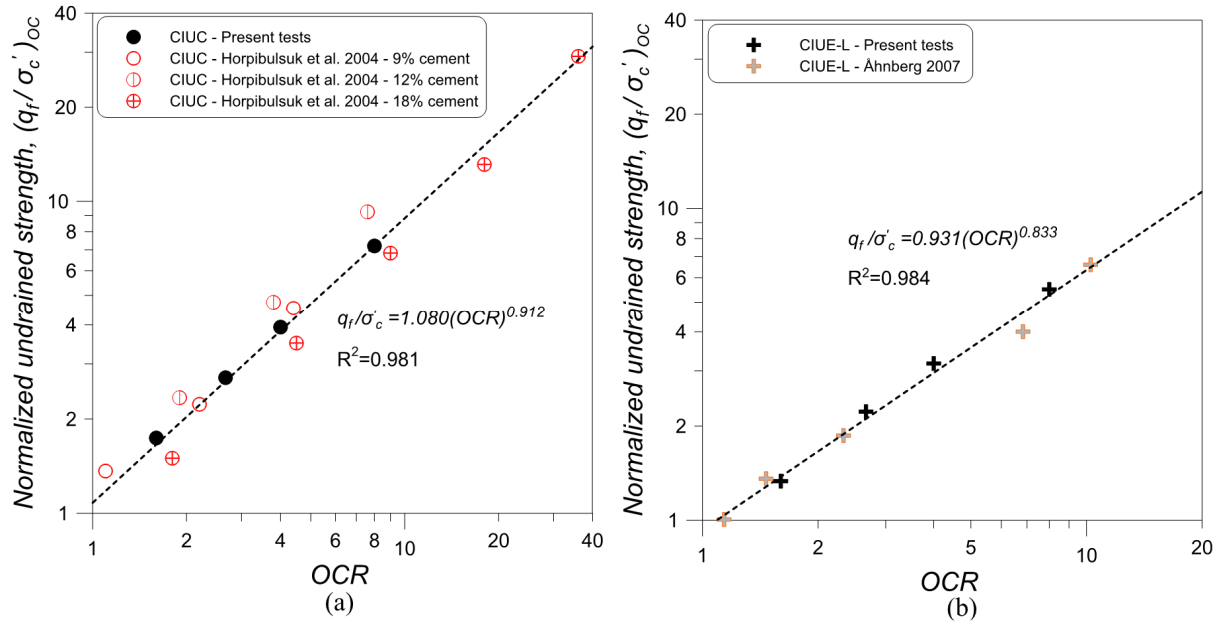

Fig. 4-11: Comparison of SHANSEP normalization for other reported improved clays: (a) CIUC tests; (b) CIUE-L tests

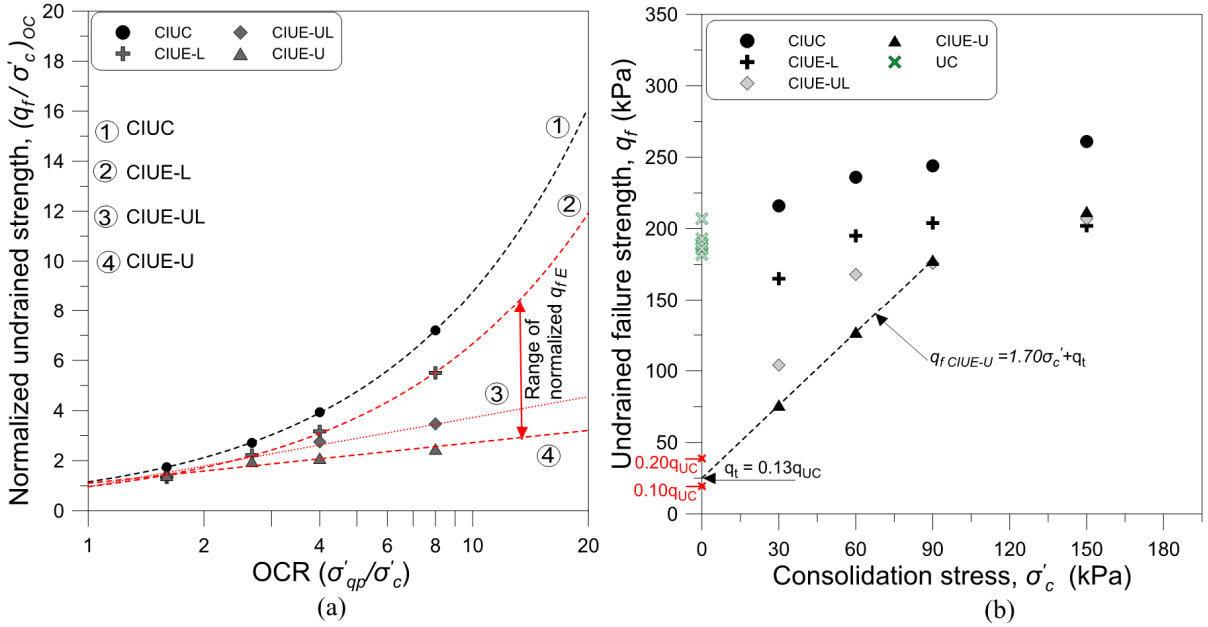

Fig. 4-12: (a) Range of normalized undrained strength; (b) Evaluation of unconfined tensile strength from CIUE-U tests.

Fig. 4-12a shows the range of the normalized undrained strength at different consolidation stresses lower than σ'_{qp}, i.e. in the overconsolidated region. The slope of the regression lines of CIUE-U tests shows that q_f at low values of σ'_c is significantly less influenced by *OCR* compared to CIUC and CIUE-L tests but is strongly related to the applied σ'_c in the overconsolidated region. The influence of σ'_c on q_f for CIUE-U tests is illustrated in Fig. 4-12b. A linear relationship between σ'_c and q_f is indicated up to a level of q_f approximately equal to q_{UC}. The intercept of the straight line of the CIUE-U tests with the vertical axis at σ'_c = 0 is analogues to q_t. A ratio q_t/q_{UC} equal to 0.13 is predicted by extrapolating the q_f of the CIUE-U tests, which is in good agreement with previously presented results regarding the unconfined tensile strength of different types of cement improved soils (Terashi et al. 1980, Koseki et al. 2005, Consoli et al. 2010 and 2012, Kitazume and Terashi 2013, Pan et al. 2016).

4.4.3.4 Drained strength

In recent years, some advanced constitutive material models describing the mechanical behavior of cemented soils have been proposed (Kasama et al., 2000, Liu and Carter 2002, Suebsuk et al. 2010 and 2011, Horpibulsuk et al. 2010, Horpibulsuk and Liu 2015, Nguyen et al. 2014, Arroyo et al. 2012, Robin et al. 2015, Xiao et al. 2017). In a majority of these models, an enlarged elliptical yield surface and a failure surface parallel to that of the untreated clay are adopted. The effect of bonding due to cementation as well as cementation degradation is considered in some of the models through a modified mean effective stress and by introducing model parameters and additional hardening rules to capture the hardening behavior up to peak stress and softening behavior post-peak. Although the main features of the material behavior from compression laboratory data are captured realistically, an isotropic yield and failure surface is assumed and the material strength is thereby independent of the direction of the principal stresses.

The results of the presented tests clearly show that a shear failure occurred for drained stress paths corresponding to axial and lateral loading while samples subjected to axial unloading stress paths failed in tension. Actually, the experimental data of these tests are conceptually similar to those presented by Namikawa and Mihira (2007) and Namikawa et al. (2017) from CIDC and CIDE-U tests

on cemented sand. It is often convenient to express the failure criteria in terms of stress invariants p' and q:

$$p' = (\sigma_1' + \sigma_2' + \sigma_3')/3 = I_1/3 = (\sigma_1' + 2\sigma_3')/3 \text{ (for } \sigma_2' = \sigma_3') \quad (17)$$

$$q = \sqrt{3J_2} = \sqrt{\frac{1}{2}[(\sigma_1' - \sigma_2')^2 + (\sigma_2' - \sigma_3')^2 + (\sigma_1' - \sigma_3')^2]} = \sigma_1' - \sigma_3' \text{ (for } \sigma_2' = \sigma_3') \quad (18)$$

where I_1 is the first invariant of the stress tensor σ_{ij}' and J_2 is the deviatoric stress tensor.

The Mohr-Coulomb failure function can be expressed in the general form of stress invariants p' and q as:

$$\mathrm{F}(\sigma_{ij}') = \sqrt{J_2}\left(\cos\theta - \frac{1}{\sqrt{3}}\sin\theta\sin\emptyset'\right) - c'\cos\emptyset' - p'\sin\emptyset' = 0 \quad (19)$$

where θ is the Lode's angle and the special case of axially symmetric triaxial compression and extension stress conditions are expressed by $\theta = \frac{\pi}{6}$ and $\frac{-\pi}{6}$, respectively. Equation (19) can be rewritten as:

$$F = q - Mp' - Nc' = 0 \quad (20)$$

where

$$M = \frac{3\sin\emptyset'}{\sqrt{3}\cos\theta - \sin\theta\sin\emptyset'} \quad (21)$$

$$N = \frac{3\cos\emptyset'}{\sqrt{3}\cos\theta - \sin\theta\sin\emptyset'} \quad (22)$$

The Mohr circles determined from the effective principal stresses at the axial strain corresponding to q_f from CIDC and CIDE-L tests are presented in Fig. 4-13 together with the Mohr circles of the CIDE-U tests. The results show that the failure strength of CIDC and CIDE-L tests is proportional to the normal stresses and the Mohr-Coulomb failure criterion, with $\emptyset'$ and c' according to Table 4.4, which have been superimposed in Fig. 4-13, can be employed with reasonable agreement with the experimental data for these stress paths.

Table 4-4: Evaluated material properties of Mohr-Coulomb failure criterion

Case	$\emptyset'$	c' (kPa)
Triaxial compression - CIDC	35.8°	40
Triaxial extension - CIDE-L	32.9°	32

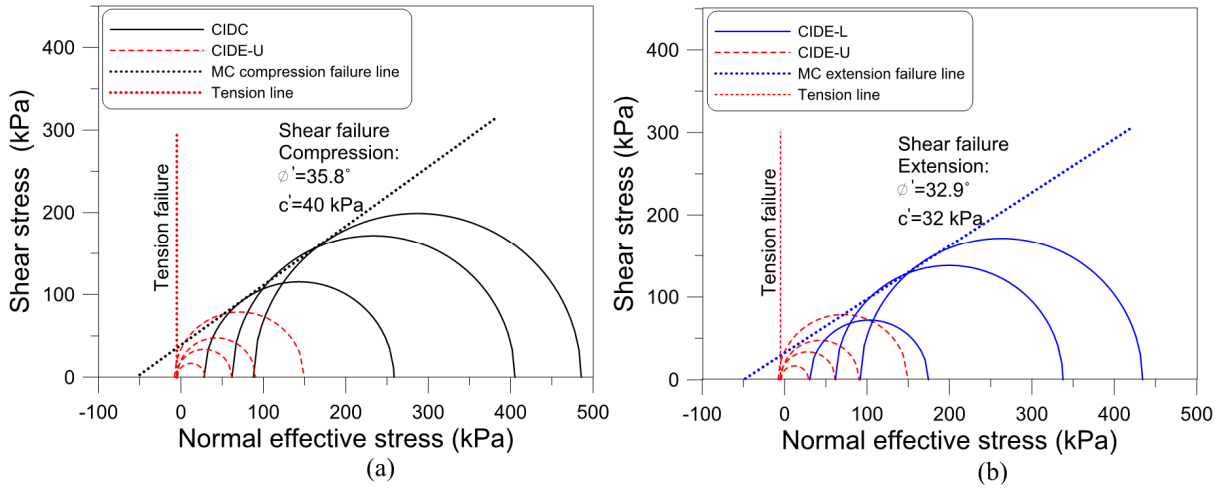

Fig. 4-13: Mohr's circles at failure: a) CIDC and CIDE-U tests; b) CIDE-L and CIDE-U tests

It is well recognized that both the friction angle and cohesion intercept for natural and cemented granular soils are stress path dependent and change with the change in ratio between the three main principal stresses, defined as $(\sigma_2 - \sigma_3)/(\sigma_1 - \sigma_3) = b$ where $b = 0$ for triaxial compression and $b = 1$ for triaxial extension, (Reddy and Saxena 1993, Matsuoka and Nakai 1974, Lade and Duncan 1973, 1975, among others). Generally, $\emptyset'$ and c' have been found to increase with increasing value of b. However, this material behavior could not be identified from these conventional compression and extension tests. On the contrary, the Mohr-Coulomb parameters of the shear failure $\emptyset'$ and c' from the CIDE-L tests were found to be lower compared to the CIDC tests. In order to investigate the effect of variation of the Lode's angle and to describe the failure criterion of lime-cement improved clay in the octahedral plane, further investigations under general stress path conditions where all three main principal stresses can be varied independently need to be conducted.

From the CIDE-U tests, the experimental data show that failure occurs when the minor principal stress reaches the tension strength line. According to Namikawa et al. (2017), the function for the tensile failure can be described as:

$$F_t(\sigma'_{ij}) = -\sigma'_3 - T_f = 0 \tag{24}$$

that can be expressed as:

$$F_t(\sigma'_{ij}) = \frac{2\sqrt{J_2}}{\sqrt{3}} \sin\left(\theta + \frac{2}{3}\pi\right) - p' - T_f = 0 \tag{25}$$

where T_f is the material tensile strength determined from direct tension tests.

By combining the two failure functions, the mean effective stress at the intersection between the tensile failure line and the compression failure line, $p'_{t\,min}$, and between the tensile failure line and the extension failure line, $p'_{t\,max}$, has been determined by Namikawa et al. (2017) as:

$$p'_t = \frac{c' \cos\emptyset' - T_f}{1 - \sin\emptyset'} + \frac{T_f \sin\emptyset' - c' \cos\emptyset'}{\sqrt{3}(1 - \sin\emptyset')} \tan\theta \tag{26}$$

where the value of p'_t changes depending on the value of θ.

For the special case of axially symmetric triaxial compression, $\theta = \frac{\pi}{6}$, and extension tests, $\theta = \frac{-\pi}{6}$, the intersection between the tension and shear failure line is thereby expressed as:

$$p'_{t\,min} = \frac{2c' \cos \emptyset' - (3 - \sin \emptyset')T_f}{3 - 3\sin \emptyset'},\ \theta = \frac{\pi}{6} \tag{27}$$

$$p'_{t\,max} = \frac{4c' \cos \emptyset' - (3 + \sin \emptyset')T_f}{3 - 3\sin \emptyset'},\ \theta = \frac{-\pi}{6} \tag{28}$$

The tensile strength evaluated as the minor principal stress at failure from CIDE-U tests, T_{fd}, is lower compared to q_t, which was determined from CIUE-U tests. These results show an analogous behavior with results presented by Namikawa et al. (2017) for samples with low cement content (q_u=500 kPa) for which the minor principal stress in a majority of the tests does not seem to reach the tensile strength line determined from the direct tension tests, while the minor principal stress in a majority of tests with high cement content (q_u= 2000 kPa) is in good agreement with T_f. The difference between q_t and T_{fd} observed for improved soil of low strength may be attributed to the development of negative Δu in the CIUE-U tests and probably also to the difference in strain rate between the test methods. In undrained tests at zero confining stress of high strength cement improved soil, lower excess pore pressure would be expected and the influence of the strain rate between test methods would also be of minor importance, resulting in a better agreement between direct tensile tests and CIDE-U tests.

By taking into consideration the difference in Mohr-Coulomb strength parameters, $\emptyset'$ and c', evaluated from the CIDC and CIDE-L tests, respectively, a better agreement with the experimental data from these tests is obtained if Equations (26) and (27) are modified as follows

$$p'_{t\,min} = \frac{2c'_c \cos \emptyset'_c - (3 - \sin \emptyset'_c)T_{fd}}{3 - 3\sin \emptyset'_c},\ \theta = \frac{\pi}{6} \tag{28}$$

$$p'_{t\,max} = \frac{4c'_e \cos \emptyset'_e - (3 + \sin \emptyset'_e)T_{fd}}{3 - 3\sin \emptyset'_e},\ \theta = \frac{-\pi}{6} \tag{29}$$

where $\emptyset'_c$, c'_c and $\emptyset'_e$, c'_e are the friction angle and cohesion intercept in compression extension, respectively, and T_{fd} is the tensile strength evaluated from drained unloading tests. The tension and shear failure function evaluated from Equations (18) and (24) is presented in Fig. 4-14 together with the experimental data. The experimental data indicate that a failure surface consisting of a tensile failure function and a shear failure function as proposed by Namikawa et al. (2017) can be adopted also for lime-cement improved clay.

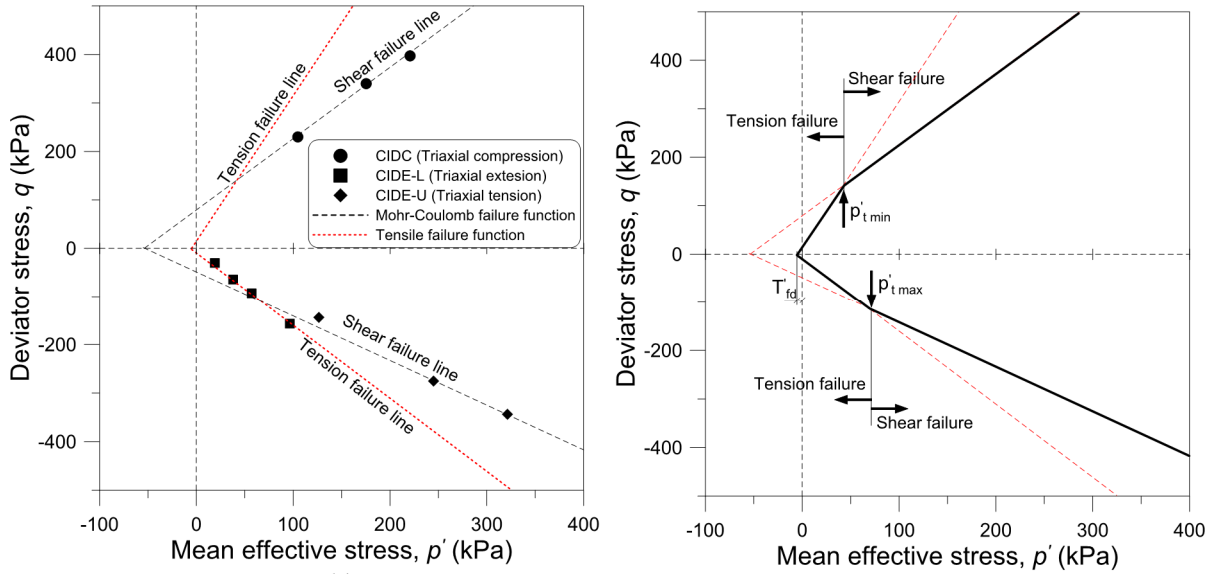

Fig. 4-14: (a) Deviator stress at failure from the experimental data in the p'-q plane; (b) Intersection of the tension and shear failure function according to Namikawa et al. (2017).

4.5 Summary

The main outcomes of the laboratory test on lime-cement improved clay are summarized as:

- The triaxial extension and tension tests showed a significantly more brittle material behavior compared to the triaxial compression tests, with very low strain at failure mobilized in the drained triaxial tension tests. Consequently, the strength of the improved and the natural soil may not be mobilized simultaneously in applications where the material is subjected to extension/tension loading.
- Samples with a degree of saturation below 98-99 % consolidated at low confining stresses behave as partly drained with effective stress paths close to those of the corresponding drained tests due to low positive excess pore pressure generated prior to failure. This behavior was found to agree with field behavior of DDM columns in field conditions.
- Samples consolidated at low effective stresses, i.e. heavily overconsolidated, subjected to undrained unloading conditions (tension or a combination of tension and extension) failed in tension while samples consolidated at high effective stresses, i.e. lightly overconsolidated, failed in a combination of shear and tension failure.
- A yield stress corresponding to the level where significant stiffness degradation occurs, equal to approximately 60-70% of the failure stress, was observed in both undrained compression and undrained extension tests that failed in shear.
- The relationship between the undrained failure strength normalized by the consolidation stress and OCR in both compression and extension could be accurately described by an exponential function, similar to the SHANSEP methodology.
- The experimental data of the drained tests show that a failure surface consisting of a shear failure function based on Mohr-Coulomb failure criterion and a tensile failure function based on the material's tensile strength and consolidation stress can be applied for lime-cement improved clay.

5. FE-ANALYSES OF FULL SCALE BRACED EXCAVATION IMPROVED BY DEEP MIXING COLUMN PANELS

5.1 Background and Study Objective

In this chapter finite element analyses of the experimental failure tests of the braced excavation supported by panels of DDM columns described in Chapter 3 and Paper II are presented.

Generally, the strength and stiffness properties of deep mixing columns are assessed from UC tests, and isotropic $s_{u\,col}$ or linear elastic material properties are commonly used in practice in the design of structures that include deep mixing columns (Navin 2005, Adams 2011, Jamsawang et al. 2015a, 2015b, 2016a, 2016b, 2017, Ignat et al. 2015). However, several researchers (Ou et al. 1996, Su 2009, Yang et al.2011) have highlighted that isotropic column strength may not represent the actual performance of deep mixing columns in the passive zone, introducing strength reduction factors to the material composite strength to consider stress-induced anisotropy. Despite the promising results obtained, these studies are generally based on hypothetical excavations and the pre- and post-failure behavior of a full-scale column type ground improvement supported excavation has not been documented in field conditions.

The current design methodology of ground improvement with lime-cement improved clay implemented in the Swedish design guidelines, TK Geo 13 (2014), Larsson (2006), is based on the assumption that the improved soil volume behaves as a composite material and the governing failure mode is a shear failure through the columns and the soil between the columns. The material properties of the improved soil volume are calculated as the weighted strength and stiffness properties of the DDM columns and the soil between the columns. A linear elastic-perfect plastic stress-strain behavior and full interaction between the DDM columns and the surrounding soil are assumed for "soft" columns ($s_{u\,col} \leq 100$ kPa). The column strength to be used in the design should be the lowest value between the drained and undrained column shear strength for the actual normal stress acting on the column. The drained strength, τ_{col}, of the columns is assumed to be proportional to the normal principal stress according to the Mohr-Coulomb failure criterion while $s_{u\,col}$ is chosen equal to 50 % of the UC strength but not higher than 100 kPa. Furthermore, for lime-cement columns installed in shear and passive zones, c' should be chosen equal to 15% and 0% of $s_{u\,col}$, respectively. These requirements result in a design where the effect of ground improvement conducted in shear and passive zones, especially to improve the stability of excavations where the main principal stress is decreasing, will be very limited.

The aim of this study is to investigate the performance of the numerical analyses compared to the experimental test results when the stress-strain behavior of the DDM column panels observed in the laboratory triaxial extension tests, described in Chapter 4, is considered. Undrained analysis were conducted with undrained strength and stiffness column properties evaluated from CIUE tests as well as drained strength and stiffness properties evaluated from CIDE tests. The results were compared with the experimental data of the field tests, presented in Chapter 3, but also with undrained analyses based on material properties chosen according to the current Swedish design guide.

5.2 Finite Element Model and Boundary Conditions

A full description of the finite element model is provided in Paper IV and is briefly summarized here. Analyses of 3D boundary problems with complex geometries (overlapping column panels), large differences in stiffness between interacting soil and structure elements in combination with advanced constitutive models for the soil properties require a very large computational effort. The geometrical model and the FE mesh of Test A are presented in Fig. 5-1.

In order to keep the computational time at a practical level, some simplifications, outlined below, were made in the FE model compared to the field tests:

- Only the DDM column panels in the passive zone of the SPW were modeled as "volume pile elements" while the area improved with a group of DDM columns installed in the active zone of the slopes (on the end sides) were modeled as a composite material
- The DDM columns were "wished in place", implying that no volume strain or disturbance of the clay parameters was taken into consideration
- To reduce the number of elements, the thickness of the frictional soil below the soft clay included in the model was only 2 m
- The ground surface and soil layers were assumed to be horizontal
- The time sequence was not taken into consideration in the analyses as both the excavation and the loading process were conducted over a relatively short period of time and undrained conditions prevailed.

A construction sequence similar to the construction sequence of the field tests was chosen assuming undrained conditions. Excavation to final depth was conducted in two steps and the strut system was activated after the first excavation step. The LDP, simulated as a rigid block (linear elastic material) with a thickness of 0.5 m and corresponding unit weight, was activated after the last excavation step. The loading process was simulated by activating a distributed load on top of the LDP. The load was increased in constant steps of 10 kPa until a failure collapse mechanism occurred, at which stage the calculations were terminated. The failure mechanism "soil body collapse" occurred in the analyses when the specified load increment for the stage in question could not be reached and the load applied is thereafter reduced in magnitude in five successive calculation steps, whereby the calculation was terminated. For comparison with the experimental tests, the maximum load that could be applied is presented as q_{peak} and the resulting load at "soil body collapse" is presented as q_{fail} .

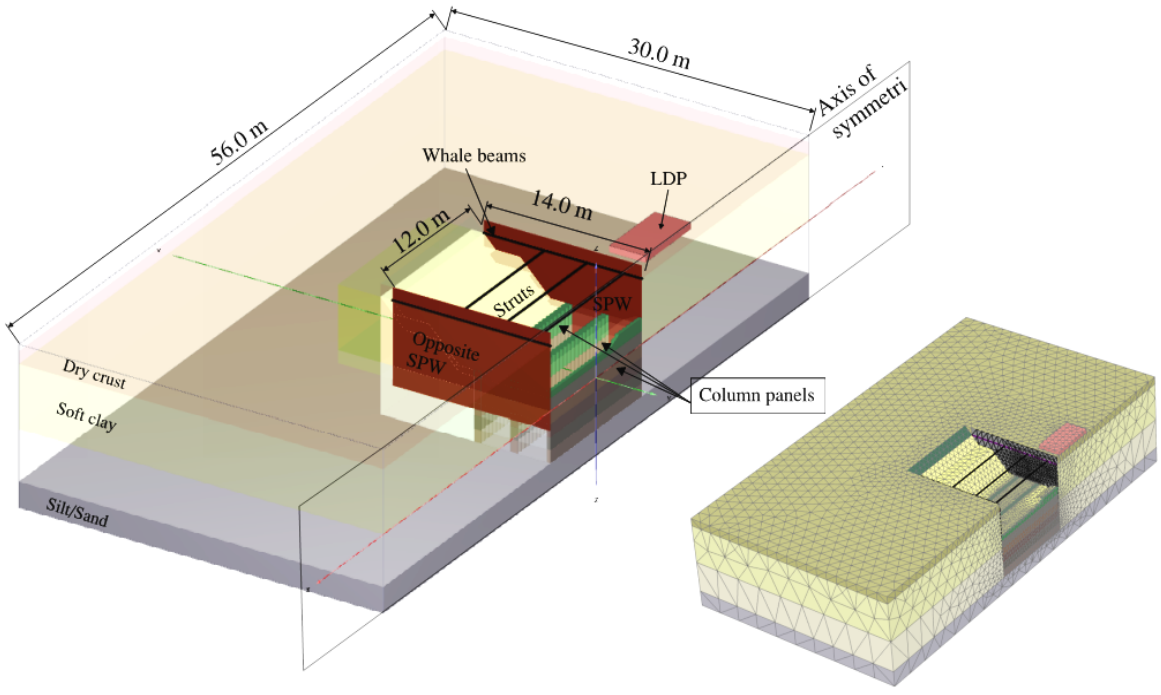

Fig. 5-1: Model geometry and FE-mesh of Test A

5.3 Constitutive Models and Model Parameters

Laboratory tests conducted on the natural clay show that the clay is very soft, lightly overconsolidated, highly sensitive, and exhibits significant fabric anisotropy. Furthermore, significant strain softening after the peak deviator stress was reached was observed in all triaxial tests, Fig. 3-3, a feature typical of very sensitive soft Scandinavian clays. This material behavior was expected to have an important impact on the test results. The constitutive material model adopted in this study for the soft clay, S-Clay1S, developed by Koskinen et al. (2002a) and Karstunen et al. (2005) originates from critical state models and is a further development of the S-Clay1 model, presented by Wheeler et al. (2003). Similar to S-Clay1, the model adopts an inclined yield surface to take into consideration initial anisotropy and a rotational component of hardening to represent the development of fabric anisotropy during plastic straining. In addition, the S-Clay1S model also incorporates the influence of bonding and destructuration by introducing an intrinsic yield surface, as presented by Gens and Nova (1993). Both S-Clay1 and its extension S-Clay1S have been successfully validated against experimental laboratory results for several typical Scandinavian soft clays (Koskinen et al. 2002b, Karstunen and Koskinen 2004 and 2008, Karstunen et al. 2005, Yildiz et al. 2009) and a full description of the model's mathematical formulation is presented by Sivasithamparam (2012). Calibration of the triaxial compression and extension tests and choice of material parameters used in these analyses are presented in Paper IV and are not repeated here.

The Hardening Soil model, HS, (Schanz et al. 1999) implemented in Plaxis was used to model the stress-strain behavior of the LCC. The HS model is an isotropic hardening double surface plasticity model that has proven to give realistic displacement results especially for excavation problems. The model combines the Mohr-Coulomb failure criterion with a hyperbolic stress-strain relationship that allows for stiffness degradation. Similar to critical stress models, different stiffness moduli are adopted in HS for primary loading and unloading-reloading conditions. The model cannot consider stress-induced strength anisotropy that was observed in the triaxial undrained tests at low σ_c'. The model's limitation was bridged for the analyses conducted with undrained material properties by choosing a direct input of $s_{u\,col}$ using ϕ_{col}'=0 and $c_{col}' = s_{u\ col}$, where $s_{u\ col}$ increased with depth according to the relationship between the normalized q_f and $\ln(OCR)$ obtained from the CIUE-UL tests. Calibration of the triaxial extension tests and choice of undrained material parameters for the DDM columns are also presented in Paper IV.

In order to compare the field test results with the design methodology implemented in the current Swedish Design Guide, TK Geo 13, analyses of both field-scale tests were also conducted by assessing drained material properties for the DDM columns. For the analyses representing the drained failure function presented in Chapter 4, material properties evaluated from the CIDE-L tests were selected to describe the shear failure surface together with a tension strength equivalent to the minor principal stress at failure evaluated from the CIDE-U tests. The HS model requires three stiffness parameters, $E_{50}^{\prime\,ref}$, E_{oed}^{ref} and E_{ur}^{ref}, that are stress-dependent reference stiffnesses, and hence not model constants. As the DDM column panels are located in the passive zone of the SPW and subjected to both unloading and lateral loading conditions, an E_{50}^{ref} based on the results of CIDC tests would significantly underestimate the "real" stiffness of the columns. As a consequence, $E_{50}^{\prime\,ref}$ was evaluated from the CIDE-U tests. The relationship between the actual modulus and the reference modulus in HS is expressed according to Schanz et al. (1999) as:

$$E_{50}' = E_{50}^{\prime\,ref}\left(\frac{c'\cos\emptyset' + \sigma_3'\sin\emptyset'}{c'\cos\emptyset' + p^{ref}\sin\emptyset'}\right)^m \tag{31}$$

where p^{ref} is the reference pressure of 100 kPa and m is an exponent controlling the stress dependency. By plotting $\ln(E_{50}')$ versus $\ln\left(\frac{c'\cos\emptyset' + \sigma_3'\sin\emptyset'}{c'\cos\emptyset' + p^{ref}\sin\emptyset'}\right)$ and fitting a linear regression line of the experimental data, the y intercept gives the value of $\ln(E_{50}^{\prime\,ref})$ and the slope of the straight line gives the value of m, as presented in Fig 5-2.

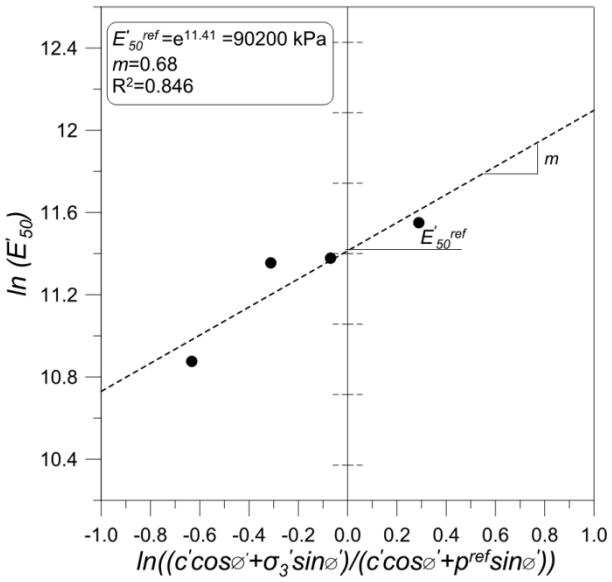

Fig. 5-2: Method of determination of $E_{50}^{\prime\,ref}$ from drained triaxial tests

Table 5-1: Material properties of DDM columns used in FE-analyses

DDM columns	**Material parameters evaluated from triaxial test results**	**Material parameters according to the Swedish Design Guide – TK Geo 13**
Material model	Hardening Soil	Mohr-Coulomb
Material behavior	Undrained Strain hardening with MC failure criterion	Undrained Linear elastic with MC failure criterion
Unit weight, $\boldsymbol{\gamma}$ (kN/m^3)	0-5 m depth:15.4 [1)] > 5 m depth: 17.1 [1)]	0-5 m depth:15.4 [1)] > 5 m depth: 17.1 [1)]
Vertical pre-overburden pressure, POP (kPa)	200 [2)]	-
Friction angle, $\boldsymbol{\phi'}$	33°	32° [3)]
Cohesion intercept, $\boldsymbol{c'}$(kPa)	32	0.1 [3)]
Secant stiffness, $\boldsymbol{E_{50}^{\prime\,ref}}$ (kPa)	90 000	-
Tangent stiffness, $\boldsymbol{E_{oed}^{ref}}$ (kPa)	$E_{50}^{\prime\,ref}$	-
Unloading/reloading stiffness, $\boldsymbol{E_{ur}^{ref}}$ (kPa)	$2.5E_{50}^{\prime ref}$	-
Power of stress level dependency, $\boldsymbol{m}$	0.7	-
Failure ratio, $\boldsymbol{R_f}$	0.9	-
Poisson's ratio for unloading/reloading, $\boldsymbol{\upsilon'_{ur}}$	0.2	-
Young's modulus, $\boldsymbol{E}$, (kPa)	-	19 300[3)]
Poisson's ratio, $\boldsymbol{\upsilon}$	-	0.30

[1)]Chosen equal to the unit weight of the clay layers
[2)]Evaluated as σ'_{qp}-σ'_{v0} at a depth of 5.0 m below the ground level
[3)]Chosen according to the Swedish Design guide

The effect of increasing effective vertical stress on $s_{u\,col}$ and τ_{col} based on the triaxial extension tests' results and also the current design methodology down to a depth of 25 m below ground surface (the maximum depth at which lime-cement columns are installed in Sweden) are presented in Fig. 5-3a-b.

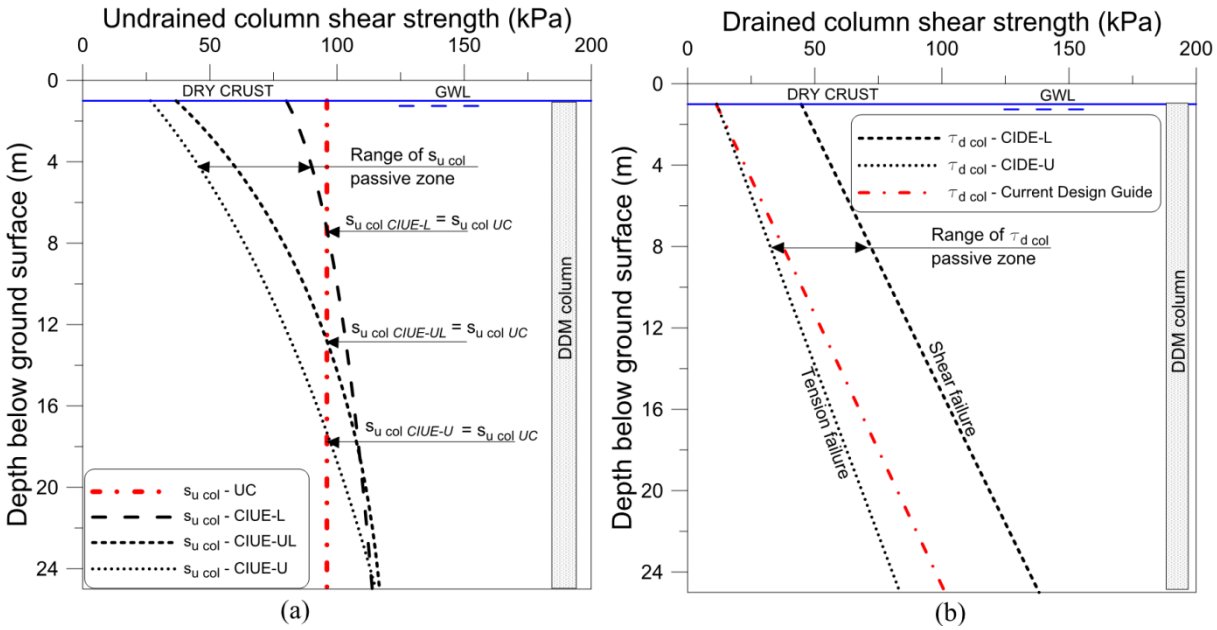

Fig.5-3: Change in column strength with depth according to laboratory test and current design guide: a) Undrained shear strength; b) Drained shear strength

5.4 Analysis Results

The results of the analyses conducted with undrained material parameters for the DDM columns and a comparison with the experimental test data are presented in Paper IV. In this chapter, in addition to the analyses conducted with undrained material parameters the results of the analyses conducted with drained material parameters for the DDM columns are also presented and discussed.

5.4.1 Failure load

The failure mechanism "soil body collapse" in Plaxis occurred when the specified load increment for the stage in question was not reached and the applied load was reduced in magnitude in five successive calculation steps, whereby the calculation was terminated. For comparison with the experimental tests, the maximum load that could be applied before reduction was chosen to be q_{peak} and the resulting load at "soil body collapse" was chosen to be q_{fail} . Evaluated $q_{peak\ FE}$ and $q_{fail\ FE}$ from the FE analyses are presented in Table 5-2 and Table 5-3, respectively, for both types of analyses conducted. Failure load predicted by analyses conducted with material properties evaluated from the triaxial extension tests was overall in good agreement, less than 10 % deviation, with the failure load of the experimental tests, $q_{fail\ exp}$. The observed failure in Test A was initiated in the clay between the DDM column panels due to the large panel center distance of 3.0 m, immediately followed by failure of the DDM columns in the panels closest to the SPW. The post-peak behavior of the clay thereby has a major influence on the magnitude of $q_{fail\ FE}$ in Test A. Observed $q_{fail\ exp}$ as well as the failure mechanism of Test B, failure simultaneously initiated in the clay and DDM column panels, were very well predicted by the FE analyses. For a center spacing between the panels of 1.5 m as in Test B, the properties of the DDM columns have a larger impact on the failure mechanism compared to Test A. On the other hand, analyses with material properties according to the Swedish Design Guide deviated significantly from the experimental data. The magnitude of $q_{fail\ FE}$ predicted in the analyses with $s_{u\ col}$ based on UC tests overestimated $q_{fail\ exp}$ in both Test A and Test B. As expected, $q_{fail\ FE}$ predicted by the analyses conducted with drained material properties according to the Swedish Design Guide underestimated $q_{fail\ exp}$ in both experimental tests and in Test B failure occurred before the first loading stage (prior to unloading, further excavation to level +1.0 and reloading until failure) could be completed.

The effect of ground improvement on predicted $q_{fail\ FE}$ was investigated by excluding the DDM column panels in the FE-model, here called Case C, and performing a similar undrained analysis of an excavation to a depth of 4.5 m followed by loading to failure. Obtained $q_{peak\ FE}$ and $q_{fail\ FE}$ from this analysis were 14.9 kPa and 14.6 kPa, respectively, significantly lower than the predicted $q_{peak\ exp}$ and $q_{fail\ exp}$ of Test A and Test B. A comparison between the analyses excluding the DDM column panels and those performed with drained material properties according to the Swedish Design Guide are presented in Table 5-4. The results clearly show that the current design methodology of assessing the column strength parameters significantly underestimates the effect of ground improvement by means of DDM columns installed in the passive zone.

Table 5-2: Predicted failure load by numerical analyses: Test A

Test	**Triaxial extension tests**	**Column shear strength**	$q_{peak\ FE}$ **(kPa)**	$q_{fail\ FE}$ **(kPa)**	$\frac{q_{fail\ FE}}{q_{fail\ exp}}$
A	Undrained (Anisotropic strength)	$s_{u\ col} = 0.5\sigma_c'(1.2ln(OCR) + 0.95)$	41.6	41.0	1.05
A	Drained	$\tau_{col} = c' + \sigma_n' \tan \emptyset'$ c'=32 kPa ; $\emptyset'$=33°	43.0	42.6	1.09
	Current Design Guide TK Geo 13	**Column shear strength**	$q_{peak\ FE}$ (kPa)	$q_{fail\ FE}$ (kPa)	$\frac{q_{fail\ FE}}{q_{fail\ exp}}$
A	Undrained (Isotropic strength)	$s_{u\ col} = 0.5q_{UC}$	51.5	50.9	1.31
A	Drained	$\tau_{col} = c' + \sigma_n' \tan \emptyset'$ c'=0 kPa ; $\emptyset'$=32°	21.2	19.8	0.51

Table 5-3: Predicted failure load by numerical analyses: Test B

Test	**Triaxial extension tests**	**Column shear strength**	$q_{peak\ FE}$ **(kPa)**	$q_{fail\ FE}$ **(kPa)**	$\frac{q_{fail\ FE}}{q_{fail\ exp}}$
B	Undrained (Anisotropic strength)	$s_{u\ col} = 0.5\sigma_c'(1.2ln(OCR) + 0.95)$	50.7	49.8	0.99
B	Drained	$\tau_{col} = c' + \sigma_n' \tan \emptyset'$ c'=32 kPa ; $\emptyset'$=33°	47.1	46.3	0.92
	TK Geo 13	**Column shear strength**	$q_{peak\ FE}$ **(kPa)**	$q_{fail\ FE}$ **(kPa)**	$\frac{q_{fail\ FE}}{q_{fail\ exp}}$
B	Undrained (Isotropic strength)	$s_{u\ col} = 0.5q_{UC}$	57.3	57.1	1.13
B	Drained	$\tau_{col} = c' + \sigma_n' \tan \emptyset'$ c'=0 kPa ; $\emptyset'$=32°	31.1*	30.1*	- *

* *Failure occurred during the first loading stage before unloading and additional excavation to level +1.0.*

Table 5-4: Effect of DDM column panels according to the Swedish Design Guide

Test	Column shear strength	Excavation depth before loading (m)	$q_{peak\ FE}$ (kPa)	$q_{fail\ FE}$ (kPa)
Case C	No DDM column panels	4.5	14.9	14.6
A	$\tau_{col} = c' + \sigma_n' \tan \emptyset'$ c'=0 kPa ; $\emptyset'$=32°	4.5	21.2	19.8
B	$\tau_{col} = c' + \sigma_n' \tan \emptyset'$ c'=0 kPa ; $\emptyset'$=32°	4.5	31.1	30.1

5.4.2 Effect of DDM column panels on failure mechanism of structure

The deformation pattern of the SPW is a good indication of how the DDM column panels influence the failure mechanism of the structure and predicted horizontal deformation of the SPW, $u_{h\ SPW}$. The results of the FE-analyses of both tests and also of the analyses with the DDM column panels excluded are presented in Fig. 5-4. By dividing the total horizontal deformations of the SPW in horizontal deformations due to translation, rotation, and bending, respectively, the change in failure mechanism is evident. Without the support provided by the DDM column panels, large $u_{h\ SPW}$ were predicted at the toe of the SPW on the loading side due to the low strength and stiffness properties of the clay. The rotation center of the loaded SPW is located at the bracing level due to the weak support below the bottom of the excavation resulting in large rotational displacements at the toe of the SPW.

The DDM column panels in Test A and Test B act as support for the SPW, reducing $u_{h\ SPW}$below the bottom of the excavation due to significantly higher strength and stiffness. In addition, with an increasing improvement ratio, the soil behind the opposite SPW is mobilized to a greater depth due to the change in location of the rotational displacements of the SPW. With increasing stiffness below the bottom of the excavation the rotation center is shifted downward in both Test A and Test B, as shown in Fig 5-4. In Test A, s_{panel}=3.0 m, a small inward rotation of the loaded SPW at the bracing level is predicted, suggesting that the support provided by the bracing system and the improved soil below the bottom of the excavation are of the same magnitude. In Test B on the other hand, s_{panel}=1.5 m, for the initial loading stage a significantly larger inward rotation of the loaded SPW at the bracing level was indicated due to increased stiffness below the bottom of the excavation, resulting in a higher mobilization of the soil behind the opposite SPW. However, in the last loading stage after the additional excavation, the rotation center of the SPW was shifted and increasing rotation-induced displacements were indicated at the toe of the SPW. The change in rotation-induced displacements from the bracing level to the toe of the SPW predicted in Test B is due to significant yielding and stiffness degradation and finally failure of the columns during the last loading stage, whereby the support below the bottom of the excavation was erased.

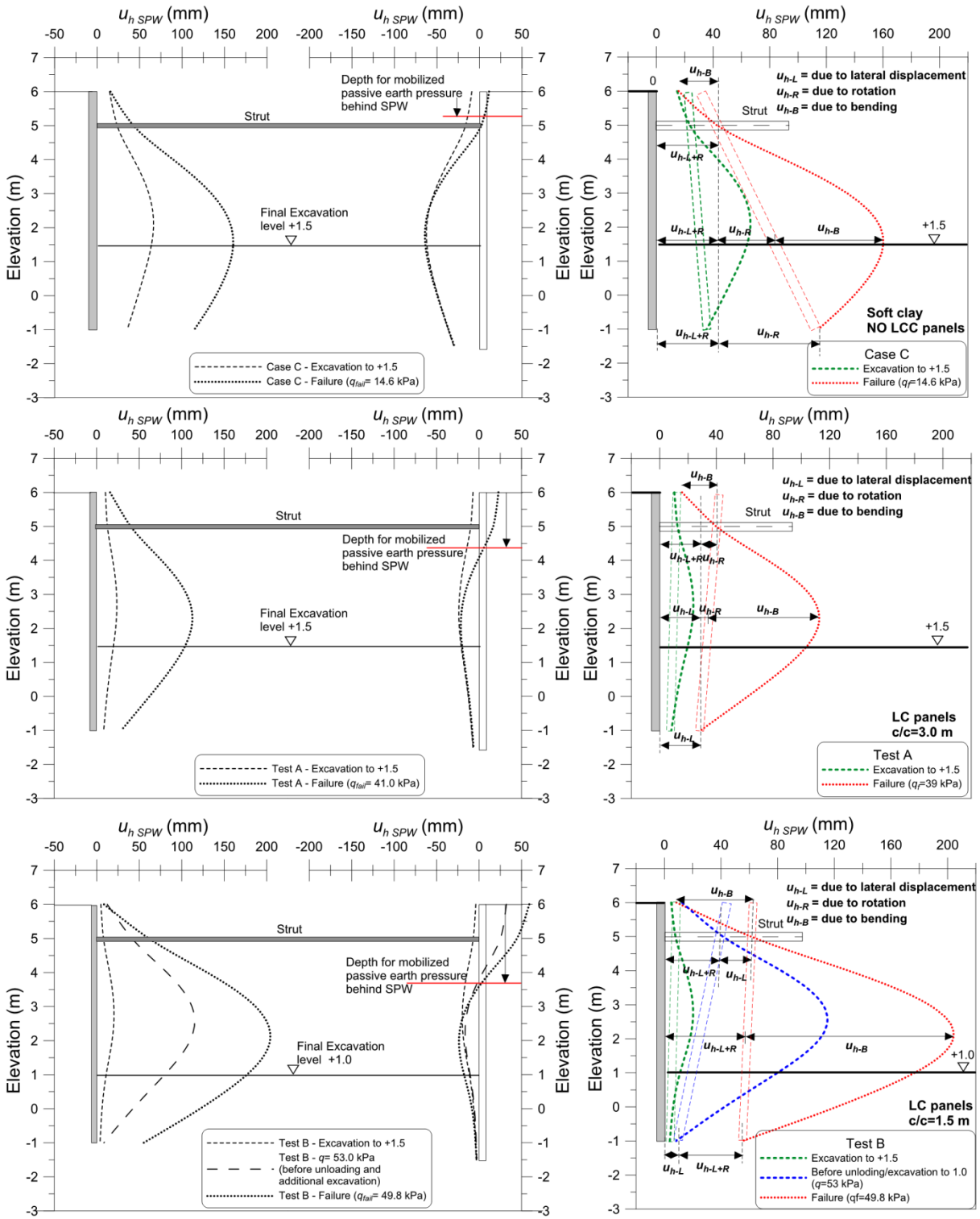

Fig. 5-4: Effect of DDM column panels on the failure mechanism of the sheet pile wall

5.5 Summary

The main outcomes of the FE-analyses are summarized as:

- Predicted failure load obtained from analyses with undrained as well as drained material properties based on results of triaxial extension/tension tests show a reasonably good agreement with the experimental data. This shows that stress-induced strength anisotropy of lime-cement improved clay needs to be considered when the stress path for the field conditions in question differs from that encountered in conventional laboratory testing.
- The FE-analyses conducted with undrained column strength and stiffness parameters evaluated from unconfined compression tests over-predicted the observed failure in both Test A and Test B. On the other hand, the results of similar analyses conducted with drained column strength and stiffness parameters evaluated according to the current Swedish Design Guide proved to be very conservative as these analyses significantly under-estimated the observed experimental failure load of both tests.
- The FE-analyses show that the DDM column panels installed in the passive zone act as support below the bottom of the excavation, giving a strut-like effect and thereby reducing lateral displacements of the SPW below the bottom of the excavation. An increasing area improvement ratio (i.e. decreasing center distance between DDM panels), changes the failure mechanism of the SPW by shifting the location of the rotation center of the SPW from the bracing level toward the toe of the SPW due to increased stiffness of the soil below the bottom of the excavation.
- A reasonably good agreement between predicted and measured horizontal displacements was obtained for the excavation stages of both tests. With increased loading, the predicted displacements mainly followed the observed trend even though the magnitude of calculated displacements did not exactly match the observations. This also shows that in order to predict reasonable deformations, which can be of vital importance during excavations in urban areas, column stiffness properties relevant for the conditions in question, i.e. unloading and lateral loading conditions, need to be considered in the design.
- Predicted strut forces at failure in Test A were in very good agreement with observed values. However, the constitutive model could not capture the post-peak stress-strain behavior of the DDM column panels, resulting in underestimation of the strut forces at failure in Test B.

6. SUMMARY OF APPENDED PAPERS

6.1 Paper I

Two- and three-dimensional analyses of excavation support with rows of dry deep mixing columns

Razvan Ignat, Sadek Baker, Stefan Larsson and Sven Liedberg

Published in *Computers and Geotechnics* (2015), Vol.66, p.16-30

The objective of this paper was to investigate the performance of a 2D model of an excavation with a tied-back sheet pile wall in interaction with perpendicular rows of overlapping DDM columns compared to a more realistic 3D model. A method to take into consideration the effect of the overlap zones between the columns in the 2D model, where the improved soil was assessed as a composite material, was investigated and the results of the 2D and 3D analyses were compared with a focus on predicted failure load, failure mechanism, and deformations. The results of these analyses demonstrate that by taking the effect of the overlap zone between columns installed in a row pattern into account, a 2D plane strain model shows reasonably good agreement regarding obtained deformations compared to a 3D model as long as the stress level in large parts of the improved soil does not reach the stated yielding criteria. The area improvement ratio of the improved soil and the quality of the overlap zone have a significant influence on how well a 2D model that incorporates the overlap zone between the columns performs compared to a 3D model.

6.2 Paper II

Behavior of braced excavation supported by panels of deep mixing columns

Razvan Ignat, Sadek Baker, Sven Liedberg and Stefan Larsson

Published in *Canadian Geotechnical Journal* (2016), Vol. 53(10), p. 1671-1687

This paper presents the instrumentation, execution and performance of two full-scale tests where a braced steel sheet pile wall interacting with rows of overlapping dry deep mixing columns was excavated and then loaded to failure. The purpose of the tests was to provide understanding of the behavior of deep mixing column panels located in a passive zone and interacting with a retaining structure. Both tests were extensively instrumented on both the active and passive side of the retaining structure. A stability failure of the retaining structure was the observed external failure mechanism of both tests, resulting in heave at the bottom of the excavation and large settlements of the ground surface behind the sheet pile wall. In the first test, with a distance between the column panels of 3.0 m, a very brittle failure developed suddenly in the clay between the panels with small deformations prior to failure. In the second test, with a distance of 1.5 m between the column panels, the failure developed in both the DDM column panels and the clay between the panels. Although a similar external failure mechanism developed, measured horizontal displacements, horizontal stresses, and pore pressure responses prior to failure differed between the two tests.

6.3 Paper III

Triaxial Extension and Tension behavior of lime-cement improved clay

Razvan Ignat, Sadek Baker, Martin Holmén and Stefan Larsson

Submitted to *Soils and Foundation*

This paper presents the results of a series of consolidated triaxial compression, extension, and tension tests on lime-cement improved clay. The different stress paths to failure, with the purpose to reflect the stress path to failure from the field-scale tests, were obtained by varying the direction of the major and minor principal stresses in a conventional triaxial test cell. From the undrained tests conducted at low consolidation stresses, corresponding to a depth of approximately 10 m below the ground surface, significant stress-induced anisotropy was observed depending on the direction of the major and minor principal stresses. Based on undrained triaxial test results, a relationship between the undrained strength, effective consolidation stress, and OCR is presented for different stress paths to failure. The results of drained triaxial tests demonstrate that for lime-cement improved clay the material behavior can be well represented by a shear failure surface, controlled by cementation bonds and friction angle, and a tension failure surface, controlled by the materials' tensile strength.

6.4 Paper IV

Numerical analyses of an experimental full scale excavation supported by panels of lime-cement columns

Razvan Ignat, Sadek Baker, Minna Karstunen, Sven Liedberg and Stefan Larsson

Submitted to *Computers and Geotechnics*

In this paper the influence of ground improvement with DDM panels of overlapping lime-cement columns on the behavior of a braced excavation loaded to failure is studied through 3D numerical analyses and compared with the reported experimental failure tests. The pre-failure strain hardening behavior observed from the triaxial tests on lime-cement improved clay was considered by using the HS model to describe the stress-strain behavior of the lime-cement column panels installed in the passive zone. The undrained shear strength dependency of the stress path to failure was considered by assessing a strength criterion based on results from isotropically consolidated undrained triaxial extension tests conducted under stress paths to failure similar to theoretical stress paths in the experimental LCC panels. The results of this study show that stress-induced strength anisotropy of lime-cement improved clay needs to be considered when the stress path for the field conditions in question differs from that encountered in conventional laboratory testing. Predicted failure load and also the location of the failure surface predicted by analyses conducted with column strength parameters evaluated from undrained triaxial extension tests were in good agreement with the obtained experimental tests results. On the other hand, analyses conducted with column strength parameters evaluated from unconfined compression tests significantly over-predicted the load at failure from the experimental tests. The analyses also show that in addition to strength parameters, the modulus of deformation consistent with the actual encountered stress path needs to be considered in order to predict reasonable results.

7. CONCLUSIONS AND FUTURE RESEARCH

This thesis presents results of the behavior of DDM column panels acting as excavation support and subjected to unloading and lateral loading conditions based on full-scale tests, laboratory tests, and numerical analyses. The main conclusions of the studies incorporated in this thesis are summarized below.

Summarizing the most important findings and conclusions from this study:

- Lime-cement columns panels installed in the passive zone acting as excavation support for a sheet pile wall will significantly increase the stability of the structure.
- Lime-cement column panels installed as excavation support are highly effective in reducing excavation induced displacements that can be of major concern for deep excavations conducted in areas with soft clay layers.
- The undrained strength of lime-cement improved clay at low consolidation stresses, representative of shallow depths in field conditions, is dependent of the stress path to failure and it was found to be significantly lower for unloading stress paths compared to lateral loading stress paths, i.e. stress induced anisotropy.
- The Young's Modulus of lime-cement improved clay evaluated from undrained triaxial extension tests was significantly higher, 2.7 to 4.1 times, compared to the corresponding Young's Modulus evaluated from the undrained triaxial compression tests. Also, significantly more brittle stress-strain behaviour was observed for triaxial extension tests compared to triaxial compression tests, regardless of applied stress path to failure and type of test, i.e. undrained/drained.
- Results of the Finite Element analysis of the conducted experimental tests show that the current Swedish Design Guide for lime-cement columns installed in the passive zone overestimates the material undrained strength but also significantly underestimates the material drained strength. Since the Swedish Design Guide specifies that the lowest of the undrained/drained strength should be chosen in the design of lime-cement columns the consequence is often a too conservative design as the strength increase in the improved clay is not properly considered.

Some suggestions for future research are presented below:

- Generally, for construction of larger structures, the retaining structure and the DDM columns installed in the passive zone to support the excavation will be active under a considerably longer period of time compared to the full-scale tests conducted in this study. Also, the triaxial tension tests conducted on lime-cement improved clay revealed a significant difference between the drained and undrained failure strength for unloading stress paths related to the generation of negative excess pore pressures in the undrained tests. It is therefore important to investigate the long term behavior of DDM columns subjected to unloading stress paths in field conditions in future projects.
- The triaxial extension tests showed that failure occurs along a randomly located horizontal plane, indicating that for an extension type of test failure takes place along a weakness plane that depends on the quality and homogeneity of the actual sample tested. However, this test series was only conducted on laboratory-mixed samples for which the samples are expected to be more homogeneous compared to in situ DDM columns. The effect of "poor" mixing on the strength of in situ DDM columns subjected to lateral loading or unloading conditions needs to be investigated by means of laboratory tests on trimmed field columns.
- Future testing conducted with techniques adequate for partly saturated soils (measurement of suction and pore air pressure) and local strain transducers/bender elements is recommended in order to adequately understand the effect of sample saturation and small strain behavior for lime-cement improved clay. Also, the effect of the intermediate principal stress on the material strength needs to be investigated in order to completely describe the material failure surface in the π plane by means of tests where all three major principal stresses can be varied independently, i.e. "true" triaxial tests.
- Further work on developing a constitutive model that can adequately describe the material shear and tension failure incorporating stress-induced anisotropy and degradation of cementation bonds in the normally consolidated region is needed.

REFERENCES

Adams, TE., 2011. Stability of levees and floodwalls supported by deep-mixed shear walls: five case studies in the New Orleans area. PhD dissertation, Virginia Polytechnic Institute and State University, Blacksburg VA.

Adams, T.E., Filz GM., Cali PR., Woodward ML., 2008. Stability Analyses of a Levee on Deep-Mixed Columns, Plaquemines Parish, Louisiana. ASCE Geotechnical Special Publication No. 178, p. 708-15.

Adams, T.E., Filz GM. and Navin, M., 2009. Stability of embankments and levees on deep-mixed foundations. In: Proceedings of the International Symposium on Deep Mixing and Admixture Stabilization, Okinawa, p.305-10.

Arroyo, M., Ciantia, M., Castellanza, R., Gens, A. & Nova, R., 2012. Simulation of cement-improved clay structures with a bonded elasto-plastic model: A practical approach. Computers and Geotechnics, Vol. 45, p. 140-150.

Axelsson, M. & Larsson, S., 2003. Column Penetration Tests for Lime-Cement Columns in Deep Mixing—Experiences in Sweden. In Third International Conference on Grouting and Ground Treatment, p. 681-694.

Baker S., 2000. Deformation behavior of lime/cement stabilized clay. PhD thesis, Gothenburg; Chalmers University of Technology.

Balasubramaniam, A.S. & Waheed-Uddin, 1977. Deformation characteristics of weathered Bangkok Clay in triaxial extension. Geotechnique, Vol. 27(1); p. 75-92.

Bergado, D.T., Taechakumthorn, C., Lorenzo, G.A. & Abuel-Naga, H.M., 2006. Stress-deformation behaviour under anisotropic drained triaxial consolidation of cement-treated soft Bangkok clay. Soils and Foundations, Vol. 46(5); p.629-637.

Bergman, B., Al-Naqshabandy, M. and Stefan Larsson., 2013. Variability of strength and deformation properties in lime-cement columns evaluated from CPT and KPS measurements. Georisk, Vol 7(1), p. 21-36.

Bjerrum, L., 1973. Problems of soil mechanics and construction on soft clays and structurally unstable soils. In Proc. 8th ICSMFE, Vol. 3, p. 111-159.

Black, D.K., Lee, K.L., 1973. Saturating laboratory samples by back pressure. ASCE, Soil Mechanics and Foundations Division, Vol. 99 no SM1, p. 75-93.

Broms, B.,1999a. Keynote lecture: Design of lime, lime/cement and cement columns. In Proceedings of the International Conference: Dry Mix Methods for Deep Soil Stabilization. Stockholm , p. 125-153.

Broms, B.B., 1999b. Progressive failure of lime, lime/cement and cement columns. In: Proceedings of the International Conference: Dry Mix Methods for Deep Soil Stabilization. Stockholm, p. 177-84.

Chai, J.C., Shrestha, S., Hino, T. & Uchikoshi, T., 2017. Predicting bending failure of CDM columns under embankment loading. Computers and Geotechnics, Vol. 91, p. 169-178.

Cheng, Q., Xiao, H., Liu, Y., Wang, W. & Jia, L., 2018. Primary yielding locus of cement-stabilized marine clay and its applications. Marine Georesources & Geotechnology; p. 1-18 (published on line).

Comodromos, E. M., Papadopoulou, M. C., & Georgiadis, K., 2018. Design procedure for the modelling of jet-grout column slabs supporting deep excavations. Computers and Geotechnics, Vol. 100, p. 110-120.

Consoli. N.C., Cruz. R.C., Floss. M.F. & Festugato. L., 2009. Parameters controlling tensile and compressive strength of artificially cemented sand. Journal of Geotechnical and Geoenvironmental Engineering, Vol. 136(5), p.759-763.

Consoli, N.C., Dalla Rosa Johann, A., Gauer, E.A., Dos Santos, V.R., Moretto, R.L. & Corte, M. B., 2012. Key parameters for tensile and compressive strength of silt–lime mixtures. Géotechnique Letters, Vol. 2(3), p.81-85.

Consoli, N.C., Prietto, P.D.M., Carraro, J.A.H. & Heineck, K.S., 2001. Behavior of compacted soil-fly ash-carbide lime mixtures. Journal of Geotechnical and Geoenvironmental Engineering, Vol. 127(9), p. 774-782.

D'Ignazio, M., 2016. Undrained shear strength of Finnish clays for stability analyses of embankments. Ph. D. thesis, Tampere University of Technology, Tampere, Finland.

Filz, G.M., Templeton, AE., Adams, TE., 2011. Stability analyses for levees on deep-mixed shear walls. Ground Improvement, Vol. 164(3), p.117–26.

Gens, A. & Nova, R., 1993. Conceptual bases for a constitutive model for bonded soils and weak rocks. In Geotechnical Engineering of Hard Soils-Soft Rocks, Athens, Greece, p. 485-494.

Guimond-Barrett, A., Nauleau, E., Le Kouby, A., Pantet, A., Reiffsteck, P.,& Martineau, F., 2013. Free–free resonance testing of in situ deep mixed soils. Geotechnical Testing Journal, Vol. 36(2), p. 283-291.

Gylland, A.S., Jostad, H.P.& Nordal, S., 2014. Experimental study of strain localization in sensitive clays, Acta Geotechnica, Vol. 9(2), p. 227-240.

Han, J., Chen, J., Hong, Z., Shen, S., 2005. Mitigation of levee failures using deep mixed columns and geosynthetics. Geomechanics and Geoengineering, Vol. 1; p. 49-55.

Han, J., Oztoprak, S., Parsons, R.L., Huang, J., 2007. Numerical analysis of foundation columns to support widening of embankment. Computers and Geotechnics, Vol. 34(6); p.435-48.

Han, J., Chen, J., Hong, Z., Shen, S., 2010. Mitigation of levee failures using deep mixed columns and geosynthetics. Geomechanics and Geoengineering, Vol. 5(1), p.49-55.

Horpibulsuk, S., Miura, N., & Bergado, D. T., 2004. Undrained shear behaviour of cement admixed clay at high water content. Journal of Geotechnical and Geoenvironmental Engineering, Vol. 130(10); p. 1096-1105.

Horpibulsuk, S., Liu, M.D., Liyanapathirana, D.S., Suebsuk, J., 2010. Behaviour of cemented clay simulated via the theoretical framework of the Structured Cam Clay model. Computers and Geotechnics, Vol. 37, p.1-9.

Horpibulsuk, S. & Liu, M.D., 2015. Structured cam clay model with cementation effect. Geotechnical Engineering Journal of the SEAGS & AGSSEA; Vol. 46(1), p. 86-94.

Hsi, J.P., & Yu, J.B.Y., 2005. Jet grout application for excavation in soft marine clay. In Proceedings of the International Conference on Soil Mechanics and Geotechnical Engineering, Vol. 16, no. 3, p. 1485-1488.

Hsieh, H.S., Wang, C.C. & Ou, C.Y., 2003. Use of jet grouting to limit diaphragm wall displacement of a deep excavation. Journal of Geotechnical and Geoenvironmental Engineering, Vol. 129(2), p. 146-157.

Huang, J., Han, J., Porbaha, A., 2006. Two and three-dimensional modeling of DM columns under embankments. GeoCongress, Geotechnical Engineering in the Information technology age, ASCE, Atlanta, GA.

Ignat R., 2015. Field and laboratory tests of laterally loaded rows of lime-cement columns, Licentiate thesis, KTH Royal Institute of Technology.

Ignat, R., Baker, S., Larsson, S., Liedberg, S., 2015. Two- and three-dimensional analyses of excavation support with rows of dry deep mixing columns. Computers and Geotechnics, Vol. 66, p.16-30.

Ignat, R., Baker, S., Liedberg, S., & Larsson, S. 2016. Behaviour of braced excavation supported by panels of deep mixing columns. Canadian Geotechnical Journal; Vol. 53(10); p. 1671-1687

Indraratna, A.S., Balasubramanian, A. K. & Khan, M.J., 1995. Effect of fly ash with lime and cement on the behavior of a soft clay. Quarterly Journal of Engineering Geology and Hydrogeology, Vol. 28(2), p.131-142.

Ismail, A.I.M. & Ryden, N., 2014. The quality control of engineering properties for stabilizing silty Nile Delta clay soil, Egypt. Geotechnical and Geological Engineering, Vol. 32(4), p. 773-781.

Jamsawang, P., Voottipruex, P., Boathong, P., Mairaing, W. & Horpibulsuk, S., 2015a. Three-dimensional numerical investigation on lateral movement and factor of safety of slopes stabilized with deep cement mixing column rows. Engineering Geology, Vol. 188, p. 159-167.

Jamsawang, P., Voottipruex, P., Jongpradist, P. & Bergado, D. T., 2015b. Parameters affecting the lateral movements of compound deep cement mixing walls by numerical simulations and parametric analyses. Acta Geotechnica, Vol. 10(6), p. 797-812.

Jamsawang, P., Boathong, P., Mairaing,W., & Jongpradist, P., 2016a. Undrained creep failure of a drainage canal slope stabilized with deep cement mixing columns. Landslides, Vol. 13(5), p. 939-955.

Jamsawang, P., Yoobanpot, N., Thanasisathit, N., Voottipruex, P. & Jongpradist, P., 2016b. Three-dimensional numerical analysis of a DCM column-supported highway embankment. Computers and Geotechnics, Vol. 72, p. 42-56.

Jamsawang, P., Jamnam, S., Jongpradist, P., Tanseng, P. & Horpibulsuk, S., 2017. Numerical analysis of lateral movements and strut forces in deep cement mixing walls with top-down construction in soft clay. Computers and Geotechnics, Vol. 88, p. 174-181.

Jardine, R. J. (1991). Some practical applications of a non-linear ground model. In Proceedings of 10th European Conference on Soil Mechanics Florence; Vol. 1, p. 223-228.

Jardine, R.J., 1992. Some observations on the kinematic nature of soil stiffness. Soils and foundations, Vol. 32(2), p. 111-124.

Kamruzzaman, A. H., Chew, S. H., & Lee, F. H. (2009). Structuration and destructuration behaviour of cement-treated Singapore marine clay. Journal of Geotechnical and Geoenvironmental Engineering, Vol. 135(4); p. 573-589.

Karlsrud, K., & Andresen, L., 2005. Loads on braced excavations in soft clay. International Journal of Geomechanics, Vol. 5(2), p. 107-113.

Karlsrud, K., Eggen, A., Nerland, O., 2015. Some Norwegian Experiences Related to Use of Dry-Mixing Methods to Improve Stability of Excavations and Natural Slopes in Soft Clays. In Proceedings of the Deep Mixing 2015 Conference, San Francisco.

Karlsrud, K. & Hernandez-Martinez, F.G., 2013. Strength and deformation properties of Norwegian clays from laboratory tests on high-quality block samples. Canadian Geotechnical Journal, Vol. 50(12), p.1273-1293.

Karstunen, M. & Koskinen, M., 2004. Anisotropy and destructuration of Murro clay. In Advances in geotechnical engineering: The Skempton Memorial conference: London, UK, on 29–31 March 2004. Edited by Jardine R.J., Potts D.M. and Higgins K.G.; Vol. 1, p. 476-487. Thomas Telford Publishing.

Karstunen M. & Koskinen M., 2008. Plastic anisotropy of soft reconstituted clays, Canadian Geotechnical Journal, Vol. 45(3), p. 314-328.

Karstunen, M., Krenn H., Wheeler S.J., Koskinen M., & Zentar R.,2005. Effect of anisotropy and destructuration on the behavior of Murro test embankment, International Journal of Geomechanics; Vol. 5(2), p.87-97.

Kasama K., Ochiai, H., Yasufuku, N., 2000. On the stress-strain behaviour of lightly cemented clay based on an extended critical state concept. Soils and Foundations, Vol. 40(5); p. 37-47.

Kasama, K., Zen, K., & Iwataki, K. 2006. Undrained shear strength of cement-treated soils. Soils and Foundations, Vol. 46(2); p. 221-232.

Khan, M.R.A., Hayano, K., Kitazume, M. 2008. Investigation on stability of sheet pile quay wall improved by cement treated sea-side ground from centrifuge model tests,. Soils and Foundations, Vol. 48(4), p. 563-575.

Kitazume, M., Yamamoto, M., and Udaka, Y.,1999. Vertical bearing capacity of column type DMM ground with low improvement ratio. In Proceedings of the International Conference: Dry Mix Methods for Deep Soil Stabilization, Stockholm; 1999. p. 245–250.

Kitazume, M., Okano, K., & Miyajima, S., 2000. Centrifuge model tests on failure envelope of column type deep mixing method improved ground. Soils and Foundations, Vol. 40(4), p. 43-55.

Kitazume, M., Maruyama, K., 2006. External stability of group column type deep mixing improved ground under embankment loading. Soils and Foundations, Vol. 46(3), p. 323-40.

Kitazume, M., Maruyama, K., 2007. Internal stability of group column type deep mixing improved ground under embankment loading. Soils and Foundations, Vol. 47(3), p. 437-55.

Kitazume, M., Terashi, M., 2013. The deep mixing method. CRC Press/Balkema

Kivelö, M., 1998. Stabilization of embankments on soft soil with lime/cement columns. PhD thesis, KTH Royale Institute of Technology, Stockholm.

Koseki, J., Sato, T., Mihira, S., Takeya, N., & Yoshizawa, M. 2005. Comparison of tensile strength of cement treated sand by various test methods. Proc. of the International Conference on Deep Mixing 05; p.95-100.

Koskinen, M., 2014. Plastic anisotropy and destructuration of soft Finnish clays. PhD-thesis, Aalto University, Helsinki.

Koskinen, M., Karstunen, M., & Wheeler, S. J., 2002a. Modelling destructuration and anisotropy of a soft natural clay. In Proceedings of 5th European Conf. Numerical Methods in Geotechnical Engineering, P. Mestat, ed., Presses de l'ENPC/LCPC,Paris, France, p.11-20.

Koskinen, M., Lojander, M., Tolla, P. & Vepsäläinen, P., 2002b. Numerical analysis on Murro test embankment. In Proceedings of 5th European Conf. Numerical Methods in Geotechnical Engineering, P. Mestat, ed., Presses de l'ENPC/LCPC, Paris, France, 397-402.

Lacasse, S., Berre, T., 1988. Triaxial testing methods for soils. Advanced triaxial testing of soil and rock. ASTM Special technical publications, STP 977, p. 264-289.

Ladd, C., 1991. Stability evaluation during staged construction. ASCE, Journal of Geotechnical Engineering, Vol. 117 (4), p. 540-615.

Ladd, C., Foott, R., 1974. New design procedure for stability of soft clays. ASCE, Journal of Geotehnical Engineering Division, Vol. 100 (GT7), p. 763-786.

Lade, P.V. & Duncan, J.M., 1973, Cubical triaxial tests on cohesionless soil. Journal of Soil Mechanics & Foundations Division, 99(Proc Paper 10057).

Lade, P.V. & Duncan, J.M., 1975. Elastoplastic stress-strain theory for cohesionless soil. Journal of Geotechnical and Geoenvironmental Engineering; 101(ASCE# 11670 Proceeding).

Lade, P. V., & Overton, D. D., 1989. Cementation effects in frictional materials. Journal of Geotechnical Engineering, Vol. *115*(10), p. 1373-1387.

Lade, P.V. & Trads, N., 2014. The role of cementation in the behaviour of cemented soils. Geotechnical Research, Vol. *1*(4), p. 111-132.

Lade, P.V. 2016. Triaxial testing of Soils. John Wiley & Sons

Larsson, R., 1977. Basic behaviour of Scandinavian soft clays. Swedish Geotechnical Institute, Linköping, 129 p.

Larsson R. & Mulabdić M., 1991. Shear moduli in Scandinavian clays; measurements of initial shear modulus with seismic cones; empirical correlations for the initial shear modulus in clay, Swedish Geotechnical Institute (SGI), Report No. 40, Linköping.

Larsson, R., 2006. Deep Mixing – Guidelines, Report 17, Swedish Deep Stabilization Research Centre, Linköping (In Swedish).

Larsson, R., Sällfors, G., Bengtsson, P.E., Alén, C., Bergdahl, U., Eriksson, L., 2007. Shear strength-Evaluation in cohesion soils, Information 3, Swedish Geotechnical Institute (SGI), Linköping (in Swedish).

Larsson, S., Broms, B.B., 2000. Shear box model tests with lime/cement columns – some observations of failure mechanisms. In: Proceedings of Geoengineering, Melbourne.

Larsson, S., 2005. State of practice report–Execution, monitoring and quality control. In International Conference on Deep Mixing, p. 732-785.

Larsson, S., Malm, R., Charbit, B., Ansell, A., 2012. Finite element modeling of laterally loaded lime-cement columns using a damage plasticity model. Computers and Geotechnics, Vol. 44, p.48-57.

Leroueil, S. & Vaughan, P.R., 1990. The general and congruent effects of structure in natural soils and weak rocks. Géotechnique, Vol. 40(3), p. 467-488.

Liao, H.J., Lin, C.C. & Huang, C.J., 2008. Modeling the effect of ground improvement on reducing movement during bermed excavation in clay. Journal of the Chinese Institute of Engineers, Vol. 31(1), p. 81-93.

Liao, H. J., & Su, S.F., 2011. Base Stability of Grout Pile–Reinforced Excavations in Soft Clay. Journal of Geotechnical and Geoenvironmental Engineering, Vol. 138(2), p. 184-192.

Lindh, P., Ryden, N. & Ekdah, U., 2005. Comparison between unconfined compression test and free–free resonant column test. In Proceedings of 2nd symposium (TREMTI), Paris, France.

Liu, M.D. & Carter, J.P., 2002. A structured Cam Clay model. Canadian Geotechnical Journal, Vol. 39(6), p.1313-1332.

Liu, Y., Lee, F.H., Quek, S.T., Chen, E.J., & Yi, J.T., 2015. Effect of spatial variation of strength and modulus on the lateral compression response of cement-admixed clay slab. Géotechnique, Vol. 65(10), p. 851-865.

Liu, Y., Pan, Y., Sun, M., Hu, J., & Yao, K., 2017. Lateral compression response of overlapping jet-grout columns with geometric imperfections in radius and position. Canadian Geotechnical Journal, (ja), https://doi.org/10.1139/cgj-2017-0280.

Lorenzo, G.A. & Bergado, D.T., 2006. Fundamental characteristics of cement-admixed clay in deep mixing. Journal of Materials in Civil Engineering, Vol. 18(2), p. 161-174.

Lowe, J. & Johnson, T.C., 1960. Use of back pressure to increase degree of saturation of triaxial test specimens. In Research Conference on shear strength of cohesive soils, ASCE, p. 819-836.

Länsivaara, T., 1999. A study of the mechanical behavior of soft clay. PhD-thesis, Norwegian University of Science and Technology, Norway.

Maccarini, M., 1987. Laboratory studies for a weakly bonded artificial soil. PhD-thesis, Imperial College London, University of London.

Malandraki, V. & Toll, D.G., 1996. The definition of yield for bonded materials. Geotechnical & Geological Engineering, Vol. 14(1), p. 67-82.

Malandraki, V. & Toll, D.G., 2000. Drained probing triaxial tests on a weakly bonded artificial soil. Géotechnique, Vol. 50(2), p. 141-151.

Malandraki, V. & Toll, D.G., 2001. Triaxial tests on weakly bonded soil with changes in stress path. Journal of Geotechnical and Geoenvironmental Engineering, Vol. 127(3), p. 282-291.

Massarsch, K. R., & Topolnicki, M., 2005. Regional report: European practice of soil mixing technology. In Proceedings of International Conference on Deep Mixing–Best Practice and Recent Advances, Stockholm; Vol. 1, p. R19-R45.

Matsuoka, H. & Nakai, T., 1974. Stress-deformation and strength characteristics of soil under three different principal stresses. In Proceedings of the Japan Society of Civil Engineers, Vol. 1974, No. 232, p. 59-70

Mayne, P.W., 1985. Stress anisotropy effects on clay strength. ASCE, Journal of Geotechnical Engineering, Vol. 111, p 356-366.

Miura, N., Horpibulsuk, S., Nagaraj, T.S., 2001. Engineering behaviour of cement stabilized clay at high water content. Soils and Foundations, Vol. 41(5), p. 33-45.

Namikawa, T., & Koseki, J. 2007. Evaluation of tensile strength of cement-treated sand based on several types of laboratory tests. Soils and Foundations, Vol. 47(4), p. 657-674.

Namikawa, T., & Mihira, S. 2007. Elasto-plastic model for cement-treated sand. International journal for Numerical and Analytical Methods in Geomechanics, Vol. 31(1), p. 71-107.

Namikawa, T., Hiyama, S., Ando, Y. & Shibata, T., 2017. Failure behavior of cement-treated soil under triaxial tension conditions. Soils and Foundations, Vol. 57(5), p. 815-827.

Navin, M.P., 2005. Stability of embankments founded on soft soil improved with deep-mixing-method columns. PhD -thesis, Virginia Polytechnic Institute and State University, Blacksburg VA.

Navin, M.P., Filz, GM., 2006. Numerical stability analyses of embankments supported on deep mixed columns. ASCE Geotechnical Special Publication No. 152; p. 1-9.

Nguyen, B., Takeyama, T. & Kitazume, M., 2016a. External failure of deep mixing columns reinforced by a shallow layer beneath an embankment. Journal of JSCE, Vol. 4(1), p. 92-105.

Nguyen, B., Takeyama, T., & Kitazume, M., 2016b. Internal Failure of Deep Mixing Columns Reinforced by a Shallow Stabilized Soil Beneath an Embankment. International Journal of Geosynthetics and Ground Engineering; Vol. 2(4), DOI 10.1007/s40891-016-0072-4.

Nguyen, B., Takeyama, T., & Kitazume, M., 2016c. Numerical analyses on the failure of deep mixing columns reinforced by a shallow mixing layer, Japanese Geotechnical Society Special Publication; Vol. 2(63), p. 2144-2148.

Nguyen, L.D., Fatahi, B., & Khabbaz, H., 2014. A constitutive model for cemented clays capturing cementation degradation. International Journal of Plasticity, Vol. 56, p. 1-18.

O'Rourke, T.D., O'Donell, C.J., 1997. Field behavior of excavation stabilized by deep soil mixing. Journal of Geotechnical and Geoenvironmental Engineering, Vol.123(6), p.516-524.

O'Rourke, T. D., McGinn, A.J. 2004. Case History of Deep Mixing Soil Stabilization for Boston Central Artery. Geotechnical Special Publication (GSP), ASCE, 126(1), p.77-136.

O'Rourke, T.D., McGinn, A.J., 2006. Lessons learned for ground movements and soil stabilization from the Boston central artery. Journal of Geotechnical and Geoenvironmental Engineering, Vol.13, p. 966-989.

Ou, C.Y., Wu, T.S., Hsieh, H.S., 1996. Analysis of deep excavation with column type of ground improvement in soft clay. Journal of Geotechnical Engineering, Vol. 122(9), p.709-16.

Ou, C.Y., Teng, F.C., Wang, I.W., 2008. Analysis and design of partial ground improvement in deep excavations. Computers and Geotechnics, Vol. 35(4), p.576-584.

Ou, C.Y., Hsieh, P.G., Lin, Y.L., 2013. A parametric study of wall deflections in deep excavations with the installation of cross walls. Computers and Geotechnics, Vol. 50, p. 55-65.

Pan, Y. T., Xiao, H. W., Lee, F. H., & Phoon, K. K., 2016. Modified isotropic compression relationship for cement-admixed marine clay at low confining stress. Geotechnical Testing Journal, Vol. 39(4), p.695-702.

Parry, R.H.G.,1960. Triaxial compression and extension tests on remoulded saturated clay. Geotechnique, Vol. 10(4), p. 166-180.

Pillai, R.J., Bushra, I. & Robinson, R.G., 2013. Undrained triaxial behavior of cement treated marine clay. Geotechnical and Geological Engineering, Vol. 31(2), p. 801-808.

Reddy, K. R., & Saxena, S. K. 1993. Effects of cementation on stress-strain and strength characteristics of sands. Soils and Foundations, Vol. *33*(4), p. 121-134.

Robin, V., Javadi, A.A., Cuisinier, O. & Masrouri, F., 2015. An effective constitutive model for lime treated soils. Computers and Geotechnics, Vol. 66, p. 189-202.

Rotta, G.V., Consoli, N.C., Prietto, P.D.M., Coop, M.R. & Graham, J., 2003. Isotropic yielding in an artificially cemented soil cured under stress. Geotechnique, Vol. 53(5), p. 493-501.

Ruggeri, P., Fruzzetti, V.M.E., Vita, A., Segato, D., Scarpelli, G., 2014 Stiffness of wall-type grouting under transversal loading. Ground Improvement, Vol.167.4, p. 301-310.

Rydén, N., Ekdahl, U., & Lindh, P., 2006. Quality control of cement stabilised soil using non-destructive seismic tests. Advanced testing of fresh cementitious materials, Lecture 34, p. 1-5.

Schanz, T., Vermeer, P.A. & Bonnier, P.G., 1999. The hardening soil model: formulation and verification. Beyond 2000 in Computational Geotechnics, p. 281-296.

Schnaid, F., Prietto, P.D. & Consoli, N.C., 2001. Characterization of cemented sand in triaxial compression. Journal of Geotechnical and Geo Environmental Engineering, Vol. 127(10), p.857-868.

Sivasithamparam. N. (2012). Development and implementation of advanced soft soil models in finite elements, PhD-thesis; University of Strathclyde, Glasgow, UK.

Su, S.F., 2009. Anisotropic strength evaluation of clay reinforced with grout piles. Journal of geotechnical and Geoenvironmental Engineering, Vol. 135(10), p. 1529-1537.

Su, S.F., & Liao, H.J., 2017. Base stability of deep excavation in clay reinforced with grout piles. In Proceedings of the Institution of Civil Engineers-Ground Improvement, p. 1-10.

Suebsuk, J., Horpibulsuk, S. & Liu, M.D., 2010. Modified Structured Cam Clay: A generalised critical state model for destructured, naturally structured and artificially structured clays. Computers and Geotechnics, Vol. 37(7-8), p. 956-968.

Suebsuk, J., Horpibulsuk, S., Liu, M.D, 2011. A critical state model for overconsolidated structured clays. Computers and Geotechnics, Vol.38(5), p.648-58.

Sukpunya, A. & Jotisankasa, A., 2016. Large simple shear testing of soft Bangkok clay stabilized with soil–cement-columns and its application. Soils and Foundations, Vol. 56(4), p. 640-651.

Tanaka, H., 1993. Behaviour of braced excavations stabilized by deep mixing method. Soils and Foundations, Vol. 33(2), p.105-115.

Tanaka, H., Locat, J., Shibuya, S., Soon, T.T. & Shiwakoti, D.R., 2001. Characterization of Singapore, Bangkok, and Ariake clays. Canadian Geotechnical Journal, Vol. 38(2), p.378-400.

Terashi, M., 1980. Fundamental properties of lime and cement treated soils, Report of PHRI; Vol. 19(1), p.33-62.

Terashi, M., Tanaka, H., & Kitazume, M., 1983. Extrusion failure of ground improved by the deep mixing method. In Proceedings of the 7th Asian Regional Conference on Soil Mechanics and Foundation Engineering, Haifa, Israel; Vol. 1, p. 313-318.

Terashi, M., 2005. Keynote lecture: Design of deep mixing in infrastructure applications. In Proceedings of International Conference on Deep Mixing-Best Practice and Recent Advances.

Thakur, V., 2007. Strain localization in sensitive soft clays. PhD-thesis, NTNU, Trondheim, Norway.

Toohey, N.M. & Mooney, M.A., 2012. Seismic modulus growth of lime-stabilized soil during curing. Geotechnique, Vol. 62(2), p. 161.

Tremblay, H., Leroueil, S., & Locat, J. 2001. Mechanical improvement and vertical yield stress prediction of clayey soils from eastern Canada treated with lime or cement. Canadian Geotechnical Journal, Vol. 38(3), p.567-579.

Toll, D.G., Malandraki, V., Ali Rahman, Z. & Gallipoli, D., 2006. Bonded soils: problematic or predictable. In Proceedings of 2nd International Conference on Problematic Soils, Malaysia, Singapore, CI-Premier, p. 55-62.

TK Geo 13, 2014. Technical requirements for geoconstructions (Trafikverkets tekniska krav för geokonstruktioner). The Swedish Transport Administration, Publ. TDOK 2013:0667, Sweden.

Uddin, K.M., Buensuceso, B.R., 2002. Lime Treated Clay: Salient Engineering Properties and a Conceptual Model. Soils and Foundations, Vol. 42(5), p. 79-89.

Verástegui-Flores, R.D., Di Emidio, G., Bezuijen, A., Vanwalleghem, J. & Kersemans, M., 2015. Evaluation of the free–free resonant frequency method to determine stiffness moduli of cement-treated soil. Soils and Foundations, Vol. 55(5), p. 943-950.

Wheeler, S.J., Näätänen, A., Karstunen, M. & Lojander, M., 2003. An anisotropic elastoplastic model for soft clays. Canadian Geotechnical Journal, Vol. 40(2), p. 403-418.

Won, J.Y., 2013. Anisotropic strength ratio and plasticity index of natural clays. In Proceedings of the 18th International Conference on Soil Mechanics and Geotechnical Engineering, ICSMGE, p. 2-6.

Yang, T., Tan, T.S., Leung, C.F., 2011. Mass behaviour of embedded improved soil raft in an excavation. Proceedings of Institution of Civil Engineers – Geotechnical Engineering, Vol. 164(GE1); p.11-25.

Yildiz, A., Karstunen, M. & Krenn, H., 2009. Effect of anisotropy and destructuration on behavior of Haarajoki test embankment. International Journal of Geomechanics, Vol. 9(4), p. 153-168.

Yoshida, S., 1996. Shear strength of improved soils at lap-joint-face. In: Proceedings of the 2nd International Conference on Ground Improvement Geosystems, Tokyo; Vol. 1; p. 461-466.

Yoshizawa, H., Okumura, R., Hoshia, Y., Sumi, M., Yamada, T., 1997. JGS TC Report: Factors affecting the quality of rested soil during execution of DMM. In: Proceedings of the 2nd International Conference on Ground Improvement Geosystems, Tokyo; Vol. 2; p. 931-937.

Xiao, H., Lee, F.H. & Chin, K.G., 2014. Yielding of cement-treated marine clay. Soils and Foundations, Vol.54(3), p. 488-501.

Xiao, H., Lee, F. & Liu, Y., 2017. Bounding Surface Cam-Clay Model with Cohesion for Cement-Admixed Clay. International Journal of Geomechanics, Vol. 17(1), p.1-22.

Zhu, J.G. & Yin, J.H., 2000. Strain-rate-dependent stress-strain behavior of overconsolidated Hong Kong marine clay. Canadian Geotechnical Journal, Vol. 37(6), p. 1272-1282.

Åhnberg, H., Johansson S.E., Retelius, A., Ljungkrantz, C., Holmqvist, L., Holm, G.,1995. Cement och kalk för djupstabilisering av jord. Report No. 48. SGI, Linköping, Sweden, p 213 (in Swedish).

Åhnberg, H., 2004. Effects of back pressure and strain rate used in triaxial testing of stabilized organic soils and clays. Geotechnical Testing Journal, Vol. 27(3), p. 250-259.

Åhnberg, H., 2006. Consolidation stress effects on the strength of stabilized Swedish soils. Proceedings of the Institution of Civil Engineers - Ground Improvement, Vol. 10(1), pp. 1-13.

Åhnberg, H., 2007. On yield stresses and the influence of curing stresses on stress paths and strength measured in triaxial testing of stabilized soils. Canadian Geotechnical Journal, Vol. 44(1), p. 54-66.

Åhnberg, H. & Holmen, M., 2008. Laboratory determination of small-strain moduli in stabilized soils. In Proceedings of International Symposium on Deformation Characteristics of Geomaterials, Atlanta, Vol. 1, p. 291-297.

Åhnberg, H. & Holmén, M., 2011. Assessment of stabilised soil strength with geophysical methods. Proceedings of the Institution of Civil Engineers-Ground Improvement, Vol. 164(3), p. 109-116.